The development of different strategies using clinically translatable models for the treatment of Triple Negative Breast Cancer

Sara El-Sahli

Thesis submitted to the University of Ottawa
in partial fulfillment of the requirements for the
Doctorate in Philosophy degree in Biochemistry

Department of Biochemistry, Microbiology & Immunology
Faculty of Medicine
University of Ottawa

uOttawa

ABSTRACT

Triple negative breast cancer (TNBC) is an aggressive form of breast cancer, that lacks targeting therapy, making chemotherapy the primary treatment option. However, chemotherapy leads to the enrichment of a subpopulation of cells with tumor initiating capacities called cancer stem cells (CSCs), that are implicated in treatment resistance, metastasis, and recurrence. To address this, I developed a triple-drug combination therapy targeting multiple aspects of tumorigenesis. Due to the limitation of conventional drug treatment, the use of nanoparticles (NPs) as a delivery system was introduced to increase therapeutic index. This triple-drug NPs suppressed bulk TNBC cells, CSC enrichment, and angiogenesis, both *in vitro* and in the clinically relevant patient-derived xenograft (PDX) model, paving the way for potential clinical application.

RNA based therapeutics have emerged as a promising alternative in cancer treatment due to higher specificity in targeting key drivers of tumorigenesis. Using NPs as a delivery system, I showed the successful delivery of mRNA agents in PDX models, highlighting the promise of RNA-based NP therapies for overcoming limitations of conventional treatments in TNBC. As tumors are heterogenous with multiple drivers in play, I developed a NP-based co-delivery platform to deliver siRNA and mRNA for multitargeted gene regulation in cancer. These RNA-loaded NPs simultaneously knocked down and expressed target genes in TNBC *in vitro* and *in vivo*, highlighting their potential for multi-targeted therapy. Overall, throughout this thesis, using PDX models, I showed the effective delivery of both Drugs-NP and RNA-agents, laying the groundwork for future therapeutic strategies in TNBC treatment.

ACKNOWLEDGEMENTS

I would first like to thank my supervisor and mentor, Dr. Lisheng Wang. Finding my way to his lab has truly been one of my greatest blessings. Dr. Wang taught me what it takes to be an incredible scientist but also a kind, patient, and compassionate mentor. Thank you for always making time, for encouraging me through every challenge, and for leading with such empathy and care for your students. You showed me that it is possible to care deeply about both the science and the people behind it. Your support meant everything on the hardest days, and your belief in me pushed me to aim higher, growing in ways I never imagined. I am incredibly grateful for your mentorship and your guidance.

I would also like to sincerely thank Dr. Suresh Gadde, for his support and mentorship throughout my degree. Your commitment to all the students you have mentored and your trust in them has been very inspiring. I am immensely grateful for all the encouragement and advice you have given me along the way. A special thanks to my thesis advisory committee, Dr. Jonathan Lee, Dr. Seung-Hwan Lee, and Dr. Zemin Yao, for their guidance and insight from the very beginning of my degree. Thank you for going beyond simply sharing your expertise and for truly supporting me throughout every step of my PhD journey.

I would like to thank the Wang lab, in particular Dr. Li Li, whose support was instrumental to the success of my experiments. Thank you for constantly sharing your wealth of knowledge and for always being ready to help when we needed you. To those who started the journey in Dr. Wang's lab with me, Shelby and Jason, thank you for your constant support and friendship over the years. To the students I have mentored in the lab, in particular,

Alyanna, Marcelle, and Divine, thank you for teaching me the value of collaboration and perspective. To Red, Julia and Toqa, thank you for your friendship both inside RGN and out. Our time together will always bond us regardless of where life takes us.

To the Faculty of Medicine staff, thank you for all that you do in assisting us navigate our degrees with care and efficiency. Additionally, thank you to the funding support I have received from the Ontario Graduate Scholarship (OGS) program and the Canadian Institutes of Health Research (CIHR), without whom this work would not be possible.

A special thanks to Adez and Marianna, friends I met very early on in my journey who quickly became best friends and ended up becoming sisters. You have been a source of strength and comfort both inside the lab and out. Thank you for all the memories we have created and for being there for me even across different countries and time zones.

To my sisters, Lujane, Yomna, and Yasmin, who have been my lifeline, thank you for being my safe space and my best friends. I have been incredibly blessed with you as my biggest cheerleaders - thank you for consistently motivating me to keep going. Your support and love has meant more than you know, and I feel so lucky to have you three by my side. To my brother-in-law, Muaz, and to Esra (Esso) and Omar, who we have always considered to be siblings, thank you for being my best friends, for always being there throughout it all and for making life that much brighter with your presence. To my aunt, Azza, thank you for all your assistance and unwavering support. To Mahmoud, thank you for joining me on the last stretch of this chapter - your presence, encouragement and support has made it that much easier.

Most importantly, I would like to thank my incredible parents, whose love and support knew no bounds throughout my life. Thank you for everything you have done for my sisters and I. Dad and Mum, my gratitude and love for you is beyond anything I could ever put into words - in these pages or anywhere else. You have taught me the true meaning of resilience, strength, and unconditional love. I am so eternally blessed to have you both, and I am so grateful you created a family that supports so completely and uplifts no matter what. This degree belongs to you just as much - if not more - because I would not be where I am without you both.

TABLE OF CONTENTS

LIST OF FIGURES & TABLES

LIST OF ABBREVIATIONS

ADC	Antibody Drug Conjugate
Akt	Protein Kinase B
ALDH	Aldehyde Dehydrogenase
ANOVA	Analysis of Variance
BL1	Basal-Like 1
BL2	Basal-Like 2
BLBC	Basal-Like Breast Cancer
BRCA1	Breast Cancer 1, early onset
CA4	Combretastatin A4
CARs	Chimeric Antigen Receptors
CSC	Cancer Stem Cell
circRNA	Circular RNA
DCIS	Ductal Carcinoma In Situ
DLS	Dynamic Light Scattering
EE	Encapsulation Efficiency
EMT	Epithelial-Mesenchymal Transition
EPR	Enhanced Permeability and Retention
ER+	Estrogen Receptor Positive
HER2+	Human Epidermal Growth Factor Receptor Positive
HIF-1α	Hypoxia-Inducible Factor 1-alpha
Hpf	Hours Post Fertilization
ICD	Immunogenic Cell Death

ICI	Immune Checkpoint Inhibitor
IDC	Invasive Ductal Carcinoma
ILC	Invasive Lobular Carcinoma
IM	Immunomodulatory
IT	Intratumoral
IV	Intravenous
IVIS	In Vivo Imaging System
LAR	Luminal Androgen Receptor
M	Mesenchymal
miRNAs	micro-RNA
mRNA	Messenger RNA
MSL	Mesenchymal Stem-Like
NF- κB	Nuclear Factor kappa-light-chain-enhancer of activated B cells.
NOD-SCID	Non-Obese Diabetic-Severe Combined Immunodeficiency
NP	Nanoparticle
pCR	Pathological Complete Response
PDX	Patient Derived Xenografts
PFS	Progression Free Survival
PI3K	Phosphoinositide 3-Kinase
PLGA-PEG	Poly (lactic-co-glycolic acid)–Polyethylene Glycol.
PR+	Progesterone Receptor Positive
PTEN	Phosphatase and Tensin Homolog
RISC	RNA Induced Silencing Complex
RNAi	RNA interference

saRNA	Self-amplifying RNA
SCID	Severe Combined ImmunoDeficient
SD	Standard Deviation
SE	Standard Error
siRNA	short interfering RNA
taRNA	Trans-amplifying RNA
TCRs	T Cell Receptors
TMIs	Tumor Initiating Cells
TNBC	Triple Negative Breast Cancer
TP53	Tumor Protein p54
VEGF	Vascular Endothelial Growth Factor
YAP	Yes-Associated Protein

CHAPTER 1: INTRODUCTION

1.1 Breast Cancer

1.1.1 Breast Cancer Incidence

Breast cancer is the most frequently diagnosed cancer in women around the world, and currently remains one of the leading causes of cancer-related deaths (after lung cancer), with the incidence rates varying across countries and geographical regions[1,2].

While the highest incidence rates are observed in more developed countries, thought to be due to lifestyle factors as well as increased screening and earlier-stage diagnosis, the mortality rate is disproportionately higher in less developed countries, likely due to improper access to diagnostic services and limited treatment options[2].

In Canada, breast cancer remains a prevalent challenge and a major burden on the public healthcare system[3–5]. As of 2022, around 2.1% of Canadian women are predicted to be breast cancer survivors, as they were diagnosed in the past two decades[5]. While the mortality rate has decreased, which is largely due to increased awareness and advancements in diagnosis and treatment, the overall rate remains around 31.5 deaths per 100,000 cases annually, varying slightly across Canadian provinces[4,6].

1.1.2 Breast Cancer Risk Factors

The incidence of breast cancer is influenced by several risk factors, some non-modifiable and others modifiable (Figure 1.1)[7]. Non-modifiable risk factors include older age, with 80% of new

cases in women >50 years of age; genetic mutations; and family history, with 13-19% of cases reporting an affected first degree relative[7,8]. Race and ethnicity have also been widely considered to be risk factors, although the mechanisms have not been fully elucidated. However, more research is required to look into the racial disparities in breast cancer incidences; while the rates are higher in non-Hispanic white women, a study by Wilkinson *et al*. (2024) found that black women are more likely to be diagnosed later at a more advanced stage with a higher mortality rate[9]. Modifiable risk factors are primarily related to environmental cues and lifestyle factors such as alcohol intake, physical inactivity, obesity, and smoking[7,10]. Growing evidence also suggests that diet and processed food are a huge risk factor for breast malignancies, with a 10% increase in the consumption of processed food being linked with an over 10% rise in breast cancer incidence[11].

1.1.3 Breast Tumorigenesis

The transformation of normal breast tissue into malignancy or breast carcinogenesis is a multistep process driven by a series of events, both genetic and environmental, that result in the well-characterized uncontrolled proliferation and growth[12–14]. Hereditary breast cancer, which constitutes around 5-10% of breast cancers, is a result of inherited mutations in one of the alleles of tumor suppressor genes such as *BRCA1*, *BRCA2*, *CHEK 2*, *TP53,* or *PTEN*, that renders them inactive[13]. These tumor suppressor genes are crucial in DNA repair, genome stability, cell cycle regulation, and apoptosis[12]. BReast CAncer gene 1 (BRCA1), for example, plays a significant role in DNA repair, protecting new DNA strands from degradation and maintaining the stability of the genome[15]. Phosphatase and tensin homolog deleted on chromosome ten (PTEN) downregulates phosphatidylinositol-3-kinase (PI3K)/protein kinase B (Akt) signaling, a significant pathway in

cell proliferation and survival[16]. The loss of PTEN activity and the subsequent overactivation of PI3K/AKT signaling is linked to aggressive disease progression and poor prognosis[16,17].

On the other end, tumor development can also result from the activation of cellular oncogenes, which promote tumor initiation[18]. Oncogene mutations can result in an increase in gene expression or the overactivity of the oncogene-encoded effector protein. Examples of oncogenes implicated in breast cancer progression are *PI3KCA*, *MYC,* and *CCND1* (encoding Cyclin D1)[19]. These play significant roles in cell survival, growth, and proliferation. Furthermore, studies over the last few decades have identified other oncogenic signaling pathways driving various cancers, particularly breast cancer, amongst them being the Hippo/YAP, Notch, TGFβ, and Wnt/β-catenin pathways[20–22]. While research is continuously exploring the mechanisms that drive carcinogenesis and tumor progression, the development of breast cancer relies on both the activation of oncogenic pathways and, at the same time, the inactivation of tumor suppressor genes.

1.1.4 Breast Cancer Subtypes

Breast cancer originates in the epithelial cells that line the ducts/lobules of the breast tissue and can be broadly classified into invasive and non-invasive types. Of the invasive types, the most common is invasive ductal carcinoma (IDC), accounting for approximately 70–80% of all cases, after which comes invasive lobular carcinoma (ILC), which makes up 10–15% of the invasive cases[23]. Non-invasive forms, such as ductal carcinoma in situ (DCIS), are confined mostly to the ducts, do not invade surrounding tissues, and are associated generally with a better prognosis[24].

Using immunohistochemical analysis, breast cancer is characterized based on the receptor status, where it is divided into 4 subtypes: estrogen receptor positive (ER+), progesterone receptor positive (PR+), human epidermal growth factor receptor positive (HER2+), and triple negative breast cancer (TNBC), called triple negative as it lacks the expression of these receptors[25,26]. At around 70%, the ER+ subtype of breast cancer represents the majority of cases and is generally linked to a better overall survival than ER- breast cancer cases, particularly in women over the age of 40[26,27]. Likewise, having PR+ expression, which commonly occurs alongside ER expression, is associated with a lower mortality risk than ER- and ER+ breast cancer[28]. On the other hand, HER-2 positive breast cancer is said to have a higher risk of recurrence and metastasis than HER-2 negative, ER/PR positive cases[29].

Further classification of breast cancer is based on gene expression profiling, which divides them into Luminal A, Luminal B, HER-2 enriched and basal-like breast cancer (BLBC)[30]. Luminal A accounts for 23.7% of breast cancer and is ER and/or PR positive, but HER-2 negative[30]. Luminal B, on the other hand, accounts for 33.2% and is ER and/or PR positive as well as, HER- 2 positive. Luminal tumors are sensitive to targeted therapies such as endocrine therapy; tamoxifen or aromatase inhibitors with Luminal A having the best prognosis out of the two[30]. HER- 2 enriched accounts for 10-20% and is ER and PR negative. The treatment option for HER-2 enriched breast cancers is typically the HER-2 monoclonal antibody, Trastuzumab[30,31]. Most BLBCs are triple negative breast cancer (TNBC), accounting for around 10-15 % of breast cancers. TNBC patients have the worst prognosis with a lower survival rate, a higher risk of relapse, and a lack of targeted therapies.

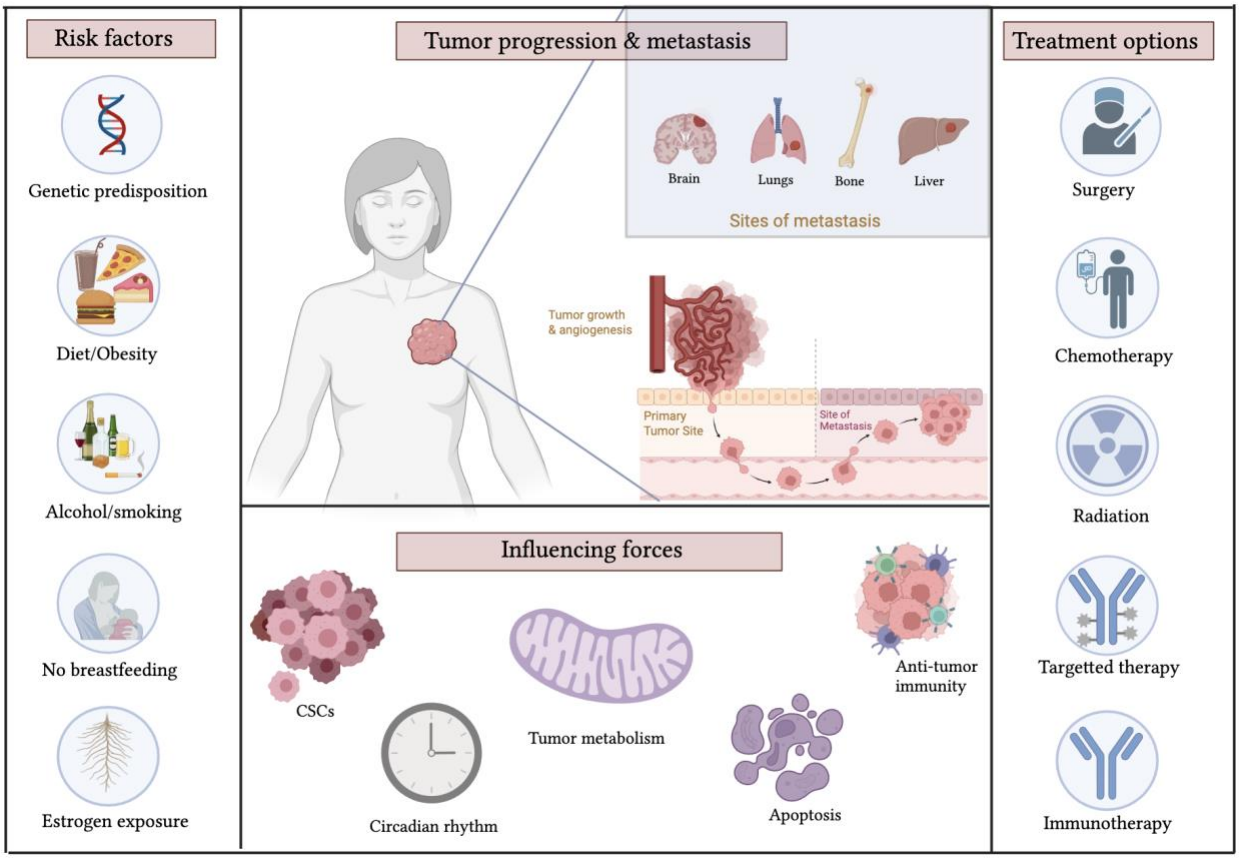

Figure 1.1. An overview of breast cancer risk factors, progression, influencing factors and treatment. Figure adapted from Xiong, X., *et al.* (2025). "Breast cancer: pathogenesis and treatments." *Signal Transduction and Targeted Therapy*, *10*(1),49 [12] Permission conveyed through Creative Commons Attribution 4.0 International License. (Creative Commons — Attribution- 4.0 International — CC BY 4.0) https://creativecommons.org/licenses/by/4.0/. Figure recreated using BioRender.com.

1.2 Triple Negative Breast Cancer (TNBC)

While TNBC only accounts for less than 15% of all breast cancer cases, it is responsible for most of the breast cancer-related deaths[32–34]. TNBC is particularly prevalent in younger women (< 40), with racial and socioeconomic disparities as its incidence is higher in non-white women and those from low-income neighborhoods[34–36]. Clinically, TNBC tumors tend to be more aggressive, with the diagnosis occurring at a later stage, partially due to the limitation of the diagnostic methods. Mammography screening, for example, has an accuracy rate of only 39.8% in the detection of TNBC tumors as they tend to be less likely to show suspicious features[37].

As TNBC is known to be a heterogeneous disease, efforts have been put towards further classifications for a deeper understanding of therapeutic strategies and their prognostic implication[34,38]. One common categorization is the Lehmann classification of TNBC which divides it into four different subtypes based on molecular differences (Figure 1.2); basal-like 1 (BL1) and basal-like 2 (BL2), which tend to be highly proliferative due to their high expression of DNA regulation genes; luminal androgen receptor (LAR), which is characterized by the high expression of the androgen receptor; and the mesenchymal (M) subtype, characterized by mesenchymal features and includes tumors with a highly immunosuppressive environment[38]. This classification is a refinement of a previous one that included the two subtypes: immunomodulatory (IM) and mesenchymal stem-like (MSL), which were found to be distinct due to immune and stromal factors rather than actual tumor cell biology[34,38].

BL1 and BL2 subtypes of TNBC are known to have high genomic instability, with BL1 having a higher frequency of tumor suppressor mutations, particularly p53 and PTEN, while BL2 displays

higher signaling activity of crucial pathways such as Wnt/β-catenin[39,40]. The M subtype tumors are specifically enriched in genes governing angiogenesis and metastasis[38,41]. Lastly, the LAR subtype tumors display a higher activity of key pathways involved in tumor growth[41]. The heterogeneity of TNBC tumors contributes to the challenges in the development of effective therapy, highlighting the significance of targeting multiple aspects in treatment.

1.2.1 TNBC Treatment: A Focus on Chemotherapy

The lack of targeted therapy makes TNBC the most complex subtypes to tackle, connected with the highest mortality rate among the breast cancer subtypes[32]. Chemotherapy, following the surgical removal of the tumor (a lumpectomy or a mastectomy), remains one of the primary treatment strategies for patients with TNBC[42]. The chemotherapy regimen used is dependent on various clinical factors, among them is the stage of diagnosis and the involvement of the lymph nodes, with the standard treatment consisting of both anthracyclines and taxanes[42]. Anthracyclines such as doxorubicin, work by causing DNA damage, intercalating into the DNA, and inhibiting topoisomerase II, triggering apoptosis and cancer cell death[43]. Taxanes, such as paclitaxel, work by disrupting microtubule function, resulting in cell cycle arrest, and inhibiting cell division[44].

Paclitaxel remains a common component of chemotherapy regimens for TNBC patients; however, it is ineffective on its own, with successful treatment depending on a combination drug regimen [42,44,45]. Database analysis of randomized controlled trials, for example, showed that taxane (paclitaxel) based combination therapy prolonged progression-free survival (PFS) and overall survival (OS) compared to taxane monotherapy[45]. Studies have also shown the increased efficacy

of paclitaxel in combination with other agents, such as bevacizumab or alisertib, prolonging PFS more than paclitaxel alone[46,47].

While chemotherapy is required for TNBC treatment in early-stage disease, possibly eliminating signs of the disease and achieving pathological complete response (pCR)[48], there are substantial challenges that limit its overall clinical efficacy and viability. Due to the systemic administration of chemotherapy, it can lead to both short- and long-term toxicity. Paclitaxel for example, leads to nausea, vomiting, and fatigue in the short-term, and peripheral neuropathy that continues post-treatment cessation in the long term[49,50]. Furthermore, multiple cycles of chemotherapy administration lead to treatment resistance and a poor outcome[51]. Perhaps even more drastically, chemotherapy is implicated in the enrichment of a subpopulation of cells known as cancer stem cells (CSCs), which are increasingly being linked to drug resistance, disease relapse, and metastasis[52–55]. Indeed, multiple reports have shown the enrichment of CSCs in TNBC cell lines and associate it with the aggressive nature of the disease[55,56].

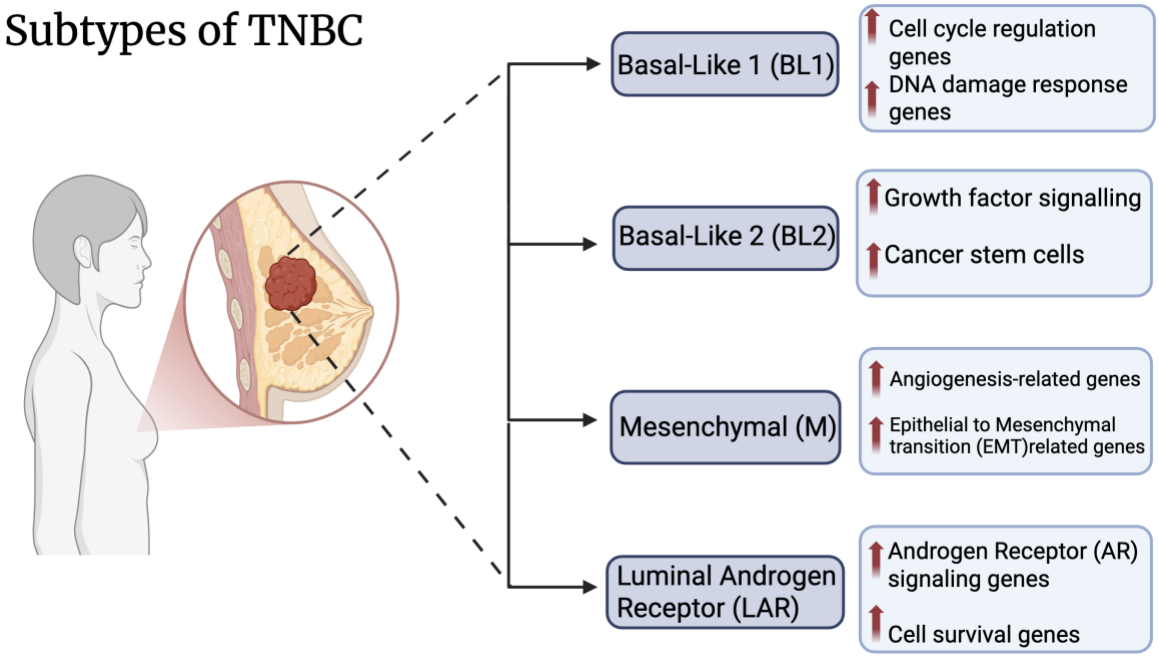

Figure 1.2. The classification of TNBC into different subtypes. Recent categorization of TNBC divides it into four subtypes, each characterized by different molecular and biological features, that showcases its heterogeneity. Figure generated based on the TNBCtype-4 classification as described by Lehmann, B. D., *et al.* (2016). "Refinement of triple-negative breast cancer molecular subtypes: implications for neoadjuvant chemotherapy selection." *PloS one*, *11*(6). Figure created using BioRender.com.

1.3 Cancer Stem Cells (CSCs)

The "cancer stem cell" model of tumor heterogeneity states that among bulk tumor cells, there is a subpopulation of cells that have self-renewing capabilities and stem-like characteristics, capable of forming new tumors[57–59]. This subpopulation is known as cancer stem cells (CSCs) and due to their ability to form new tumors, they are also known as tumor-initiating cells (TMIs)[59]. Over the last few decades, more evidence has shed light on the role of breast CSCs in tumor initiation, tumor progression, treatment resistance, and metastasis.

While the exact origins of breast CSCs are still under debate, there is strong evidence to suggest that they have acquired key stem cell characteristics[59]. Studies have shown that mutations, such as BRCA1, in breast progenitor cells led to tumor growth, and early preinvasive DCIS lesions were found to have cells with known stem cell markers[60,61]. Alternatively, it is also speculated under the stochastic model of CSC origin that a series of mutations in differentiated somatic cells results in reprogramming, acquiring CSC properties[59].

1.3.1 Breast CSC Markers

Breast CSCs are commonly characterized based on specific markers, such as cell surface protein expression. This breakthrough came when a study by Al-Hajj *et al.* (2003) revealed that the subpopulation of breast tumor cells with the greatest tumorigenic capacity (CSCs) expressed high levels of CD44, a transmembrane hyaluronic acid receptor, and low levels of CD24, a cell surface protein anchored to the membrane by glycosylphosphatidylinositol[62]. Using tumor pleural effusion from breast cancer patients, Al-Hajj *et al.* (2003) showed that cancer cells expressing the immunophenotype $CD44^{+}$ /$CD24^{-/low}$ were able to generate heterogeneous tumors at a frequency

of 100-fold higher than their $CD44^{-}/CD24^{+}$ counterparts in immunocompromised mice[62]. While these remain the conventional markers with the most clinically relevant evidence, other additional markers have also been investigated, among them are CD133, EpCAM, SSEA-3, and LGR5[63].

Internal players have also been explored as potential markers for breast CSCs, most commonly being the enzyme aldehyde dehydrogenase (ALDH)[64]. The overactivity of ALDH was previously used to isolate hematopoietic stem cells. Based on that, Ginestier *et al.* (2007) identified another group of tumorigenic breast cancer cells with stem cell-like properties as being ALDH-overexpressing or $ALDH^{+}$[65]. ALDH catalyzes the oxidization of cytotoxic aldehydes to the carboxylic acid, retinoic acid, which initiates the transcription of genes associated with the stemness characteristic of CSCs[64,65]. It has been reported that cell lines capable of producing tumorspheres *in vitro* displayed an upregulation of various ALDH isoforms, which further validates the use of ALDH as a CSC marker and the use of tumorsphere formation assays in CSC analysis *in vitro*[66].

1.3.2 CSC and Metastasis

Despite advances in cancer therapy, metastasis is responsible for over 90% of deaths from solid tumors[67]. Understanding the metastatic process by which CSCs dissociate from the primary tumor site, invade the surrounding tissue, and travel through the bloodstream to a distinct secondary site where they reconstitute the tumor becomes crucial[67,68].

The process implicated in metastasis is known as the epithelial-mesenchymal transition (EMT)[67]. EMT involves the transformation of polarized epithelial-like cells, which rest on the basement

membrane, to mesenchymal-like cells, characterized by increased migration and invasiveness. EMT is normally involved in organ development and embryogenesis, driven by tightly regulated transcription factor action and epithelial cell transformation[69]. However, this program is aggressively used by cancer cells, where the loss of cell-cell contact helps them metastasize. Cells undergoing EMT are therefore distinguished by the decreased expression of cell junction proteins, such as E-cadherin, a transmembrane protein that maintains cell-to-cell adhesion, and the increased expression of transcriptional factors that induce cytoskeleton organization and cell migration[67,69]. Breast cancer cell lines, such as MDA MB-231, that are low in E-cadherin exhibit a mesenchymal phenotype with high tumorigenicity observed *in vivo*[70,71].

A growing body of evidence has suggested that EMT is linked to CSCs, as signaling pathways upregulated in CSCs, such as Hippo/YAP signalling also serve as key regulators of EMT[72]. Moreover, aberrant activation of EMT is associated with mesenchymal CSC enrichment[73,74]. Liu *et al.* (2014) showed that breast CSCs existed in EMT and the reverse, MET states that are characterized by the expression of distinct CSC markers. $CD44^{+}CD24^{-}$ CSCs were found to be present in the invasive outskirts of the tumor and adopted a more mesenchymal or EMT-like phenotype while $ALDH^{+}$ CSCs present at the center of the tumor were found to be more proliferative with epithelial-like propertoes[73]. Of note, CSCs are able to convert between epithelial-like cells and mesenchymal-like cells, making it crucial to target both cell populations to prevent one population reconstitution.

1.3.3 CSC and Chemoresistance

Breast CSCs also contribute to cancer recurrence as they exhibit resistance to chemotherapy and

radiation[75]. There are several mechanisms by which CSCs are thought to be resistant to conventional treatment. The quiescent state of CSCs helps them evade drugs targeting fast-growing cells, the increased drug efflux through the overexpression of ABC transporters, and the upregulation of enzymes, like aldehyde dehydrogenase, that rapidly metabolize the drugs[75,76]. Patient tumor analysis revealed that following chemotherapy treatment, the proportion of ALDH positive cells increased and was associated with a worse prognosis[77]. CSCs also activate DNA damage repair pathways. Recently, it was shown that breast CSCs chemoresistance is driven by the arginine methyltransferase PRMT5 as it regulates DNA repair in response to damage induced by chemotherapy[78].

Pathway activation is another mechanism by which CSC are thought to evade chemotherapy[76]. Signaling pathways such as JAK/STAT3, NF- κB and Wnt/β-catenin are thought to play a significant role in CSC survival and chemo-resistance[52,76,79]. Jia *et al.* (2017) revealed a mechanism by which cytokines produced by TNBC cells after treatment with the chemotherapeutic agent, paclitaxel, activate both NF-κB and Wnt/β-catenin pathways. This in turn further promotes breast cancer cells to produce and secrete cytokines, forming an autocrine inflammatory forward-feedback loop that allows the enrichment of drug-resistant TNBC bulk cells and CSCs[52]. A study by Wang *et al.* (2018) investigated the mechanism by which the JAK/STAT3 pathway, when dysregulated promotes breast CSCs. They found that STAT3 signalling controls CSC lipid metabolism, upregulating fatty acid oxidation and its inhibition re-sensitized cells to chemotherapy[79].

While more research is required to decipher all the mechanisms by which CSCs adopt chemo-

resistant characteristics, preclinical research has increasingly shifted to targeting the CSC population as a way to halt tumor growth and recurrence after chemotherapy.

1.4 The Hippo/YAP pathway: Key Pathway Implicated in TNBC and CSCs

The Hippo signalling pathway is a significant pathway implicated in tumorigenesis and CSC enrichment[80]. Normally, it plays a crucial role in controlling organ size, organism development, cell differentiation, proliferation, and apoptosis. A major downstream effector of this pathway, known as Yes-associated protein (YAP), has been extensively explored as a potential target in cancer therapy[80,81]. YAP functions as a transcription factor along with the transcription factor TEAD, promoting the transcription of genes such as Cyclin D1 (cell cycle progression), CTGF, and Cyr61 (angiogenesis factors)[82,83]. Activation of Hippo signalling, which usually occurs either through mechanical cues or the activation of intersecting pathways, initiates the phosphorylation of YAP by serine/threonine kinases, primarily the LATS1/LATS2 kinase. This phosphorylation of YAP sequesters its function as it leads to its accumulation in the cytoplasm, ubiquitination, and eventual degradation[80–83]. YAP activity has also been found to be controlled by other oncogenic pathways such as Wnt/β-catenin, and PI3K/AKT[84,85].

The overactivation of YAP, either through aberrant dysregulation of the Hippo pathway as a result of mutations in key components or the activation of oncogenic signaling in TNBC, is associated with increased disease aggressiveness, poor clinical outcome, and chemoresistance[20,86,87]. Evidence increasingly points to YAP's role in CSCs, maintenance of a stem-like phenotype, and the EMT process[20,88]. Notably, YAP expression correlated with the metastatic potential of breast cancer, the expression of $CD44^{+}$ $CD24^{-}$ surface marker, and the loss of E-cadherin, which

characterizes EMT[20,82,89]. YAP is known to directly bind and upregulate pluripotent genes, such as the gene expressing Oct4, which helps maintain the CSC phenotypes[90,91]. Studies have previously shown that YAP knockdown reduced the CSC population and that YAP inhibition led to treatment sensitivity in TNBC cells, highlighting the importance of YAP suppression in targeting CSC along with standard therapy[92,93]. Over the past decade, research has shifted into exploring small molecule inhibitors or repurposing existing approved drugs that have shown potential in the inhibition of YAP activity, such as HK24[94], Verteporfin[95], Simvastatin[96], and YZ-6[97], although more work is required to fully understand their mechanism of action, elucidate their effect on CSC enrichment, and their efficacy in combination therapy.

1.5 Angiogenesis in TNBC

Angiogenesis, widely known as the process by which new blood vessels are formed, is crucial to normal physiological processes such as healthy tissue repair, muscle growth, and development[98]. Upon dysregulation, it is a strong driver of solid tumor growth and the metastatic process[98,99]. Angiogenesis begins with the degradation of the vascular basement membrane by endothelial cells upon stimulation, after which these cells migrate and proliferate toward the angiogenic signal, creating new vessels that eventually connect with existing ones. During the first stage of tumor development, tumor growth is avascular, relying on nutrients via passive diffusion. However, as the tumor grows, resources become scarce, resulting in a hypoxic microenvironment[98]. This promotes the release of angiogenic factors such as vascular endothelial growth factor (VEGF), triggering the angiogenic process[98].

Research has highlighted the significance of the angiogenic process in TNBC progression[100,101]. Studies have shown that TNBC tumors exhibited higher levels of VEGF compared to non-TNBC patients and elicited a worse prognosis[100,102]. Hypoxia, the non-physiological reduction in tissue oxygen levels, is a common phenomenon in the tumor microenvironment of most malignant tumors, driving tumorigenesis in part by stimulating angiogenesis to allow the formation of the new blood supply required for rapid tumor growth. Hypoxia is also said to promote tumor escape from immune cell surveillance, conferring resistance to immunotherapy[103]. Additionally, TNBC tumors are known to be hypoxic, which is thought to further explain their aggressive nature and their susceptibility to metastasis and poor outcomes[104]. More specifically, TNBC tumors have been found to overexpress hypoxia-inducible factor 1-alpha (HIF-1 α), a transcription factor that makes up one of the two subunits of HIF-1 and is crucial to the cell's response to hypoxia[105]. HIF-1α in turn, can activate genes involved in the cellular regulation of hypoxia such as, VEGF, as well as genes related to other signaling pathways. In particular, HIF-1α interplays with several key CSC-related pathways such as, Wnt/ β-catenin and NF-κB signaling, playing a major part in the increased expression of pluripotency genes like *SOX2*, *POU5F1,* and *NANOG*[106,107]. This sheds light on the significant role HIF-1α plays in TNBC progression and identifies it as a target to combat the disease. Indeed, studies have found that the inhibition of HIF-1α suppressed TNBC tumor growth and angiogenesis, as well as increased anti-cancer immunity[103,104,108].

1.6 Models in Cancer Research

Cancer models are the cornerstone of cancer research, serving as essential tools to study tumorigenesis and disease progression. These models used in the lab pave the way for clinical

application, making the most successful preclinical screening heavily dependent on the validity and strength of the model used.

1.6.1 Cell-Line Based Models

In vitro cell culture has been the conventional method of analyzing tumor biology, mechanisms, and drug response for decades[109]. Cancer cells are harvested from a primary or metastatic patient tumor and passaged for years, where they can grow indefinitely in culture under *in vitro* conditions, or they can be injected into the mammary fat pads of immunocompromised mice for a cell line based *in vivo* xenograft model used for various analyses.

While *in vitro* cell culturing presents a convenient and cost-effective platform for a multitude of investigations, they have extensive limitations. Culturing cell lines under *in vitro* conditions over an extended period can lead to genetic drift (the random accumulation of mutations over multiple cell divisions) and clonal selection (the dominance of certain traits after the genetic changes in a cell population)[110]. This is particularly true in breast cancer research, where certain commonly used subtypes have a high mutation frequency. Serial passaging would then lead to cells that differ from the starting source, causing more discrepancies and variations across studies, which would poorly replicate the tumor of origin[111]. This is highlighted by a study by Ben-David *et al.* (2018) analyzing the same breast cancer cell line from different sources and finding marked diversity with differences in gene activation profiles, cell morphologies, and proliferation rate[110].

Likewise, *in vivo* cell line-based tumor models, while they can more accurately mimic tumor microenvironment than *in vitro* models, allowing for a better investigation of tumor growth and

metastasis, they present with several drawbacks. These xenografts are derived from single cell lines, and the culturing-induced clonal selection leads to the failed recapitulation of the parent tumor's heterogeneity[112]. Furthermore, the clinical complexity of the metastatic process cannot be accurately investigated using cell line-based xenografts. A study by Liu *et al.* (2019) found that some of the commonly used breast cancer cell lines had little genomic similarities to the transcriptomes of metastatic breast cancer patient samples[113]. Metastasis is heavily influenced by the cell type heterogeneity in a growing tumor as well as the tumor microenvironment. This partially explains why spontaneous metastasis is less frequently seen *in vivo* cell line-based models as compared to actual patient disease course[114,115].

Despite their limitations, the use of cell line-based models remains an important tool in preclinical analysis due to their feasibility, ease of genetic manipulation for mechanistic studies, and cost-effectiveness.

1.6.2 Patient Derived Xenografts (PDX): Clinically Translatable Tumor Models

Patient-derived xenografts (PDX) mouse models have emerged over time as an effective alternative method for preclinical assessment in breast cancer research. This model involves the extraction of breast cancer tissues from human patients and their orthotopic surgical implantation into the mammary fat pads of immunocompromised mice, such as athymic nude mice, severe combined immunodeficiency (SCID) mice, or non-obese diabetic-severe combined immunodeficiency (NOD-SCID) mice. These tumors are allowed to grow and can be further segmented and reimplanted in mice for serial passaging[114].

Unlike cell line-xenografts, PDX models preserve the original patient tumor's organization including its architecture, heterogeneity, vasculature, as well as stromal and extracellular components, conserving as much of the original tumor's biology and microenvironment as possible[114,116]. Research has found that PDX models can replicate *in vivo* patient tumors, and multiple studies have shown a strong correlation between results obtained from PDX experiments and actual patient responses[114,116,117]. Owonikoko *et al*. (2016) analyzed the *in vivo* response of PDX derived from patients in a phase II clinical trial receiving arsenic trioxide. The results showed that the treatment response of *in vivo* PDX-implanted mice corresponded to the patient's response in clinical trial[117,118]. Another study by Roife *et al.* (2016) investigated the use of *ex vivo* tissue cultures obtained from PDX fragments as a predictor of clinical outcomes. The sensitivity of these fragments to chemotherapies was assessed and was found to correlate with clinical responses, highlighting the strength of *ex vivo* fragments in preclinical analysis[118]. These studies suggest that PDX models are more accurate models for tumor metastasis, closely mimicking patients' disease course[119,120]. Orthotopic PDX engraftment can at least in part maintain the tumor's natural microenvironment and molecular features, which is essential in the progression of the disease[119]. As such, the use of PDX models to investigate treatment strategies will facilitate ultimate clinical translation.

1.6.3 Models for Angiogenesis: A Focus on Zebrafish (Danio rerio)

Angiogenesis is typically studied using *in vitro* and *ex vivo* techniques that rely on isolated endothelial cells. While these models are useful in understanding the mechanisms behind the angiogenic process, they are limited as they fall short in factoring in effects in a whole organism[121,122]. Zebrafish (Danio rerio) have increasingly been used as an effective *in vivo* model

of angiogenesis. This has been in part due to the transparency of the zebrafish embryo and how fast development begins post-fertilization, making it easier to handle, more efficient to use for high-throughput screening, as well as more cost-effective. Zebrafish are also easier to genetically manipulate through the microinjection of RNA/DNA material early in their development, allowing for uniform expression[123].

Significantly, comparative studies have demonstrated a high degree of genetic conservation between zebrafish and humans, particularly for angiogenesis and tumorigenesis[124]. This makes zebrafish a reliable model to deepen our understanding of the tumor angiogenic process and to test potential therapies that target angiogenesis and metastasis.

1.7 Overcoming Therapeutic Limitations: Nanoparticles as a Delivery System

1.7.1 Limitations of Conventional Therapy

Despite significant advancements in pre-clinical testing and developments in TNBC therapy using drugs such as chemotherapy, immunotherapy, and small molecule inhibitors, conventional drug success remains limited by several factors. Many anti-cancer drugs have relatively low and poor water solubility as well as low bioavailability, requiring a higher dose administration to achieve therapeutic levels[125,126]. Moreover, the systemic administration means that they can have various off-target effects and could lead to toxicity to other organs[127]. While continuous research explores the development of new, safer small molecule inhibitors against tumorigenesis, many lack an active site, making them undruggable[128]. The current approved drugs are thought to target only 0.05% of the human genome as they interact with less than 700 gene products, limiting our ability to target many key players in cancer progression[129].

1.7.2 Nanoparticles in Drug Delivery

The development of nanoparticles (NPs) in cancer treatment can circumvent these challenges, allowing for an efficient drug delivery system with higher therapeutic index. This is largely due to the drugs' retained blood circulation, decreased off-target toxicity, and higher drug accumulation in the tumor[130–132]. Indeed, NPs as carriers of therapeutic agents displayed favourable pharmacodynamic profiles with a reduction in normal cell toxicity and achieved notable success in pre-clinical testing, and some have been approved for clinical use[132].

While the methods by which NPs accumulate at the tumor site are not yet fully understood, it is thought that this occurs through the enhanced permeability and retention (EPR) effect. The EPR effect is due to pathological characteristics of solid tumors; the abnormal and leaky tumor vasculature with wide fenestration as well as the lack of lymphatic drainage. which allows for the entrapment and accumulation of nanoparticles and macromolecules at tumor sites[133]. Furthermore, NPs can bypass drug resistance barriers such as efflux via P-glycoprotein, allowing for a higher accumulation of drugs inside the tumor cells[134].

Over the years, many different nanoformulations were developed carrying various anti-cancer agents, with the most prominent ones including albumin NPs, antibody–drug conjugate (ADC), liposomes, and polymer-based NPs[135]. Clinical studies have found that nab-paclitaxel, a nanoparticle albumin-bound paclitaxel, led to better outcomes, a higher pCR, and invasive disease-free survival in TNBC patients than paclitaxel alone, showcasing the significance of NP use in TNBC treatment[132,136,137]. A phase III clinical trial designed to assess the efficacy of Genexol-PM,

a lyophilized polymeric micellar formulation of paclitaxel, compared to standard therapy in breast cancer patients found that Genexol-PM led to an improved overall response rate, with manageable toxicity[138]. Another phase III trial investigated sacituzumab govitecan, an antibody–drug conjugate consisting of an antibody against the cell surface antigen, human trophoblast cell-surface antigen 2, and attached to a small molecule inhibitor targeting topoisomerase I, resulting in tumor-specific cell death. Patients receiving sacituzumab govitecan demonstrated better overall survival than those receiving standard chemotherapeutic treatment[139].

Recent discoveries have also revealed the synergic efficacy of such ADCs in delivering the cytotoxic payloads to antigen-expressing tumor cells, where they not only induce tumor cell death but also trigger immunogenic cell death (ICD). This process enhances immune cell infiltration and is thought to potentiate response to immune checkpoint inhibitors (ICIs), monoclonal antibodies that block inhibitory immune checkpoints and amplify the anti-tumor response[140,141]. Notably, preliminary results from a Phase III trial showed that patients treated with sacituzumab govitecan combined with the PD-1 inhibitor pembrolizumab achieved superior PFS compared to those receiving pembrolizumab along with standard treatment[142]. While these early clinical findings underscore the promise of combining ADCs with ICIs, concerns about increased toxicity remain significant and necessitate vigilant monitoring[143].

More recent preclinical research explored the use of NPs encapsulating emerging anti-cancer agents and small molecule inhibitors for potential TNBC treatment. Kumari *et al*. (2021), developed a polymeric NP system to target TNBC encapsulating curcumin, a natural product used in traditional medicine, showcasing its apoptotic potential *in vitro*[144]. Mukhopadhyay *et*

al. (2020) investigated the co-encapsulation of curcumin and gemcitabine using a polymeric NP system and found an increase in P-glycoprotein suppression and apoptosis *in vitro* as well as a higher therapeutic efficacy *in vivo* than single-drug NP[145]. However, research on NP systems co-encapsulating a combination of different therapies and small molecule inhibitors remains scarce, particularly in TNBC.

1.7.3 RNA-Based Therapeutics.

RNA-based therapeutics have emerged as a powerful approach to treatment in cancer research. RNA agents, such as short interfering RNA (siRNA) and microRNA (miRNAs), can effectively and specifically suppress genes that encode proteins involved in tumor cell proliferation, invasion, drug resistance, and metastasis, while messenger RNA (mRNA) can induce expression of genes countering tumor growth and immune evasion[146]. Moreover, these RNA-agents can knock down target genes/proteins that are ineffectively targeted using a classical drug or small molecule inhibitor, helping to overcome a major hurdle in cancer treatment[146,147].

RNA interference (RNAi) is a multi-step biological mechanism by which siRNA or miRNA exert their effect (Figure 1.3). The first step involves the processing of the exogenous agent by the RNase II enzymes, Dicer and Drosha, into a siRNA, which are short, double-stranded RNA with a distinct structure[148]. The siRNA is then incorporated into other proteins and loaded into the effector complex; RNA-induced silencing complex (RISC). Within RISC, siRNA is then unwound, the single-stranded siRNA is exposed, and the less stable antisense strand remains part of RISC while the sense strand is degraded. The RISC complex, along with the siRNA strand, then scans the target complementary mRNA and binds to it to induce mRNA cleavage and degradation[147,148].

miRNA is an endogenous single-stranded small non-coding RNA. Like siRNA, it also exerts its gene expression suppression through RNAi, involving several processing steps before the incorporation into RISC and the degradation (or repression, depending on the level of base pair complementarity) of mRNA[149]. However, miRNA is less specific than siRNA as they regulate gene expression via imperfect base pairing, while siRNA is specific to its target[149]. This specificity makes siRNA a useful agent in the targeting of oncogenes to halt tumor development and progression. Research has also explored the use of siRNA alongside chemotherapy to reverse chemoresistance. Donmez & Gunduz (2011) found that using siRNA agents targeting multidrug protein 1 mRNA (whose product is P-glycoprotein, an efflux pump in multidrug resistance) resulted in 70% re-sensitization to doxorubicin in breast cancer cells *in vitro*.[150] This exemplifies how direct and specific targeting can address conventional therapy shortcomings and the longstanding issues in TNBC resistance and recurrence.

More recently, mRNA-based therapeutics have been introduced for their potential to specifically interfere with the oncogenic process through the expression of tumor suppressor genes such as p53 or PTEN, or the expression of tumor antigens to trigger anti-tumor T cell or B cell responses[151,152]. mRNA can also encode cytokines, immunomodulatory proteins, or chimeric antigen receptors (CARs) to improve the anti-cancer immune response and inhibit tumor growth[152]. While RNA-based agents are relatively simple, they come with limitations that must be overcome to achieve clinical therapeutic potential.

In particular, RNA-based agents are hydrophilic, with a large molecular weight and a negative charge, hindering their ability to passively cross cell membranes. Furthermore, their entrapment within endosomes during endocytosis means that most of the siRNA delivered cannot reach the cytoplasm. Lastly, they are highly susceptible to degradation by nucleases in the bloodstream and circulating immune cells[153]. Therefore, RNAi agents need to be protected, ensuring effective delivery and accumulation at the tumor sites instead of other vital organs, to reduce undesired side effects.

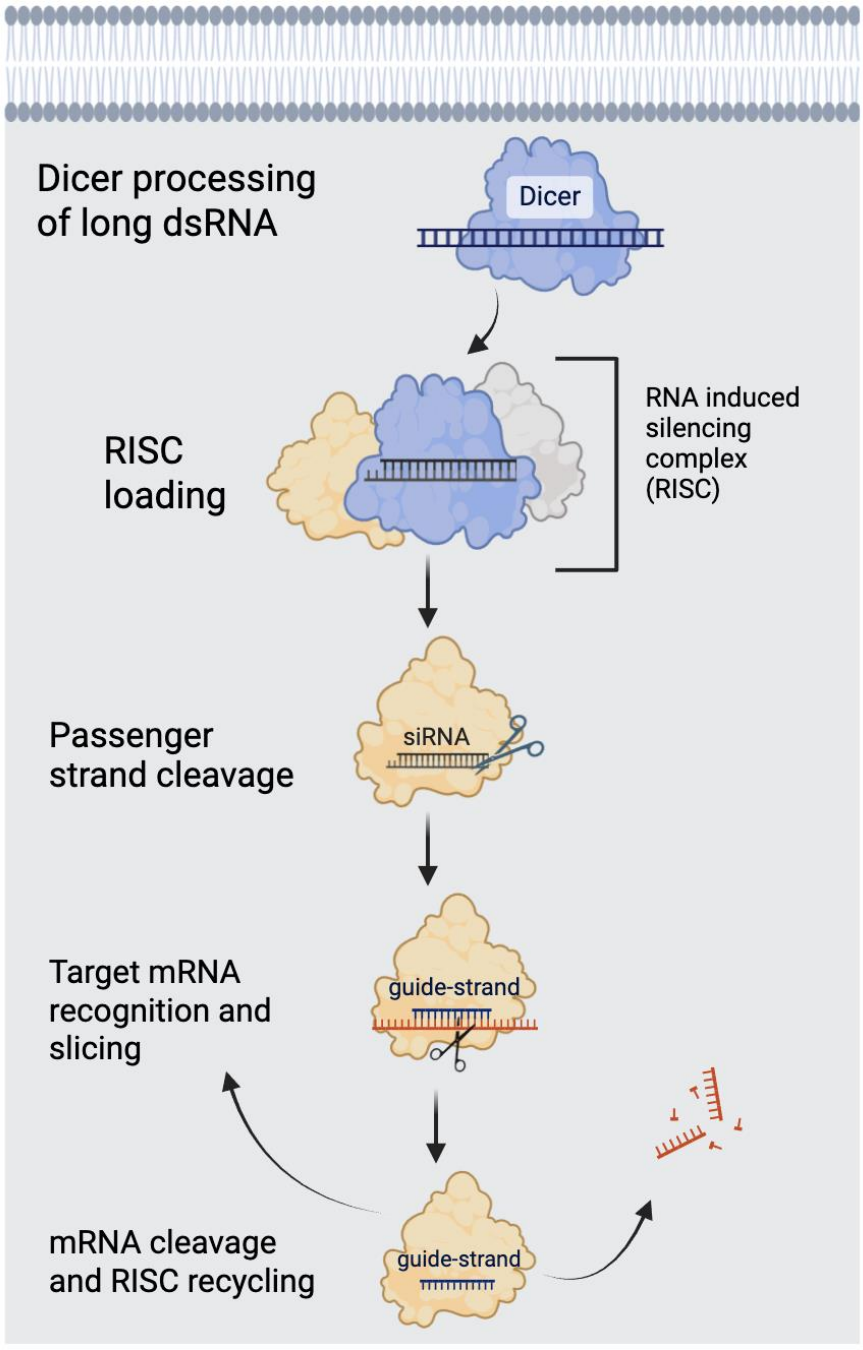

Figure 1.3. RNA interference mechanism for gene silencing. siRNA mediated silencing occurs through the processing of long double stranded RNA, RISC loading and strand cleavage, and the eventual target mRNA binding and degradation. Figure adapted from Dana, H., *et al*. (2017). "Molecular mechanisms and biological functions of siRNA." *International journal of biomedical science: IJBS*, *13*(2), 48[154] Permission conveyed through Creative Commons Attribution 2.5 Generic License. (Creative Commons — Attribution- 2.5 Generic— CC BY 2.5) https://creativecommons.org/licenses/by/2.5/. Figure recreated using Biorender.com.

1.7.4 Nanoparticles in the Delivery of RNA-based therapeutics

To overcome the limitation of conventional therapy and the inherent instability of RNA, nanomedicine has evolved to incorporate RNA-based agents for gene expression modulation through encapsulation and targeted delivery. NP-based RNAi delivery systems have shown great potential as they are capable of encapsulating high amounts of RNAi agents, increasing their uptake by tumor cells to safely deliver the gene silencing agents into the cytoplasm[146,151]. These NP delivery vehicles can also improve the pharmacological profiles by protecting RNAi from serum nucleases and renal filtration achieving higher tumor concentrations. NP-RNAi agents have recently been approved for clinical usage, opening a new treatment avenue[155].

Recent research explored the use of siRNA-NP therapy in TNBC, showing some promising preclinical results. A study by Wan *et al.* (2021) developed a polymeric NP system with siRNA targeting epidermal growth factor receptor and bromodomain-containing protein 4, both known to be oncogenic regulators. They found that siRNA-NP treatment reduced tumor growth *in vivo,* as well as the expression of various key players in TNBC tumorigenesis using a cancer cell line-based model[156]. More recently, Yin *et al.* (2025) constructed lipid-based NPs for the co-delivery of chemotherapeutic agent, docetaxel, and siRNA to target receptor tyrosine kinase-like orphan receptor 1. This co-delivery was able to reduce tumor burden *in vivo* more significantly than single-agent treatment while also increasing immune cell infiltration in a cancer cell line-based model system[157]. Other work designed a nanoformulation consisting of the tumor suppressor miR-200c, which was found to inhibit metastasis-related genes and was effective at halting tumor growth[158].

These studies and others underscore the efficacy of RNA agents' delivery to the tumor site and their potential for specific gene silencing[155–159].

Studies have also investigated the use of mRNA - NPs to combat TNBC by the upregulation of tumor suppressor genes. Researchers developed an NP platform consisting of paclitaxel with p53 mRNA NP, and results showed a greater efficacy than nab-paclitaxel, with a reduction in tumor growth and a significant increase in mice survival *in vivo*[160]. However, to date, research has largely used mouse and/or human-based cell lines, which could lead to discrepancies in the clinical translation of these results. The delivery of RNA-based agents in a clinically translatable PDX model has yet to be achieved.

CHAPTER 2: A TRIPLE-DRUG NANO-THERAPY TO TARGET BREAST CANCER CELLS, CANCER STEM CELLS, AND TUMOR VASCULATURE

2.1 Preface

This chapter contains original research showing the development of a triple-drug nano-therapy to target multiple aspects of tumorigenesis in TNBC. This research was published in Cell Death & Disease.[161]

El-Sahli, S., Hua, K., Sulaiman, A., Chambers, J., Li, L., Farah, E., McGarry, S., Liu, D., Zheng, P., Lee, S.H., Cui, J., Ekker, M., Cote, M., Alain, T., Li, X., D'Costa, V.M., Wang, L.,* & Gadde, S.* (2021). A triple-drug nanotherapy to target breast cancer cells, cancer stem cells, and tumor vasculature. *Cell death & disease*, *12*(1), 8.

Author Contributions:

LW, SG and SE conceived and planned the study. All authors were involved in data collection, analysis, and final editing.

2.2 Abstract

Triple-negative breast cancer (TNBC) is the most aggressive subtype of breast cancer, accounting for the majority of breast cancer-related death. Due to the lack of specific therapeutic targets, chemotherapeutic agents (e.g., paclitaxel) remain the mainstay of systemic treatment, but enrich a subpopulation of cells with tumor-initiating capacity and stem-like characteristics called cancer stem cells (CSCs); thus development of a new and effective strategy for TNBC treatment is an unmet medical need. Cancer nanomedicine has transformed the landscape of cancer drug development, allowing for a high therapeutic index. In this study, we developed a new therapy by co-encapsulating clinically approved drugs, such as paclitaxel, verteporfin, and combretastatin (CA4) in polymer-lipid hybrid nanoparticles (NPs) made of FDA-approved biomaterials. Verteporfin is a drug used in the treatment of macular degeneration and has recently been found to inhibit the Hippo/YAP (Yes-associated protein) pathway, which is known to promote the progression of breast cancer and the development of CSCs. CA4 is a vascular disrupting agent and has been tested in phase II/III of clinical trials. We found that our new three drug-NP not only effectively inhibited TNBC cell viability and cell migration, but also significantly diminished paclitaxel-induced and/or CA4-induced CSC enrichment in TNBC cells, partially through inhibiting the upregulated Hippo/YAP signaling. Combination of verteporfin and CA4 was also more effective in suppressing angiogenesis in an *in vivo* zebrafish model than single drug alone. The efficacy and application potential of our triple drug-NPs were further assessed by using clinically relevant patient-derived xenograft (PDX) models. Triple drug-NP effectively inhibited the viability of PDX organotypic slide cultures *ex vivo* and stopped the growth of PDX tumors *in vivo*. This study developed an approach capable of simultaneously inhibiting bulk cancer cells, CSCs, and angiogenesis.

2.3 Introduction

Breast cancer is the most common cancer among women and the second leading cause of cancer-related death in women[162]. Triple-negative breast cancer (TNBC), a subset of breast cancer, accounts for the majority of breast cancer death due to the lack of specific treatment targets, as TNBC does not express estrogen receptor, progesterone receptor, and human epidermal growth factor receptor-2[163]. As such, chemotherapeutic agents (e.g., paclitaxel) remain the current first-line therapy for the patients with TNBC. While chemotherapeutic drugs effectively kill bulk cancer cells, ample evidence has demonstrated that chemotherapy enriches a subpopulation of cells known as cancer stem cells (CSCs), capable of initiating new tumors[164]. Breast CSCs are known to resist treatments and are key to cancer progression, recurrence, and metastasis4. Indeed, multiple reports have revealed the enrichment of CSCs in TNBC cell lines and associate it with the aggressive nature of TNBC[165,166].

The Hippo signaling pathway is implicated in tumorigenesis and CSC enrichment. Its major downstream effector, Yes-associated protein (YAP), is known to play a significant role in the maintenance of a stem-like phenotype[81]. Furthermore, YAP expression correlates with the metastatic potential of breast cancer and is a well-known driver in CSCs[81]. Verteporfin, an FDA-approved drug used in the treatment of macular degeneration, was found to inhibit cancer cell proliferation by inducing the cytoplasmic sequestration of YAP[167].

Tumor growth and metastasis is also dependent on angiogenesis, the process by which new blood vessels are generated from existing ones[168]. The vascular disrupting agent, combretastatin A4 (CA4) is currently in phase II/III clinical trials and has been shown to be an effective

antiangiogenesis agent[169]. In addition, CA4 is a tubulin binding chemotherapeutic agent and is shown to suppress a variety of cancers[169,170]. However, the effect of CA4 on CSC remains poorly explored. Given that TNBC aggression is a multifaceted process without specific targets, we sought to develop a new therapeutic strategy capable of simultaneously inhibiting bulk tumor cells, CSCs, and angiogenesis by the combination of paclitaxel, verteporfin, and CA4.

While combinational therapies have several advantages, dissimilar pharmacokinetics and off-target toxicities arising from the drug combinations hamper potential clinical application[171]. To reduce free drug toxicity, improve their pharmacokinetics, and induce an overlap in pharmacological profiles of the drugs, we employed a nanomedicine-based multidrug delivery platform[172]. Nanomedicine in cancer treatment has allowed for a better drug delivery with higher therapeutic index by virtue of features, such as improved circulation in blood, reduced off-target toxicity, and higher drug accumulation in the tumor[172,173]. This is thought to occur through the enhanced permeability and retention (EPR) effect, where molecules exceeding a certain size accumulate in tumor tissue due to the aberrant blood vasculature and the lack of lymphatic drainage within the tumor[174].

Clinical translation of therapeutics tested *in vivo* is often limited by the use of cell line-based tumor models due to their artificial nature, which has created a gap between preclinical and clinical research[114]. Patient-derived xenograft (PDX) tumors, obtained from the patients and surgically implanted in mice, are capable of simulating *in vivo* patient tumors and display a strong retrospective correlation with actual patient responses[114,175]. In this study, we use an *ex vivo* and *in*

vivo PDX tumor models that retain original tumor architecture, composition, vasculature, and heterogeneity in addition to *in vitro* TNBC cell line and *in vivo* zebrafish model.

We showed that paclitaxel and CA4 inhibited the viability of bulk TNBC cells, while enriching CSCs and upregulating oncogenic YAP signal, both of which can be effectively counteracted by verteporfin. As a result, triple drug-nanoparticle (NP) not only inhibited bulk TNBC cell viability, cell migration, but also suppressed CSC enrichment. Using an *in vivo* zebrafish model, we found that combination of CA4 and verteporfin more effectively abrogated angiogenesis than single drug alone. Furthermore, triple drug-NP effectively inhibited viability of PDX organotypic cultures *ex vivo* and disrupted the growth of TNBC PDX tumors *in vivo*. Given that the drugs and nanomaterials used in this report have been proved safe and employed in the clinic, this new nanomedicine-based approach tested in clinically relevant PDX models may lead to an effective treatment for TNBC patients.

2.4 Materials and Methods

2.4.1 Nanoparticles synthesis and characterization

Lipid-polymer hybrid nanoparticles (NPs) were made through a nanoprecipitation method as previously reported[176]. Lecithin and DSPE-PEG_{2K} in the molar ratio of 6.5:1 were dissolved in 4% ethanol aqueous solution (0.02% w/v) and heated for 2 mins at 68 ^{o}C while maintaining gently stirring. PLGA (poly lactic co-glycolic acid) and the selected drug/drugs (10:1 w/w ratio) in either acetonitrile (ACN) were then added dropwise at 0.6ml/min rate while stirring at room temperature to allow the formation of self-assembled hybrid NPs. After 6 hours of stirring, NPs were concentrated and purified by centrifugal filters and characterized for size, surface charge and

structure by ZetaView, Malvern Zetasizer (DLS) and TEM. To test the stability of NPs in biologically relevant conditions, NPs were incubated in 5% FBS for 4 hours and size was measured using ZetaView.

2.4.2 Assessment of drug release of paclitaxel, verteporfin and combretastatin in 72 hours

The amounts of paclitaxel and combretastatin remaining in the NPs at different time points were assessed using HPLC at 204 nm, with H_2O:acetonitrile mobile phase and with 5%–90% acetonitrile gradient. The amount of verteporfin remaining in the NPs at the different time points was quantified using NanoDrop at 430 nm absorbance. The amounts of drugs calculated were then expressed as percentage of drug released from the NPs.

2.4.3 Cell culture

MDA-MB-231 cell line was purchased from the American Type Culture Collection (Manassas, VA, USA). MDA-MB-231 cells were transfected with pLVX-Tet-On Advanced and pLVX-Tight-Puro MDA-MB-231 cells overexpressing E-cadherin were generated using pLVX-Tight-Puro containing an E-cadherin gene insert according to manufacturer's instructions (Clontech, Mountain View, California, United States). MDA-MB-231 cells without overexpression of E-cadherin (control) were generated using an empty vector of pLVX-Tight-Puro. Stable clones were selected after 3 days using G418 (Clontech) and puromycin dihydrochloride (Thermo Fisher) at a concentration of 1000 µg/mL and 1 µg/mL respectively for 14 days. For maintenance, 250 µg/mL of G418 and 0.25 µg/mL of puromycin were added in the culture medium. E-cadherin expression was activated by adding 1 µg/mL doxycycline hydrochloride (Thermo Fisher) to the cell culture every 2-3 days. E-cadherin levels were examined following RNA extraction by RT-qPCR and

protein levels by western blotting. MDA-MB-231 cells were grown in DMEM-F12 media that contained 10% fetal bovine serum (HyClone, Logan, UT, USA) and 1% penicillin/streptomycin. For the tumorspheres formation assays, E-cadherin high MD-MB-231 cells were seeded in low attachment plates and cultured in serum-free conditions (DMEM/F12 medium containing 1mM sodium pyruvate, 1×B27, 20 ng/mL bFGF and 20 ng/mL EGF).

SUM149 breast cancer cells were obtained from Asterand (Detroit, MI, USA) and cultured in Hams F-12 media (Mediatech, Manassas, VA, USA) containing 5% FBS, 5 µg/ml insulin, 1 µg/ml hydrocortisone, 10 mM HEPES and 1% penicillin/streptomycin. Cells were cultured at 37°C in a 5% CO2 incubator. Insulin, Hydrocortisone, HEPES, and bovine serum albumin were purchased from Sigma-Aldrich (St. Louis, MO, USA).

MCF10A cells (an immortalized, non-transformed epithelial cell line derived from human mammary tissue) were obtained from ATCC. They were cultured in DMEM:F12 (1:1) medium supplemented with 1× antibiotics (penicillin and streptomycin), EGF (10 ng/mL), insulin (10 µg/mL), cholera toxin (1 µg/mL), hydrocortisone (1 µg/mL), and heat-inactivated horse serum (5%) (Invitrogen). All cell lines were incubated at 37 °C in a humidified 5% CO_2 atmosphere. All cell lines used have been recently ruled out for mycoplasma contamination using RT-qPCR.

2.4.4 Cell viability assay

MTT stock was diluted in PBS to make 5 mg/mL, aliquoted and stored in -20 °C. Cells were seeded into a 24 well plate (1.5 x 10^3 cells per well) and treated for 120 hours (unless otherwise stated). MTT was then added to the media in a 1:20 ratio and incubated for 3 hours at 37 °C. Reaction was

terminated by aspirating the media and adding 600 µL DMSO to each well. The wells were incubated for 20 min at 37 °C. Triplicates from each well/treatment were aliquoted into a 96 well plate and absorbance at 570 nm was measured using Gen 3.0. Alamar blue assay was performed according to the manufactures' instructions (Thermo Fisher, Waltham, Massachusetts, United States).

2.4.5 Cell migration assay

MDA-MB 231 cells were seeded in 6-well plates and grown to confluence; they were then scratched with a sterile pipette tip, washed with PBS to remove detached cells and debris, and then incubated with 2% mitomycin for 4 hours and then washed with PBS. Cells were then incubated with various treatments for 48 hrs. The scratch was then photographed at different time points using a Zeiss Axiovert 40 CFL microscope (Carl Zeiss AG, Feldbach, Switzerland). The open area was quantified on each photo to obtain a diameter and normalized to that of 0 hours.

2.4.6 Luciferase Assay to assess HIF-1α activity

MDA-MB-231 TNBC cells were seeded into 12-well plates and transfected with 1000 ng of HRE-luciferase (HIF-1α, Plasmid #26731, a gift from Dr. Navdeep Chandel[177]) construct in conjunction with 1000 ng Renilla pRL-SV40P (Addgene Plasmid #27163, a gift from Dr. Ron Prywes[178]) construct using Lipofectamine 3000 (Invitrogen, Carlsbad, California, United States) according to the manufacturer's instructions. After 18 hours, cells were treated with control and different drugs as described in the Figure legends for 24 hours, after which cells were lysed and both Firefly and Renilla luciferase activities were quantified using a Dual-Luciferase® Reporter Assay System (Promega, Madison, Wisconsin, United States) following the manufacturer's instructions.

2.4.7 Flow cytometry analysis

Dissociated cancer cells were filtered through a 4 μm strainer and suspended in PBS supplemented with 2% FBS and 2 mM EDTA (FACS buffer). One μL of mouse IgG (1 mg/mL) was added and incubated at 4 °C for 10 minutes. The cells were then re-suspended in 1× binding buffer and anti-CD44 (APC) in combination with anti-CD24 (PE) antibodies (BD, Mississauga, ON, Canada) according to the manufacturer's instructions for 30 min. The cells were washed twice with FACS buffer and 7-aminoactinomycin D (7-AAD, eBioscience, San Diego, CA) and Annexin-V/V450 (BD) was added and incubated for 15 minutes at room temperature to assess dead and apoptotic cells. Flow cytometry was performed on the BD LSRFortessa. Data were analyzed with FlowJo software (Ashland, OR, USA).

2.4.8 RT-qPCR

To assess mRNA levels, total RNA was extracted from the frozen pellets of MDA MB- 231 using the RNeasy mini kit (Qiagen, Germantown, MD, USA). Nanodrop 1000 (Thermo Fisher) was used to determine mRNA concentration and purity. cDNA was obtained from the mRNA using iScript cDNA Synthesis Kit (Bio-Rad, Hercules, California, United States) and GeneAmp PCR System 2700 (R&D Systems, Minneapolis, Minnesota, United States). Gene expression levels were determined through quantitative real-time PCR (qPCR) analysis using the Bio-Rad MyiQ (Bio-Rad, USA). Reaction mix per well constituted 37.5% RNAase-free H_2O, 50% SyBr Green (Bio-Rad, USA), 2.5% cDNA and 5% forward and reverse primers of the gene of interest. Reaction conditions were 1 cycle at 95 °C for 20 seconds, 45 cycles at 95 °C for 3 seconds, and 60 °C for 30 seconds. Data obtained were normalized using the housekeeping gene, 18S or GAPDH and

relative fold changes of gene expression were calculated via the ^{2DD}CT method and determined by comparing it to the appropriate controls. Table S1 contains the primer sequences used.

2.4.9 Zebrafish treatment and visualization

Animal care and handling: all zebrafish husbandry and experimental procedures used in the experiments were compliance with University of Ottawa Animal Care Committee following guidelines of the Canadian Council on Animal Care. Transgenic line Tg(*fli*:eGFP) was used for this study and maintained at 28.5^{0}C, unless stated otherwise and staged as described earlier[179].

For *in vivo* zebrafish drug treatment, transgenic Tg(fli:eGFP) embryos were dechorionated at 6 hours-post-fertilization (hpf) using 10 mg/mL Pronase (Sigma-Aldrich) and treated with paclitaxel, verteporfin, combretastatin or various combinations at a final concentration of 5 nM, 250 nM and 5 nM respectively at 8 hpf in 6-well plates with 10 embryos per well and incubated at room temperature in the dark for 48 hours. Solutions were refreshed daily.

2.4.10 Zebrafish RT-qPCR

RNA was extracted from pools of 5 whole zebrafish larvae following drug treatment using pestle for homogenization in TRIzol reagent (Invitrogen, Carlsbad, California, United States) following manufacturer protocol. Integrity of RNA was checked by gel electrophoresis, and purity of RNA was determined using the NanoDrop 1000 Spectrophotometer (Thermo Fisher, Waltham, Massachusetts, United States). Only samples with clear 28S and 18S rRNA bands at an approximate intensity ratio of 2:1 and an A260/280 absorbance ratio of 1.8-2.1 were used for cDNA synthesis using the iScript™ Reverse Transcription Supermix for RT-qPCR kit (Bio-Rad) according to the manufacturer protocol. For all genes, standard 10 µL RT-qPCR reactions were

assembled as follows: 5 µl of SsoFast™ EvaGreen® Supermix (Bio-Rad), 0.4 µl of forward primer (10 µM), 0.4 µl of reverse primer (10µM), 4 µl of template cDNA and 0.2 µl of nuclease-free water. For no template negative controls, template cDNA was replaced by nuclease-free water. All reactions were carried out in triplicate using the Bio-Rad CFX96 system. The PCR conditions were 95 ºC for 30 seconds, followed by 40 cycles of 95 ºC for 5 seconds and 59 ºC for 5 seconds. Normalized gene expression values were determined using the comparative Cq method and each gene was normalized against three reference genes, *elongation factor 1 alpha* (*ef1α*), *ribosomal protein l13a* (*rpl13a*), and *tyrosine 3-monooxygenase/tryptophan 5-monooxygenase activation protein, zeta polypeptide* (*ywhaz*). All the primers are listed in Table S2.

2.4.11 Treatment of TNBC MDA-MB-231 tumors growing in mice

All mouse studies illustrated in this paper were performed according to the ethical guidelines set by the University of Ottawa and in pathogen free conditions. Athymic nude mice were obtained from Charles River Laboratories (Senneville, QC, Canada). The MDA-MB-231 breast cancer cells were mixed 1:1 with Matrigel and injected under aseptic conditions into the mammary fat pads (n = 5 for each group, 2×10^6 cells per fat pad). When the tumor reached a mean diameter of ~3 mm, mice were injected with empty–nanoparticles, free drugs or same concentrations of drugs-encapsulated in nanoparticles *via* tail vein every 2-day.

2.4.12 Assessment of *ex vivo* viability of PDX organotypic slice cultures and *in vivo* tumor growth of PDX transplants after treatments

All protocols described throughout this manuscript regarding animal studies were performed in strict pathogen-free conditions and in accordance with guidelines approved by the Animal Care

Committee at the University of Ottawa. TNBC PDX HCI-002 tumor chunks (2 mm x 4 mm) were transplanted into the mammary fat pad of athymic nude mice (Charles River Laboratories, Senneville, Quebec, Canada). PDX HCI-001 and HCI-002 tumors were originally generated from two patients with TNBC. They have been well characterized, including tumor histology/immunohistology, clinical markers, drug treatment and response, whole exome sequencing, RNA sequencing, RPPA analysis, and growth curve, which have been described in details in the spreadsheet of PDXNet and in the supplemental results published elsewhere[180].

For the *ex vivo* organotypic slice culture experiment, HCI-001 tumors were harvested and fragmented into a 48 well plate. Alamar blue viability assay was preformed *via* incubation with 4% Alamar blue solution (Thermo Fisher Scientific, Waltham, MA, USA) for 4 hours after which florescence at 560 nm excitation and 590 nm emission was determined to measure baseline viability. Drugs-NPs were then incubated with tumor fragments for 120 hrs and Alamar blue viability assay was conducted again and calculated by subtracting the values of baseline viability in each group, followed by comparison amongst different groups.

For *in vivo* transplantation and treatment, HCI-002 PDX tumors were passaged twice in athymic nude mice without treatment. Treatment began when the tumors grew to a mean diameter of 3 mm. Mice were randomized into 2 cohorts and treated with either vehicle (empty nanoparticles) or lipid-polymer hybrid nanoparticles co-encapsulating paclitaxel, combretastatin and verteporfin (PVC-NP) every 2 days for 20 days (n=3 mice/group). Tumor growth was measured consistently using a caliper and tumor volume was determined using the formula: $V=1/2(\text{Tumor Length} \times \text{Tumor Width}^2)$.

2.4.13 Statistical analysis

Data are represented as means +/- standard deviation (SD) or standard error (SE) without data transformation. For relative comparison, the data were normalized to control group and then compared as indicated in each figure. Statistical tests were performed using Functions of MS Excel Variances. Data distribution was tested by one-way analysis of variance (ANOVA). Wherever appropriate, statistical differences between groups were assessed by unpaired Student's two tailed t-test (comparison of two groups) and reported as * for $p < 0.05$, ** for $p < 0.01$, *** for $p < 0.001$, and **** for $p < 0.0001$. Unless otherwise stated, experiments have a minimum of three biological repeats.

2.5 Results

2.5.1 Nanoparticle synthesis and characterization

Lipid-polymer hybrid NP were synthesized using FDA-approved, biodegradable, and biocompatible poly (lactic-co-glycolic acid) (PLGA), polyethylene glycol (PEG) polymers, and encapsulated with single drug or triple drugs (paclitaxel, verteporfin, and CA4). All formulations of drug-NPs had a spherical morphology with surface charge of −5 to −50 mV and an average range of 100–150 nm in size. All NPs were incubated with fetal bovine serum (FBS) to assess stability; NP sizes were then measured and found to be stable in serum (Figure S2.1A-E). The release rates of three drugs from the encapsulated NPs were also assessed (Figure S2.2).

2.5.2 Combination of verteporfin-NP, paclitaxel-NP, and/or combretastatin-NP suppressed both bulk TNBC cells and cancer stem cells

A viability assay was conducted to determine the effect of drugs-NP on TNBC MDA-MB-231 bulk cells *in vitro*. Results showed that paclitaxel-NP and CA4-NP in combination was more significant in decreasing bulk cell viability than each drug-NP alone, while verteporfin-NP exhibited minimal effect on bulk cells (Figure 2.1A). The combination of the three drug-NP treatment also inhibited TNBC cell viability of the SUM149 cell line (Figure S2.3).

Since breast CSCs are known to be key in cancer progression, metastasis, and recurrence[73,166], targeting the CSC population with tumor-initiating capacity has been considered an effective strategy for successful treatment. To determine the effect of the NP-encapsulated drug treatment on CSCs, we carried out an *in vitro* tumorsphere assay, which is a method used commonly in cancer research to assess the function of CSCs in a 3D suspension culture[181]. Epithelial-like MDA-MB-231 cells (overexpressing E-cadherin) were grown in non-adherent and serum-free conditions, in which only CSC-like cells could survive and grow[181]. NP encapsulating drugs were then added to the cultures. After incubation for 120 hrs, tumorspheres were photographed and viability was assessed to determine CSC enrichment after different treatments. While paclitaxel-NP and CA4-NP inhibited bulk TNBC cells, they either enhanced CSC enrichment or did not exhibit inhibitory effects on CSCs (Figure 2.1B, C). In contrast, although verteporfin-NP did not significantly inhibit viability of bulk TNBC cells, it markedly suppressed CSCs. Furthermore, verteporfin-NP in combination with paclitaxel-NP and/or CA4-NP significantly suppressed both bulk cells and CSCs (Figure 2.1A-C). Consistently, flow cytometric analysis showed that the frequencies of apoptotic CSCs ($CD44^+$ $CD24^-$ Annexin-V^+ $7AAD^-$) in TNBC cells were significantly increased after

treatment with verteporfin alone or verteporfin in combination with paclitaxel and CA4. In contrast, paclitaxel and/or CA4 treatments did not show significant changes (Figure S2.4).

These data suggest that three drug-NPs in combination not only suppress TNBC bulk tumor cells, but also inhibit CSCs, which cannot be achieved by either paclitaxel-NP nor CA4-NP alone. Verteporfin was essential to suppress the CSC enrichment and as such, the combination of three drug-NPs is required to suppress both bulk and CSCs for the development of an effective treatment for TNBC.

To evaluate the *in vitro* toxicity, non-transformed epithelial mammary cells (MCF-10A) were treated with P-NP, C-NP, V-NP, and different combinations. While drug-NPs significantly reduced cancer cell viability (Figure 2.1A), they exhibited little effect on these non-transformed epithelial mammary cells (Figure S2.5A).

2.5.3 Verteporfin-NP effectively inhibits the migration of TNBC cells *in vitro*

Since cell migration has been attributed to cancer metastasis[182,183], we assessed the effect of drug-NPs in combination on TNBC cell migration. An *in vitro* scratch assay was performed where TNBC MDA-MB-231 cells were exposed to mitomycin to stop cell proliferation, followed by a scratch. While verteporfin-NP was inadequate at inhibiting the viability of TNBC bulk cells (as shown in Figure 2.1A), it effectively halted cell migration approximately two-fold greater than empty-NP control after a 48-hr treatment (Figure 2.2A, B). Moreover, the three drug-NPs in combination suppressed migration effectively, highlighting the efficacy of verteporfin-NP and the

three drug-NPs in halting the migration of TNBC cells in addition to promoting CSC apoptosis (shown in Figure S2.4).

2.5.4 Verteporfin-NP fully suppresses YAP target genes upregulated by paclitaxel-NP and/or combretastatin-NP

Of the many signaling pathways, YAP has recently been identified as an oncogene in several cancers, including TNBC[184], and is closely associated with CSCs and poor prognosis in cancer patients[185]. Since paclitaxel-NP and CA4-NP treatment enriched CSCs, we asked whether the YAP signaling pathway was upregulated after treatment with these two drugs, and whether V-NP could abolish their upregulation of YAP activity. We assessed the effect of single drug-NP, and double or triple drug-NPs in different combinations on CSC-associated YAP target genes using RT-qPCR. While paclitaxel-NP and CA4-NP upregulated key YAP target genes, verteporfin-NP downregulated them. Importantly, triple drug-NPs in combination was able to suppress the YAP target genes upregulated by paclitaxel-NP and CA4-NP (Figure 2.2C, D). These results suggest that suppression of YAP signal by verteporfin-NP in the triple drug-NP combination may contribute to the CSC inhibition (i.e., suppressing tumorsphere formation and promoting CSC apoptosis) as shown in Figure 2.1 and Figure S2.4.

2.5.5 Drug combination effectively inhibits angiogenesis in an *in vivo* zebrafish model

We further determined the effect of drug combinations on angiogenesis, the process by which new blood vessels are generated from the existing ones to promote tumorigenesis and tumor metastasis[168]. The zebrafish embryo model is the most effective way to study *in vivo* angiogenesis and is considered to be comparable to angiogenesis occurring in the clinic[186]. We used a transgenic

fluorescent zebrafish, Tg(fli-GFP), which has GFP-expressing endothelial cells (lining the inside of blood vessel in the body) under the control of fli1 promoter to allow the visualization of blood vessels[187]. CA4 has been previously shown to inhibit angiogenesis in zebrafish[169], we sought to determine the effect of verterporfin and CA4 in combination on angiogenesis. Zebrafish embryos at 8 hrs post fertilization were treated with drugs for 48 hrs. Since paclitaxel at the clinically relevant concentration had no effect on blood vessel formation (Figure S2.6), it was not further tested in combinations. Consistent with literature, CA4 significantly inhibited angiogenesis in zebrafish as indicated by shortened/misshapen intersegmental vessels in comparison to the control (Figure 2.3A-C). More significantly, combination of verteporfin and CA4 inhibited angiogenesis ~1.5-fold and 5-fold more than single drug alone, respectively (Figure 2.3D-F).

To understand the mechanism underlying the antiangiogenic effect of the combination therapy, we analyzed angiogenesis-associated genes in zebrafish embryos and found a significant reduction in vascular endothelial growth factor A (*VEGFA*) and the VEGF receptor after treatment with verteporfin and CA4. Both drugs in combination suppressed these gene expressions more than single drug alone *in vivo* (Figure 2.3G, H).

2.5.6 Verteporfin also inhibits HIF-1α activity and the angiogenetic gene VEGF *in vitro* in human TNBC cells

To determine the effect of the three drugs on angiogenetic activity in human TNBC cells, an *in vitro* luciferase assay was carried out to measure the activity of hypoxia-inducible factor 1-alpha (HIF-1α), a key transcription factor controlling angiogenic genes, tumorigenesis, and stemness factors[188,189] (Figure 2.4A). We found that HIF-1α activity was suppressed after treatment with

verteporfin and the three drugs in combination in TNBC MDA-MB-231 cells (Figure 2.4B). Verteporfin was also able to inhibit the HIF-1α activity upregulated by paclitaxel and CA4 (Figure 2.4B), and the VEGF gene expression upregulated by paclitaxel in TNBC MDA-MB-231 cells (Figure 2.4C). Taken together, these results suggest that the three drugs in combination more effectively inhibit the viability of bulk TNBC cells, diminish CSC enrichment, suppress angiogenesis, and circumvent the weaknesses/side effects of paclitaxel and/or CA4 to enhance the treatment efficacy.

2.5.7 Combination of verteporfin-NP, paclitaxel-NP, and combretastatin-NP decreases *ex vivo* viability of PDX organotypic slice cultures

To translate our results to a clinical setting, we tested our drug-NPs on PDX organotypic slice cultures. Fragments of organotypic slices were prepared from the PDX tumor and grown *ex vivo* in a culture dish (Figure 2.5A), which has been considered a clinically relevant model[114]. *Ex vivo* 3D PDX slice cultures contain human tumor cells, stroma cells, extracellular matrices, and other tumor compositions, different from the uniform cancer cell lines cultured *in vitro* that have gone through a high degree of selection[114]. Because of the limited availability of PDX tumor tissues for *in vivo* transplantation and substantial experimental logistics, we used organotypic PDX slice cultures that provide a predictable and cost-effective tool for *ex vivo* selection of drugs for subsequent *in vivo* PDX transplantation experiments[114]. We surgically engrafted TNBC PDX tumors into athymic mice, passaged and expanded them two to three times in mice. After that, we dissected the tumors, cultured tumor slices, and carried out an Almar blue viability assay after a 120-hr treatment with single drug-NP or the different combinations. The results showed that only

the combination of triple drug-NP, or the combination of paclitaxel-NP and CA4-NP achieved a two-fold decrease in tumor slice viability (Figure 2.5B).

Since the combination of three drug-NPs also inhibited tumorsphere formation and enhanced CSC apoptosis (Figure 2.1 and Figure S2.4), co-treatment with three drug-NPs seems to be the most effective approach.

2.5.8 Three drugs co-encapsulated in one NP stopped the growth of TNBC PDX tumor *in vivo*

While free drugs effectively suppressed MDA-MB-231 cells *in vitro* (Figure S2.7A), they did not delay the growth of MDA-MB-231 tumors *in vivo* when the mice were treated with free paclitaxel and verteporfin in combination. In contrast, NPs encapsulated with paclitaxel and verteporfin delayed the growth of MDA-MB-231 tumors *in vivo* (Figure S2.7B). In addition, there were no body weight loss and no signs of toxicity observed after 20 days of treatment with NPs encapsulated with drugs (Figure S2.5B), suggesting the tolerability of combinational treatment with drugs-NPs in mice. These results provide a rationale for testing drugs-NPs in more clinically relevant PDX models.

We then asked whether co-encapsulation of three drugs would be more effective than combination of individual drug-NPs. We encapsulated all three drugs into single NPs (Figure 2.6A and Figure S2.1). As shown in Figure S2.1, encapsulation of all three drugs in single NP did not significantly increase the NP size neither did it affect its stability. However, three-drugs co-encapsulated in one NP was more effective than the combination of three separate single drug-NPs

at inhibiting the viability of TNBC cell lines (both SUM149 and MDA-MB-231) *in vitro*, as well as the viability of PDX slice cultures *ex vivo* (Figure 2.6B and Figure S2.3).

We then surgically engrafted TNBC PDX tumors[180] into athymic mice. When the tumors reached a mean diameter of 3 mm, mice were randomized and treated with control E-NPs (empty NPs), or triple drug in one NP (NP co-encapsulated with 1 mg/kg of paclitaxel, 2 mg/kg verteporfin, and 1 mg/kg of combretastatin), every 2 days for 20 days via tail vein injection. The treatment significantly halted PDX tumor growth (Figure 2.6C), confirming the efficacy of triple drug in one NP in an *in vivo* transplantation model. Of note, by the end of the treatment, there were no body weight loss in the mice carrying PDX tumors (mouse body weight: empty-NP 24.16 ± 2.64 g vs PVC-NP 26.40 ± 0.20 g) and no signs of toxicity observed.

2.6 Discussion

TNBC is one of the most aggressive subtypes of breast cancers and accounts for the majority breast cancer-related death due to the lack of a specific target for effective treatment[163]. Targeting CSCs or angiogenesis has been considered effective therapeutic strategies[73,168]. However, chemotherapy enriches CSCs and the disorganized structure of tumor neovasculature impedes free drug delivery and accumulation in the tumors[168,173]. We attempted to circumvent the aforementioned limitations by the development of a three-in-one nanotherapy to inhibit bulk cancer cell, CSCs, and angiogenesis simultaneously (Figure 2.7). Individual free drugs selected in this study have been commonly and safely used in patient treatment. The side effects could be further reduced with NP encapsulation, as drugs-NPs have been shown to accumulate more in the tumor[174].

Nanomedicine has greatly improved the efficacy of drug/small-molecule delivery to the tumor, while minimizing drug off-target toxicities. In this study, we developed and characterized PLGA-PEG NPs encapsulating drugs individually and in combination. The NPs were stable in plasma with NP sizes ~100 nm, which is considered optimal for longer blood circulation and higher accumulation in tumor due to the EPR effect[174,190,191].

Consistent with existing literature and our previous studies[52,192,193], paclitaxel-NP effectively suppresses bulk cells but enriches CSCs that have accounted for tumor recurrence after chemotherapy withdrawal in clinic (Figure 2.1 and Figure S2.4). We also found that CA4-NP exhibits certain characteristics similar to paclitaxel-NP: inhibiting bulk cancer cell but enriching CSCs, and upregulating CSC-related YAP signal. A possible explanation for this stems from the mechanism of action of CA4. CA4, as an antimitotic agent, acts by binding at the interface of the αβ tubulin heterodimers to inhibit the assembly of microtubules[194]. Recently, a lower expression of αβ tubulin has been associated with a lower degree of differentiation but a higher level of expression of "stemness"/CSC markers[195]. It is possible that CSCs adopt resistance to CA4 by interrupting tubulin heterodimers and microtubule assembling.

Our results also showed that CA4 upregulates YAP target genes, and YAP activation has been associated with anti-tubulin drug resistance[196]. However, the exact mechanistic links between CA4, YAP, and tubulin isotype expression and microtubule assembling remain unclear, warranting further investigations. Of note, verteporfin-NP was able to offset the paclitaxel-NP and CA4-NP-mediated CSC enrichment, highlighting the necessity for combination therapy. Our results also showed that verteporfin-NP effectively decreased cell migration. The inhibitory effect of

verteporfin-NP on cancer cell migration and CSCs might be partially attributed to its suppression of YAP activity, which is known to promote EMT/migration and CSCs. The inhibitory effect of verteporfin on CSC enrichment is crucial as suppression of CSCs is well known to prevent tumor recurrence[164,165]. This further highlights the requirement of verteporfin in addition to CA4 and paclitaxel in devising an effective treatment for TNBC to reduce relapse.

While CA4 or verteporfin has been suggested to exhibit antiangiogenic potential separately[95,169], we showed that combination of two drugs was more effective to suppress angiogenesis in an *in vivo* transgenic zebrafish model (Figure 2.3). Our results also suggest that CA4 exerting its antiangiogenic effect might be partially through the inhibition of Wnt pathway (Figure S2.6D). The Wnt pathway is crucial in the functioning of vascular endothelial cells. Wnt signaling controls endothelial cell proliferation, survival, and migration through transcriptional regulation of VEGF[197]. However, the exact mechanism by which CA4 interacts with the Wnt pathway remains a subject for further investigation.

In addition, we found that verteporfin also decreased the activity of HIF-1α and the gene expression of VEGF in human TNBC cells. HIF-1α is a transcriptional factor regulating a wide range of genes involved in angiogenesis (e.g., VEGF), tumorigenesis, and metabolic adaptation of cancer cells, and is commonly linked to poor prognosis in the clinic[189]. We showed that verteporfin was able to subdue paclitaxel-enhanced HIF-1α activity. Paclitaxel-induced HIF-1α activity has been reported to promote breast CSC enrichment and increase the expression of multidrug resistance[198]. Of note, verteporfin has been shown to inhibit HIF-1α DNA-binding ability and HIF-1α-YAP-binding capacity in a liver cancer model[199]. Verteporfin may also exert antiangiogenic

effect in TNBC via YAP and/or HIF-1α by counteracting paclitaxel/CA4-upregulated HIF-1α and/or YAP activities. Taken together, our results show that paclitaxel and CA4 are important to decrease the viability of bulk cancer cells, CA4 and verteporfin in combination significantly suppress angiogenesis, and verteporfin reduces CSC enrichment following paclitaxel and CA4 treatment. Therefore, combination of three drugs will improve the outcomes. Of note, those drugs have been individually and safely used in clinic, and combinations of two or three drugs did not further inhibit MCF-10A viability compared to single drug in our experiments (Figure S2.5A); no body weight loss and no toxicity were observed in mice after the treatment with E-NPs vs PVC-NPs. These results indicate a possible tolerability of this treatment.

Using an appropriate model in cancer research is crucial for potential clinical translation. PDX organotypic slice cultures and PDX *in vivo* transplantation have been recognized, as clinically relevant platforms[118]. Various studies have reported that treatment of *ex vivo* cultured PDX tumor slices correlates with *in vivo* PDX results, allowing for a more feasible and efficient drug screening[118]. Accordingly, we screened the efficacy of different drug-NPs using *ex vivo* PDX organotypic slice cultures first, and then assessed the most potential drug-NP in an *in vivo* PDX model. This has circumvented cost and time consumption, as well as a number of logistic challenges encountered *in vivo* PDX transplantation.

Using TNBC cell line, *in vivo* zebrafish model, and clinically relevant PDX models, this study showed the efficacy of a new triple-drug NP system made of FDA-approved biomaterials in TNBC tumors, moving one-step further toward clinical application.

2.7 Figures

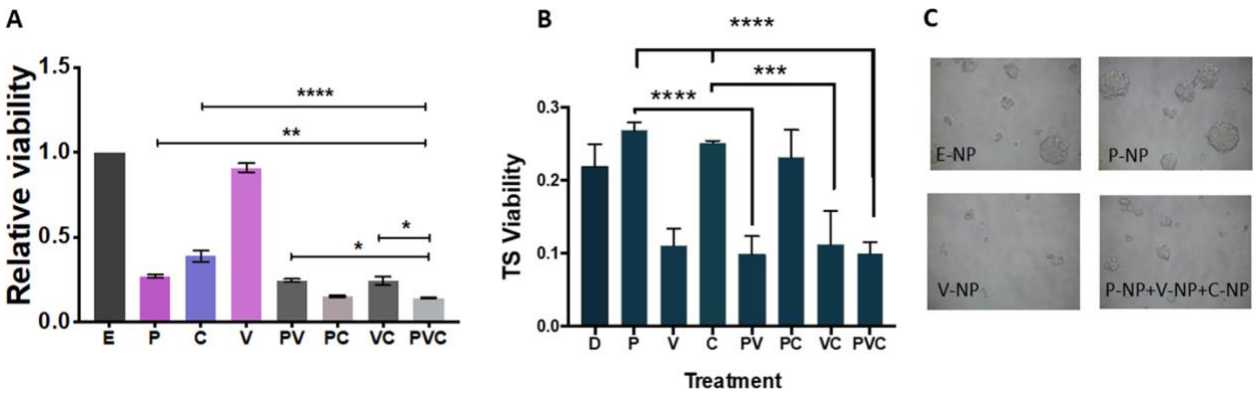

Figure 2.1 Combination of verteporfin-NP, paclitaxel-NP, and/or combretastatin-NP suppressed both bulk tumor cells and cancer stem cells. (A) The viability of TNBC MDA-MB-231 cells was determined by MTT assay after 120-hr treatment with E-NP (empty-nanoparticle), P-NP (paclitaxel-NP, 5 nM), V-NP (verteporfin-NP, 250 nM), C-NP (combretastatin-NP, 5 nM), or different combinations. (B) Tumorsphere (TS) formation, an *in vitro* assay indicating cancer stem cells (CSCs) after different treatments with drug-NPs. MDA-MB-231 cells overexpressing E-cadherin were grown in low attachment and serum-free conditions, and treated for 120 hrs as described in A, followed by MTT viability assay. (C) Representative photographs of TS shown in B. Data represent means ± SD, $*P < 0.05$, $**P < 0.01$, $****P < 0.001$.

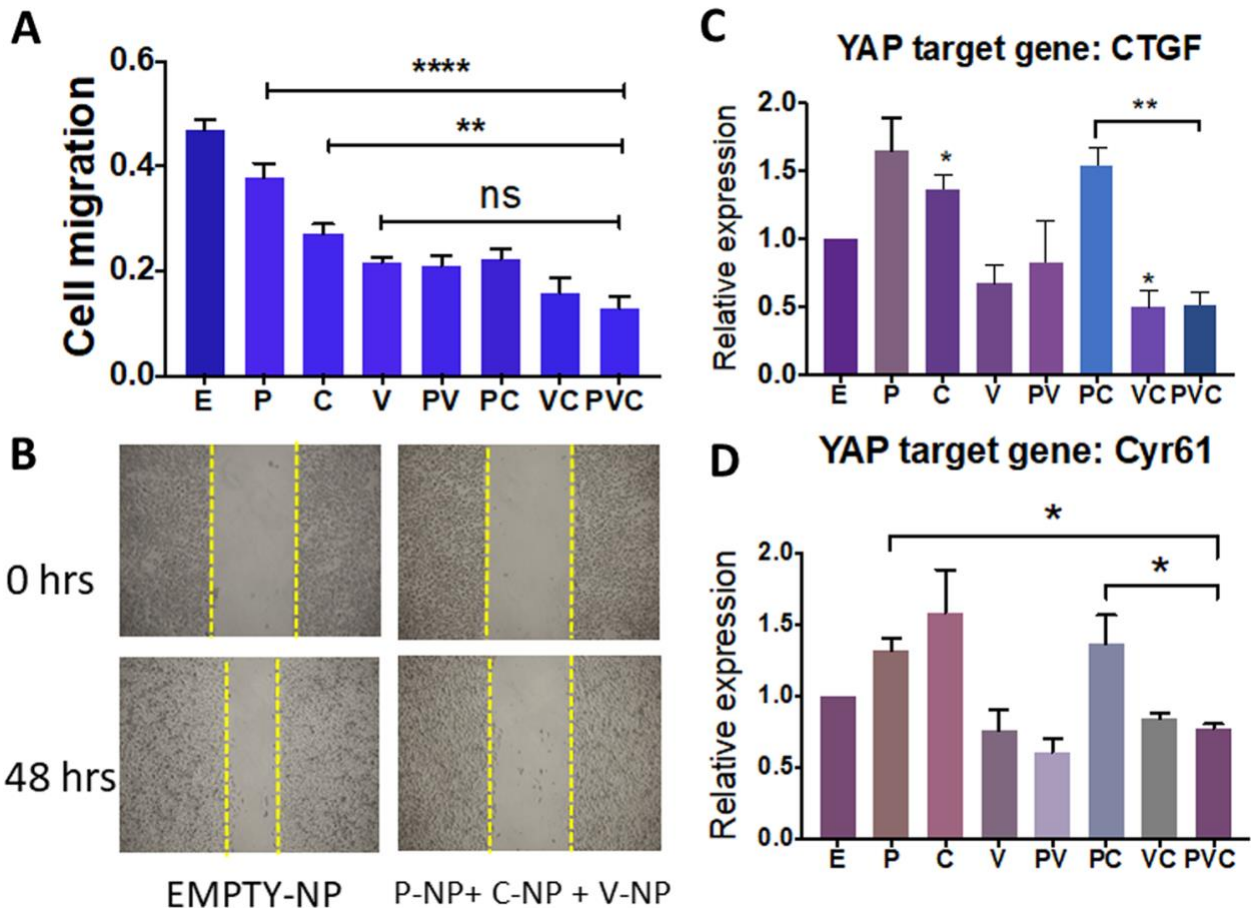

Figure 2.2 Verteporfin-NP more effectively inhibits the migration of TNBC cells and fully suppresses YAP target genes upregulated by paclitaxel-NP and/or combretastatin-NP. (A) TNBC MDA-MB-231 cells were grown to confluence, treated with mitomycin to inhibit cell proliferation, and then scratched and quantified for migration after incubation with E (empty-NP), 5 nM P (paclitaxel-NP), 250 nM V (verteporfin-NP), 5 nM C (combretastatin-NP), or different combinations for 48 hrs. (B) Representative images of A. (C), (D) RT-qPCR analysis of changes of YAP target gene in MDA-MB-231 cells after 24 -hr of treatment with E (empty-NP), 25 nM P (paclitaxel-NP), 1.25 μM V (verteporfin-NP), 25 nM C (combretastatin-NP), and different combinations. Data represent means ± SEM, $*P < 0.05$, $**P < 0.01$, $****P < 0.0001$.

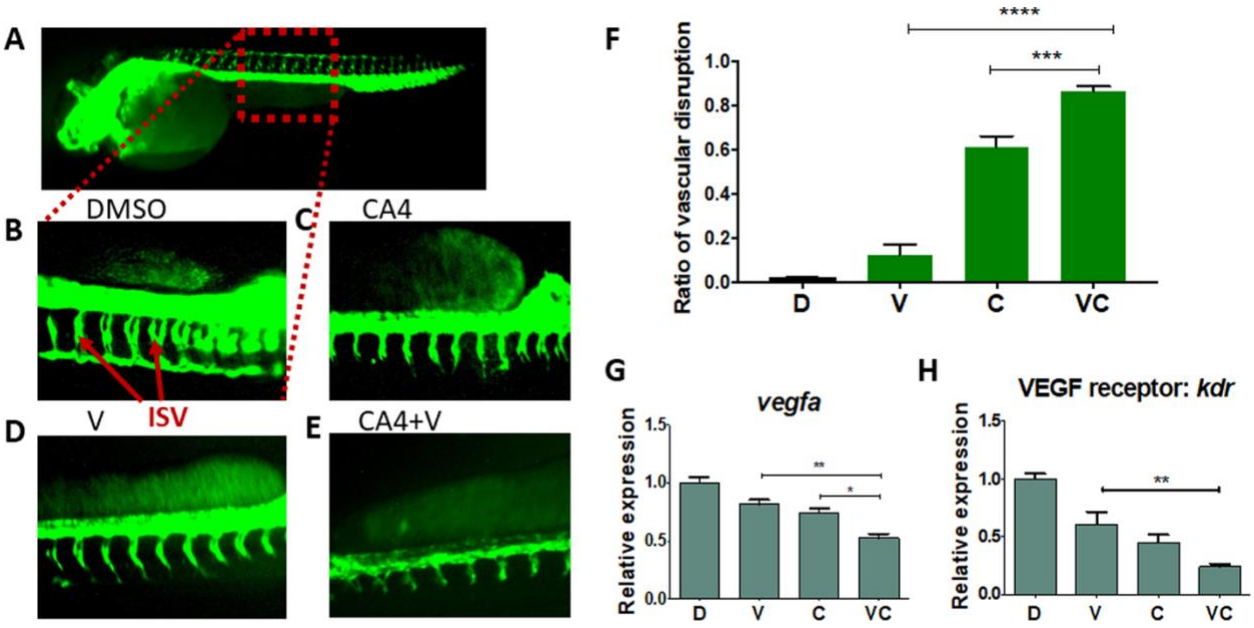

Figure 2.3 Verteporfin in combination with combretastatin more effectively inhibits vasculature in transgenic zebrafish (Tg, fli:eGFP) embryos. The zebrafish embryos at 8-hrs post fertilization were treated with drugs for 48 hrs. (A) Healthy zebrafish embryo taken at 8× magnification. Intersegmental vessel (ISV) phenotypes in a sectional view of: (B) DMSO; (C) CA4, 5 nM; (D) V, verteporfin, 250 nM; (E) V + CA4. (F) Graphical summary showing the ISV disruption ratio of B–E. Data are expressed as mean ± SEM, $n = 5$ embryos. (G), (H) RT-qPCR analysis of vascular endothelial growth factor A (*VEGFA*, an angiogenesis gene) and VEGF receptor *kdr* in zebrafish embryos after treatments. Data are expressed as mean ± SEM, $n = 4$ embryos. $^{*}P < 0.05$, $^{**}P < 0.01$, $^{****}P < 0.0001$.

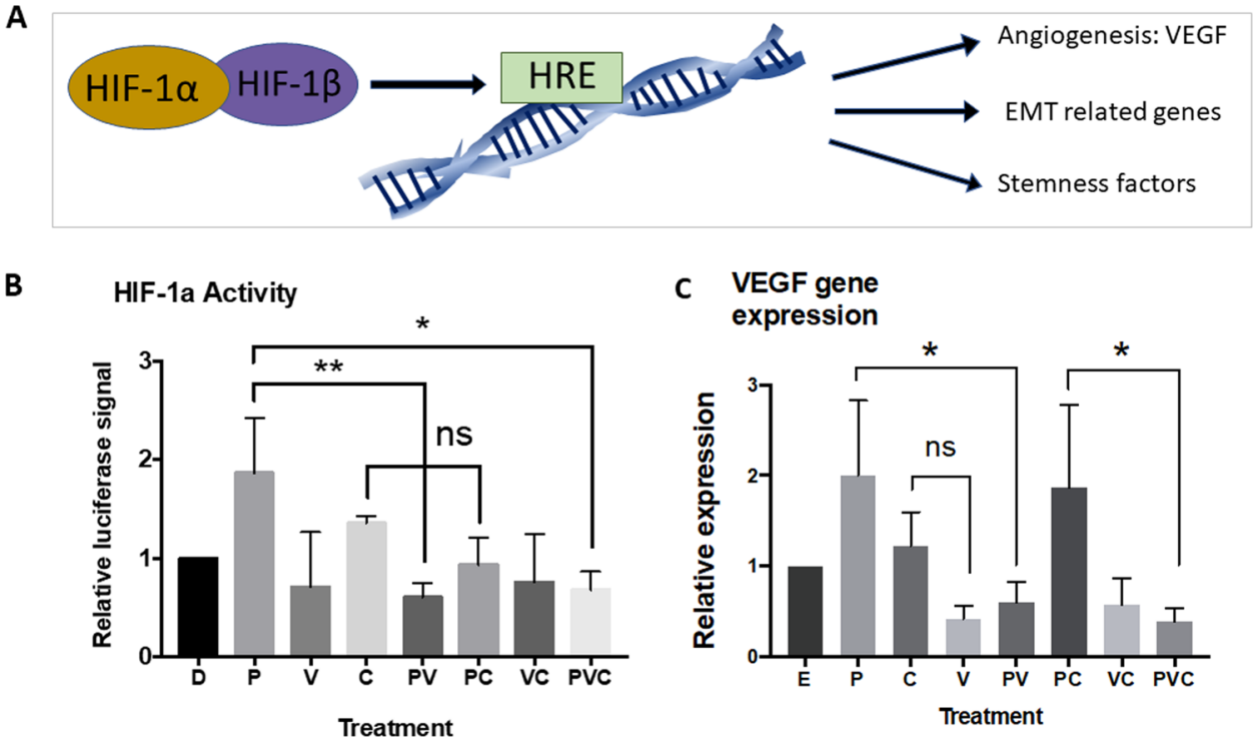

Figure 2.4 Verteporfin-NP also inhibits angiogenesis-associated genes *in vitro* in human TNBC cells. (A) Schematic showing that HIF-1α is a master regulator in angiogenesis and other tumorigenic processes. (B) Luciferase reporter activity of HIF-1α activities in MDA-MB-231 cells treated with control DMSO, paclitaxel (25 nM), verteporfin (1.25 μM), CA4 (25 nM), and different combinations for 24 hrs. (C) RT-qPCR analysis showing the changes of VEGF gene expression in MDA-MB-231 cells after 24 hrs of treatment with E (empty-NP), 25 nM P (paclitaxel-NP), 1.25 μM V (verteporfin-NP), 25 nM C (combretastatin-NP), and different combinations. Data are expressed as mean ± SD, $n = 3$. *$P < 0.05$, **$P < 0.01$.

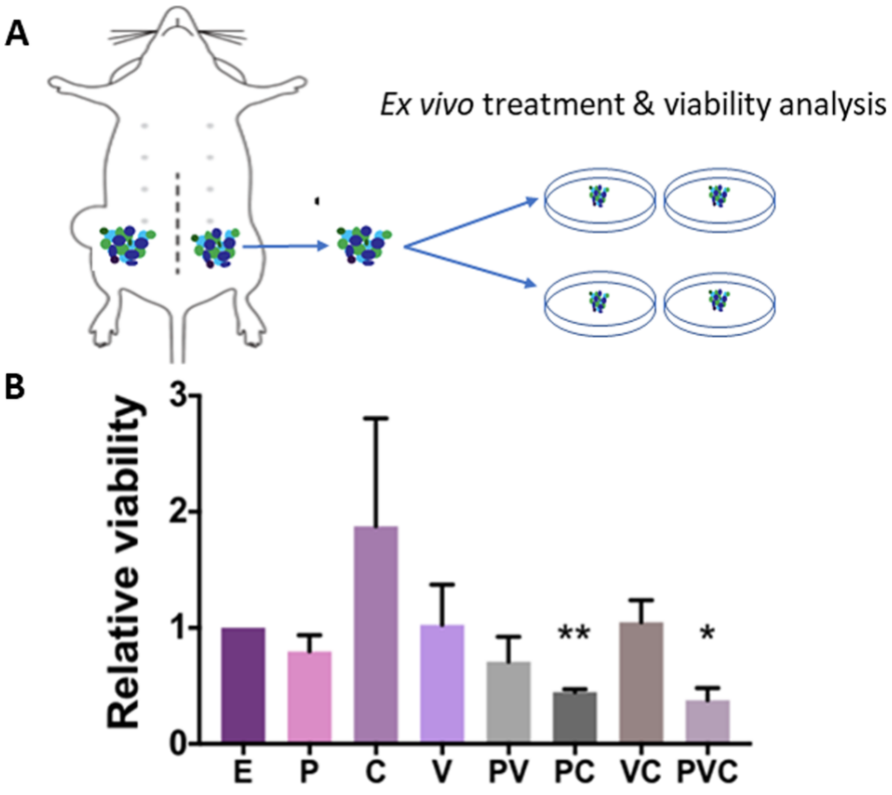

Figure 2.5 Combination of verteporfin-NP, paclitaxel-NP, and combretastatin-NP decreased *ex vivo* viability of PDX organotypic slice culture. (A), (B) *Ex vivo* viability analysis (Almar blue assay) of PDX (HCI-001) organotypic slice culture after 120-hr treatment with E-NP (empty-NP), P-NP (paclitaxel-NP, 5 nM), V-NP (verteporfin-NP, 250 nM), C-NP (combretastatin-NP, 5 nM), or different combinations. Data represents means ± SEM, $n = 3$, $^{*}P < 0.05$, $^{**}P < 0.01$.

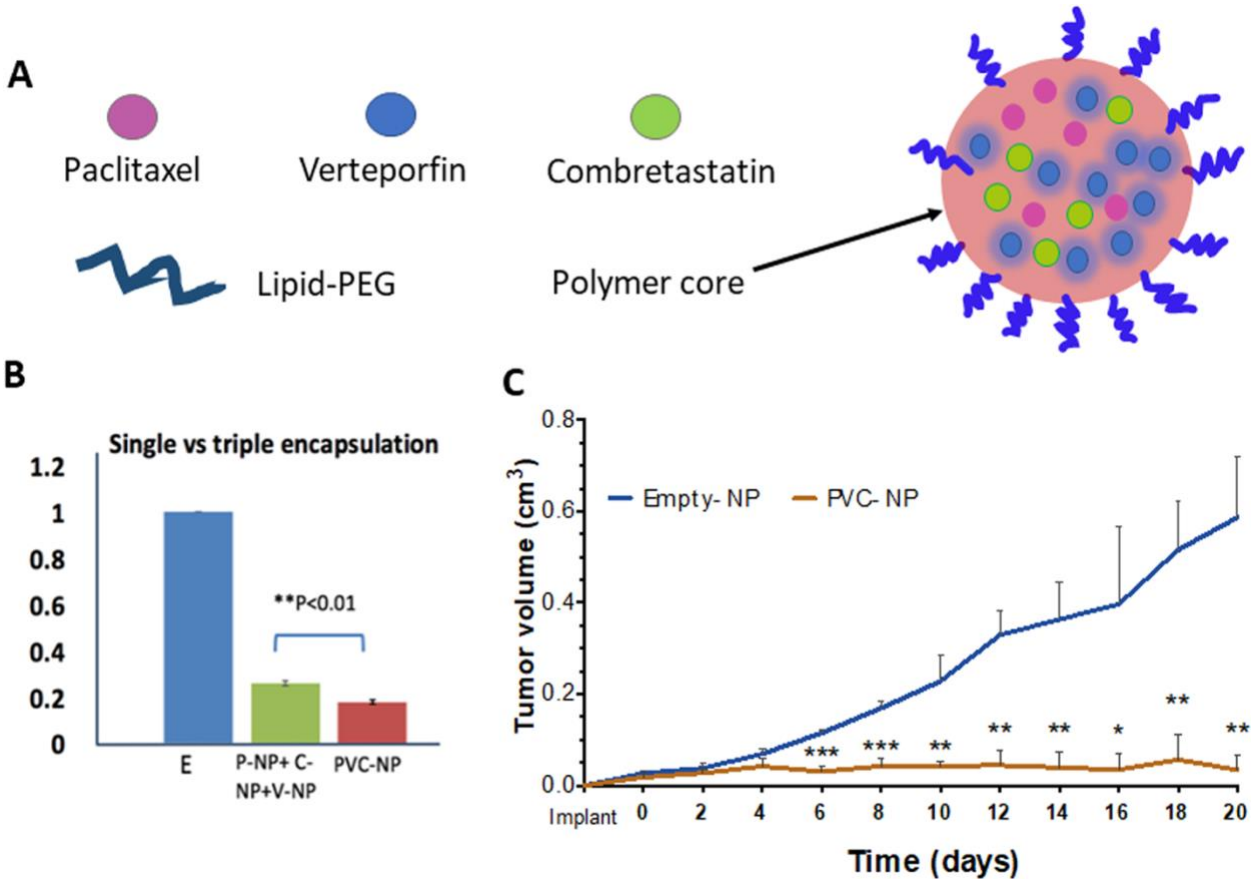

Figure 2.6 Triple drugs co-encapsulated in one NP stopped TNBC PDX tumor growth in *vivo*. (A) Schematic showing the development of a triple-drug NP system co-encapsulating CA4, paclitaxel, and verteporfin. (B) Viability analysis using an MTT assay after 120-hr treatment with empty-NP (E), paclitaxel-NP (P-NP) + verteporfin-NP (V-NP) + combretastatin-NP (C-NP), or PVC-NP at a 1:2:1 ratio. Drug-NPs were added at 0 and 72 hr. Three drugs co-encapsulated into NP showed better efficacy than combination of individual drug-NPs. (C) PDX (HCI-002) tumor fragments were engrafted into the mammary fat pads of athymic mice and treated with either control (empty-NP), or PVC-NP (1 mg/kg of paclitaxel and 2 mg/kg verteporfin, 1 mg/kg CA4 co-encapsulated in NP) every 2 days for 20 days. Data are expressed as mean ± SEM, $n = 3$, $^{*}P < 0.05$, $^{**}P < 0.01$, $^{***}P < 0.001$.

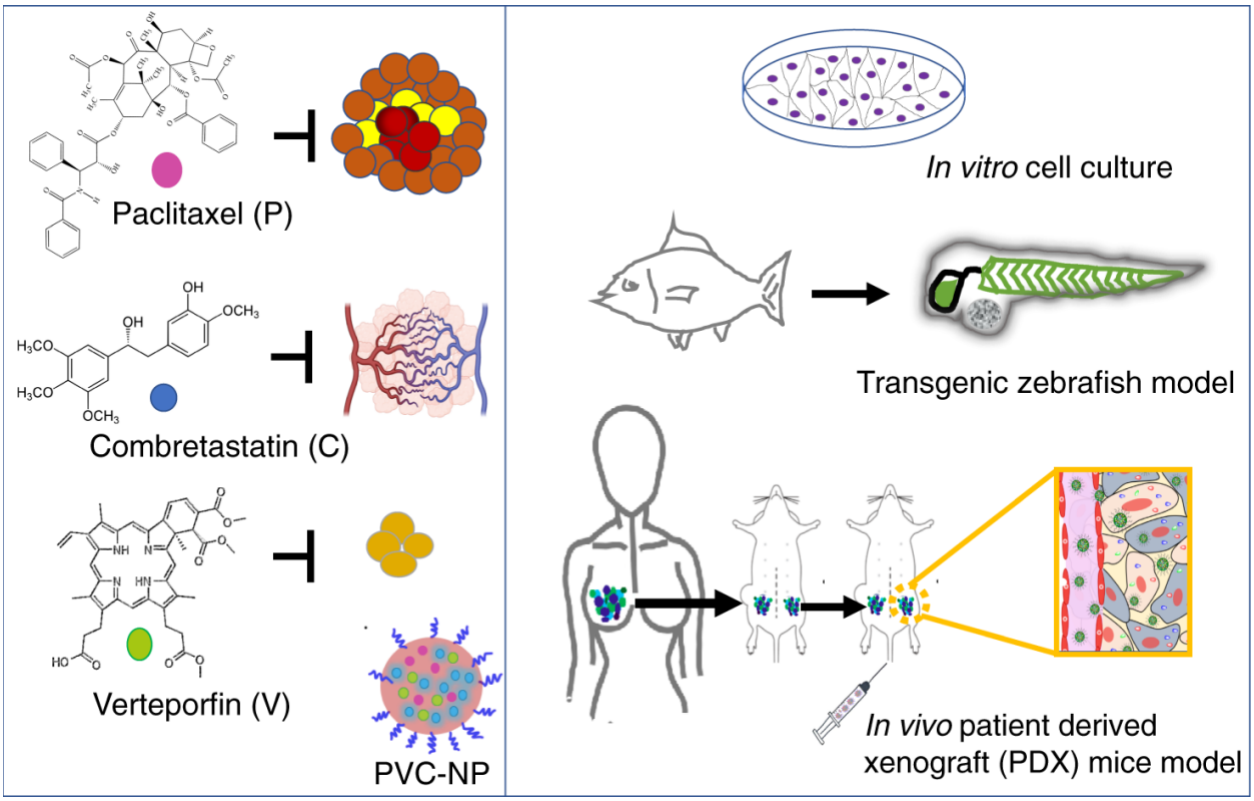

Figure 2.7 A schematic representation of experimental design using cell culture, transgenic zebrafish, and patient-derived xenograft models to study bulk cancer cells, angiogenesis, and CSCs. PDX: established TNBC PDX fragments were isolated from mice, and engrafted in mice again for in *vivo* transplantation and for *in vitro* organotypic slice culture. Biorender was used to construct part of the figure.

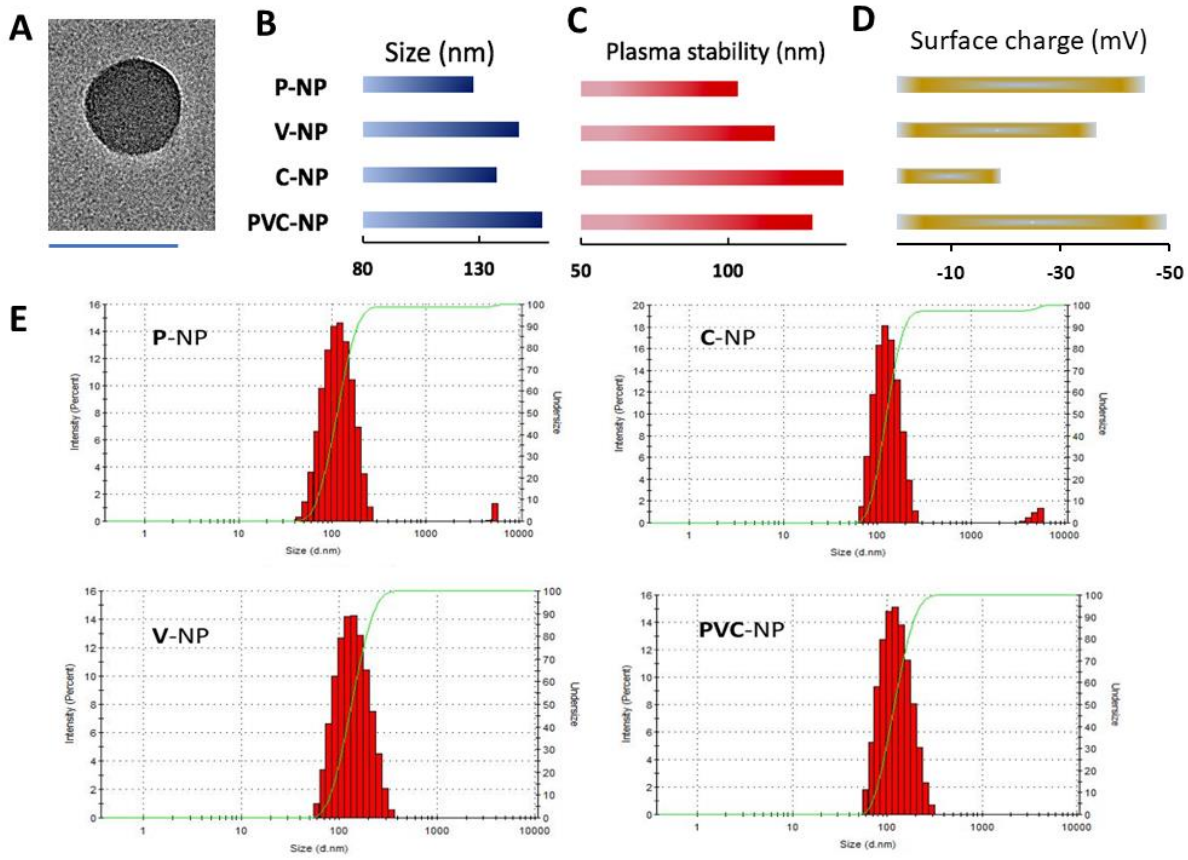

Figure S2.1. Development of lipid polymer nanoparticles (NPs) encapsulated with paclitaxel, verteporfin and/or combretastatin and their physiochemical properties. (A) TEM microscopic image of NP encapsulated with three drugs (scale bar, 100 nm). (B) and (C) Sizes of single and triple encapsulated NPs measured by Dynamic Light Scattering (DLS) before incubation with serum (B) and after incubation with serum (C) for 4 hours. (D) Zeta potential showing surface charge of single and triple encapsulated NP. (E) Representative size distribution.

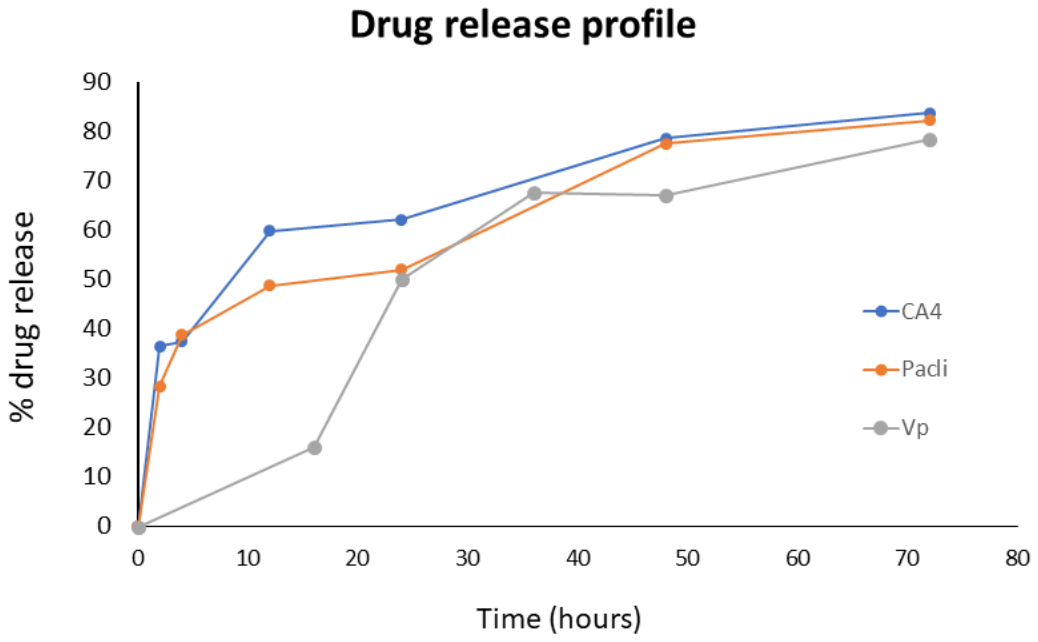

Figure S2.2 Drug release profile of paclitaxel, verteporfin and combretastatin in 72 hours. The amounts of paclitaxel (Pacli) and combretastatin (CA4) remaining in the NPs at different time points were analyzed using HPLC at 204 nm, with H2O:acetonitrile mobile phase and with 5%–90% acetonitrile gradient. The amounts of verteporfin (Vp) remaining in NPs at the different time points were quantified using NanoDrop at 430 nm absorbance. The amounts of drugs were expressed as percentage of drug released from the NPs.

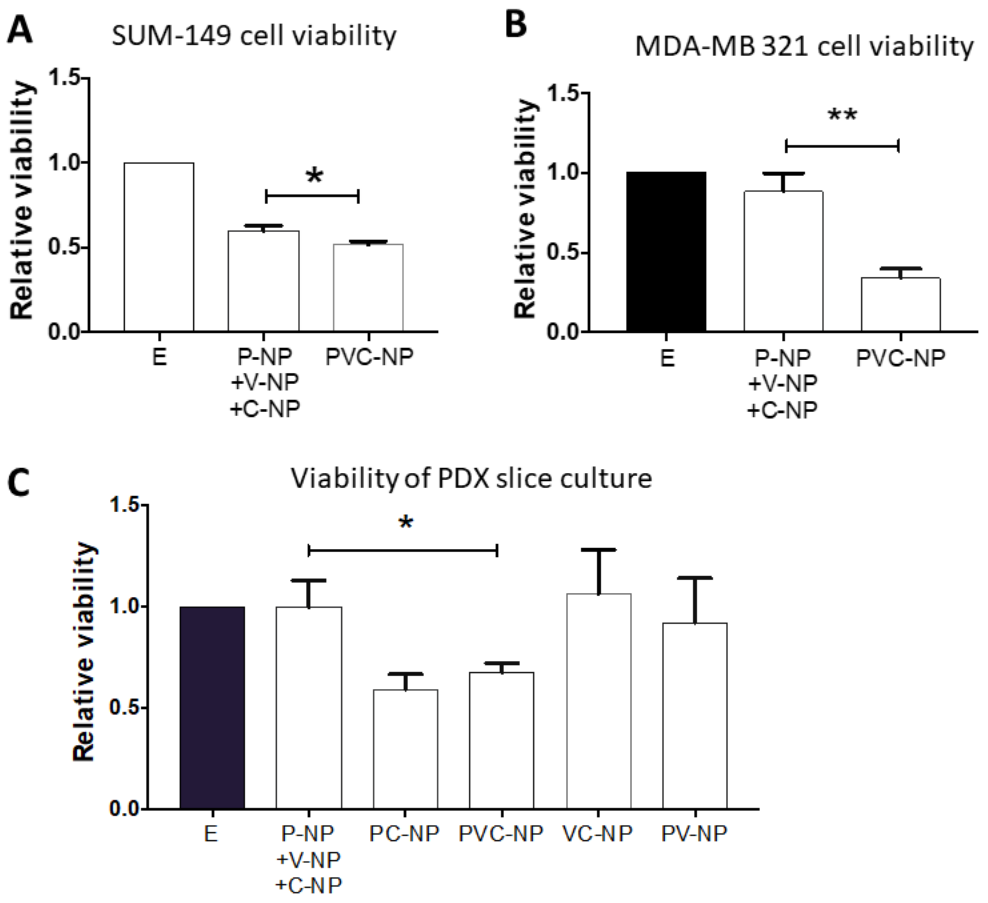

Figure S2.3. Triple drug-encapsulated NPs are more effective at suppressing TNBC cells and TNBC slice cultures than the combination of single drug-encapsulated NPs. (A) and (B) The viability of SUM149 and MDA-MB-231 TNBC cells was determined by MTT assays after 48-hour treatment. (C) Viability of PDX (HCI-001) *ex vivo* slice culture assessed by Alamar blue assay after 72-hour treatment, with statistical difference. NP (nanoparticles), E (empty-NP), P-NP (5nM), V-NP (10 nM), C-NP (5 nM), VC-NP (10nM:5nM), PV-NP (5nM:10nM), PC-NP (5nM:5nM), PVC-NP (5nM:10nM:5nM). n = 3 for (A) and (B), n = 5 for (C). Data represent means ± SEM, * $p < 0.05$, ** $p < 0.01$.

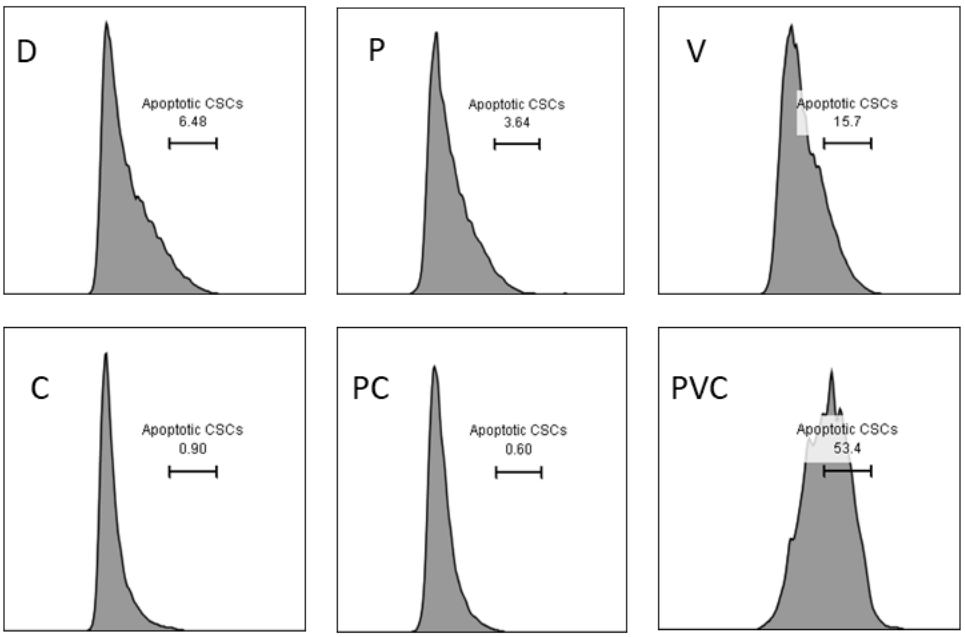

Figure S2.4. Verteporfin enhances CSC apoptosis. Flow cytometric analysis of $CD44^{+}$ $CD24^{-}$ CSCs and Annexin V^{+} MDA-MB-231 cells after 96 hours of treatments with verteporfin, paclitaxel, combretastatin, or in different combinations.

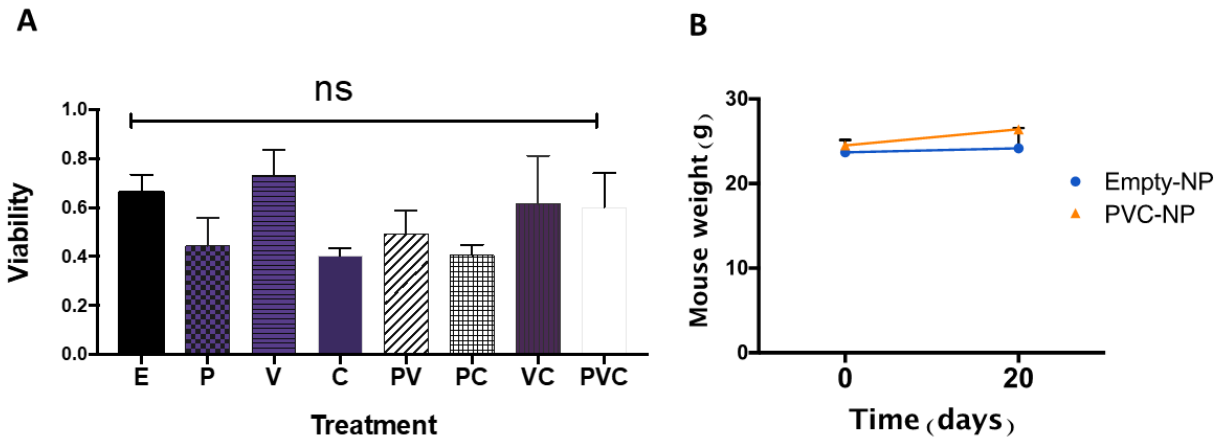

Figure S2.5. The combination of drug-NP treatment does not significantly inhibit non-transformed mammary epithelial cells *in vitro*, and does not cause the loss of mouse body weights *in vivo. (*A) The viability of MCF-10A cells was determined by an MTT assay after 120-hour treatment with E (empty-nanoparticle), P (paclitaxel-NP, 5nM), V (verteporfin-NP, 250 nM), C (combretastatin-NP, 5 nM), or different combinations. (B) There was no body weight loss observed after treatment with empty-NP (empty-nanoparticles) or nanoparticle encapsulated with drugs for 20 days. N = 3 mice in each group.

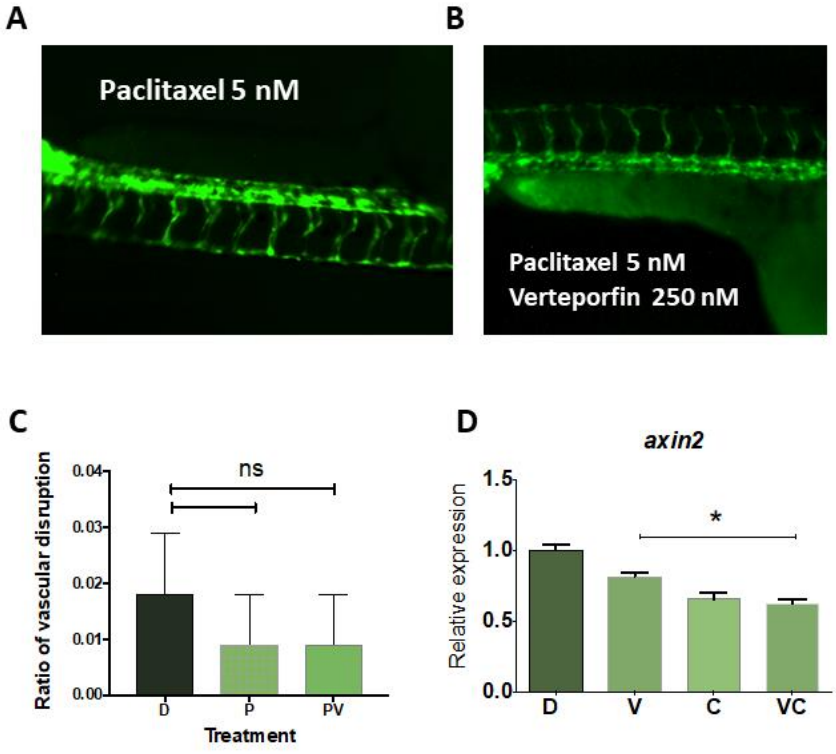

Figure S2.6. The effect of drug treatment on ZF embryos. (A-B). Representative images of zebrafish embryos after treatment with paclitaxel or paclitaxel + verteporfin, which were not shown in Figure 3. Zebrafish embryos were treated when they were 8 hours post fertilization (hpf) for 48 hours. At 56 hpf, they were imaged for vascular disruption. (C) Quantitative analysis of A-B. (D) RT-qPCR analysis of Wnt target gene *axin2* in zebrafish embryos.

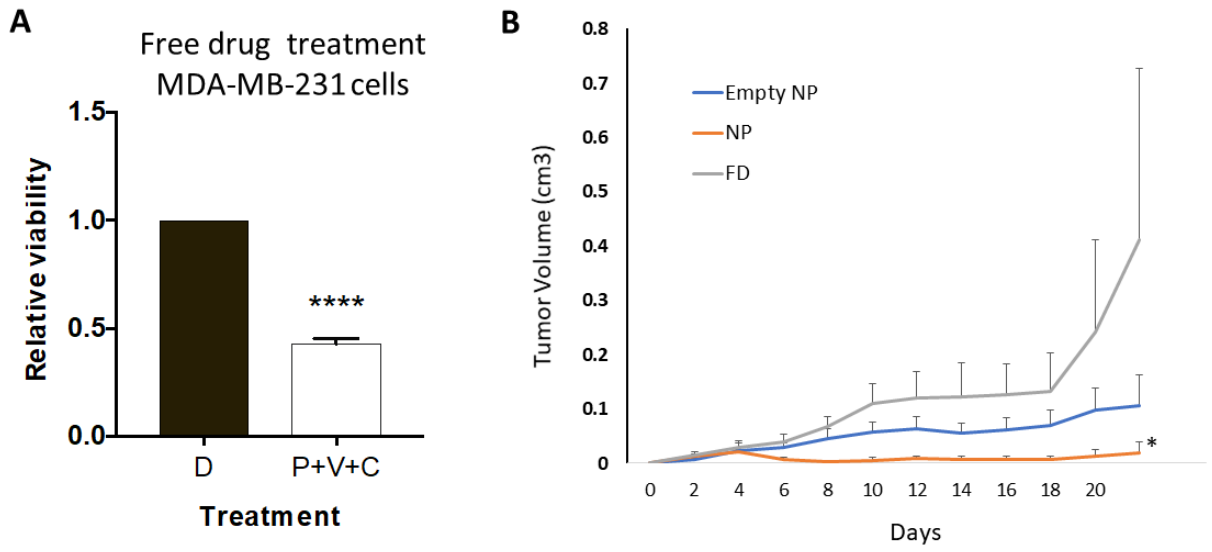

Figure S2.7. The effect of free drugs and drugs-NPs on TNBC cells *in vitro* and on MDA-MB-231 tumors *in vivo*. (A) The viability of TNBC MDA-MB-231 cells was determined by MTT assays after 48-hour treatment with D (DMSO), or combination of free drug P (paclitaxel, 5 nM), V (verteporfin, 10 nM), and C (combretastatin, 5 nM). N = 3, **** $p < 0.0001$ compared to control. (B) MDA-MB-231 TNBC cells were injected into the mammary fat pads of athymic nude mice (2×10^6 cells per mammary pad). When the tumors reached a mean diameter of ~3 mm, mice were treated with empty-NP (empty nanoparticles), FD (free drug, paclitaxel 1mg/kg and verteporfin 10mg/kg), or NP (nanoparticles encapsulated with paclitaxel and verteporfin at the same concentration as free drugs). Free drugs did not exhibit inhibitory effect on tumor growth after treatment for 20 days while drug-NP treatment delayed tumor growth. N = 5 mice in each group, * $p < 0.05$ compared to free drug group or empty-nanoparticle group.

Table S2.1. Primers used for the assessment of gene expressions of human TNBC cells by RT-qPCR

Primer	Forward primer 5'-3'	Reverse primer 5'-3'
CTGF	AGGAGTGGGTGTGTGACGA	CCAGGCAGTTGGCTCTAATC
Cyr61	AGCCTCGCATCCTATACAACC	TTCTTTCACAAGGCGGCACTC
18S	AACCCGTTGAACCCCATT	CCATCCAATCGGTAGTAGCG
GAPDH	ACAGTCAGCCGCATCTTCTT	GACAAGCTTCCCGTTCTCAG

Table S2.2. Primers used for the assessment of gene expressions of zebrafish by RT-qPCR

Primer	Forward Sequence 5'-3'	Reverse Sequence 5'-3'
axin2	GGACACTTCAAGGAACAACTAC	CCTCATACATTGGCAGAACTG
vegfa	TCCAGGAGTATCCCGATGAG	GCTTTGACTTCTGCCTTTGG
flt-1	ATGGGAACAGCAGCACTCTT	TTGAAGACGGAGGGACAATC
kdr	TGTGGTCAGCTATGCTGGAG	AGCCTCTCATGCTGTGGACT
ef1α	CTGGAGGCCAGCTCAAACAT	ATCAAGAAGAGTAGTACCGCTAGCATTAC
rpl13a	TCTGGAGGACTGTAAGAGGTATGC	AGACGCACAATCTTGAGAGCAG
ywhaz	TCTGCAATGATGTGTTGGAGC	TCAATGGTTGCTTTCTTGTCGTC

CHAPTER 3: NANOPARTICLE-MEDIATED MRNA DELIVERY TO TRIPLE-NEGATIVE BREAST CANCER (TNBC) PATIENT-DERIVED XENOGRAFT (PDX) TUMORS

3.1 Preface

This chapter contains original research demonstrating the delivery of nanoparticles encapsulating mRNA to a clinically translatable *in vivo* model. This research was published in ACS Pharmacology & Translational Science[200]

El-Sahli, S., Manturthi, S., Durocher, E., Bo, Y., Akman, A., Sannan, C., Kirkby, M., Iroakazi, C.D., Deyell, H., Kaczmarek, S., Lee, SH., Iqbal, U., Cote, M., Wang, L., & Gadde, S. (2025). Nanoparticle-Mediated mRNA Delivery to Triple-Negative Breast Cancer (TNBC) Patient-Derived Xenograft (PDX) Tumors. *ACS Pharmacology & Translational Science*.

Author Contributions:

LW, SG, SE and SM conceived and planned the study. SE. and SM contributed equally to the manuscript. All authors were involved in data collection, analysis, and final editing.

3.2 Abstract

mRNA-based therapies can overcome several challenges faced by traditional therapies in treating a variety of diseases by selectively modulating genes and proteins without genomic integration. However, due to mRNA's poor stability and inherent limitations, nanoparticle (NP) platforms have been developed to deliver functional mRNA into cells. In cancer treatment, mRNA technology has multiple applications, such as restoration of tumor suppressors and activating antitumor immunity. Most of these applications have been evaluated using simple cell-line-based tumor models, which failed to represent the complexity, heterogeneity, and 3D architecture of patient tumors. This discrepancy has led to inconsistencies and failures in clinical translation. Compared to cell line models, patient-derived xenograft (PDX) models more accurately represent patient tumors and are better suitable for modeling. Therefore, for the first time, this study employed two different TNBC PDX tumors to examine the effects of the mRNA-NPs. mRNA-NPs are developed using EGFP-mRNA as a model and studied in TNBC cell lines, *ex vivo* TNBC PDX organotypic slice cultures, and in *vivo* TNBC PDX tumors. Our findings show that NPs can effectively accumulate in tumors after intravenous administration, protecting and delivering mRNA to PDX tumors with different genetic and chemosensitivity backgrounds. These studies offer more clinically relevant modeling systems for mRNA nanotherapies in cancer applications.

3.3 Introduction

mRNA technology and its applications in COVID-19 vaccines have opened new avenues for drug development[201,202]. RNA-based therapies can overcome several challenges faced by traditional therapies in treating a variety of diseases, as around 85% of the genome might be undruggable using small molecule-based treatments[203,204]. In cancer therapies, mRNA-based applications offer multifactorial benefits[151]. They can be designed to carry optimized genetic information and be translated into the production of encoded proteins without genomic integration[151]. This allows them to encode desired tumor suppressors, tumor antigens, cytokines, chimeric antigen receptors (CARs), and T cell receptors, thereby inhibiting cancer cell proliferation and triggering antitumor immune responses in the tumor microenvironment[151,205–208]. Additionally, mRNAs can be designed to target gene editing and disrupt tumor survival genes, leading to improved treatment efficacy with fewer repeated treatments compared to traditional cancer therapies[205–207,209–212].

Clinical translation of mRNA remains challenging due to mRNA's inherent limitations, such as the immunogenicity of *in vitro* transcribed mRNA, possible TLRs/PPRS activation and proinflammatory cytokine production, stability, and the necessity of intracellular delivery for efficacy[201–204,213]. Advances in nanomedicine technologies have enabled the in *vivo* delivery of mRNA[201,202,214,215]. Nanoparticles (NPs) are nanosized drug delivery systems capable of encapsulating a variety of therapeutic agents, protecting them from degradation, delivering them to disease sites, avoiding healthy organs, and minimizing the toxic side effects[215–218]. Nanotechnology applications in cancer are particularly promising, as NPs can accumulate into tumors via passive and active mechanisms that are not yet completely understood[219–221]. mRNA-based nanotechnology applications in cancer focused on restoring tumor suppressor genes to

inhibit tumor growth or producing tumor antigens or cytokines to trigger antitumor immune responses[151]. While promising, these studies often employed cell-line-based animal models to evaluate mRNA-NP therapeutic effects[205,206]. Conventional cell-line-based xenografts, despite being convenient and widely used, have a lack of predictive value, which led to discrepancies between preclinical results and clinical outcomes[222,223]. Cancer cell lines are often derived from a single cell. This may be due to the process of establishing and maintaining cell lines, which involves selection pressure that can favor the survival of certain subclones over others, potentially eliminating important cell populations present in the original tumor. Cancer cell lines lack heterogeneity, supporting cells and extracellular matrices, and a three-dimensional architecture. They often undergo genetic and epigenetic changes that differ from the original tumor, which alter their behavior and make them less representative of the primary cancer[222]. In contrast, patient-derived xenograft (PDX) models, where tumors are taken from the patient and surgically implanted in immunocompromised mice, have revolutionized preclinical testing[114,116,180,223]. PDX models retain key characteristics of patient tumors, including histologic features, genomic signatures, and cancer cell heterogeneity, as well as stromal and immune cells from patients[116,223]. This results in a strong correlation with actual patient clinical responses[114,116,224].

The primary focus of this study is to investigate mRNA delivery to clinically relevant triple-negative breast cancer (TNBC) PDX tumors in *vivo*. We used EGFP mRNA as a model mRNA to develop NPs by using a robust PLGA-PEG nanoparticle system and evaluated them in PDX models. TNBC is a particularly aggressive and hard-to-treat subtype of breast cancer, accounting for disproportionate numbers of breast cancer deaths[161,224]. TNBC lacks specific therapeutic targets, making chemotherapy the primary treatment option, despite issues with drug resistance,

cancer stem cell (CSC) enrichment, and tumor relapse[161]. In this context, the development of mRNA-based therapies for TNBC might address the limitations of current therapies. Therefore, we employed two TNBC PDX models, HCI001 and HCI002, to study our NPs[161,224,225]. HCI-001 is derived from a patient with disease progression and is resistant to paclitaxel, whereas HCI-002 comes from a patient who has not been previously exposed to chemotherapy. We used both paclitaxel-sensitive and -resistant PDX tumors to determine if our NPs could introduce model genes effectively in both types of tumors. Our results demonstrated the successful delivery of functional mRNA both *in vitro* and *in vivo* in clinically relevant TNBC PDX models. This proof-of-concept study could pave the way for future preclinical studies exploring mRNA therapeutics to combat tumor growth.

3.4 Materials and methods

3.4.1 Materials

PEI (polyethylenimine) and fetal bovine serum were purchased from Sigma-Aldrich (UK), $mPEG_{5K}$-$PLGA_{10K}$ was procured from PolySciTech (West Lafayette, IN), and EGFP-mRNA (N1-Methylpseudouridine/m1Ψ) was purchased from GenScript Biotech (USA). Centrifuge filters were purchased from Pall Corporation (USA), and DMSO was from Fisher Scientific (Canada). Copper grids were obtained from Ted Pella Inc. (USA), UranyLess EM stain was from Electron Microscopy Sciences, and RiboGreen assay reagent was from Thermos Fisher Scientific (USA). Trypsin was obtained from Corning Inc., and Dulbecco's Modified Eagle's Medium was purchased from Wisent Bioproducts (Canada).

3.4.2 Nanoparticle Synthesis and Characterization

EGFP-mRNA and Empty-NPs were synthesized via a self-assembly process using the nanoprecipitation method under cold conditions. Briefly, a 1:2 ratio of EGFP-mRNA (50 μg) in sterile water and PEI-C_{14} lipid (0.1 mM) in DMSO were mixed gently in a glass vial. To this mixture, mPEG–PLGA (0.2 mM) in DMF was added, followed by the addition of excess sterile water, and spun for 2 h (the same concentration of PEI-C14 and mPEG–PLGA was used for Empty-NP synthesis without EGFP-mRNA). After 2 h of stirring, NPs were concentrated at 4 °C by two rounds of centrifugal filtration using 100,000 MWCO filters at 3000 rpm for 10 min. Subsequently, NPs were characterized for size and surface charge by diluting them in 1 mL of sterile water with a dilution ratio of 2:100. The concentrated NPs were stored at 4 °C for further use, and NPs were stable for 2–3 weeks from synthesis. The particle size distribution and morphological appearance of GFP-mRNA were examined under TEM. Briefly, 10 μL of the NP sample was spread onto a Cu grid (300 mesh) for 30 s and allowed to stain using 10 μL of UranyLess. The grid was dried before visualizing under a JEM-1400Plus Transmission Electron Microscope operated at 120 kV. The images were acquired on a FIJI ImageJ software (Java Version). Also, NPs were tested for stability by incubating them for 6 h in 5% or 10% of fetal bovine serum (FBS) at 37 °C, followed by size measurement.

3.4.3 Cell Culture

MDA-MB-231 breast cancer cells were purchased from the American Type Culture Collection (ATCC, Manassas, VA, USA) and maintained in Dulbecco's Modified Eagle Medium (DMEM) supplemented with 10% Fetal Bovine Serum (FBS) and 1% penicillin/streptomycin. SUM149 breast cancer cells were obtained from Asterand (Detroit, MI, USA) and cultured in Hams F-12

media (Mediatech, Manassas, VA, USA) containing 5% FBS, 5 μg/mL insulin, 1 μg/mL hydrocortisone, 10 mM HEPES (pH 7), and 1% penicillin/streptomycin. Both cell lines were cultured at 37 °C in a 5% CO_2 incubator. For all transfection studies, both cell lines were utilized up to the fifth passage.

3.4.4 Fluorescence Microscopy and Flow Cytometry for *In Vitro*

TNBC cell lines, MDA-MB-231 and SUM149 cells, were seeded in a 12-well plate at 50,000 cells per well. The next day, cells were treated with 10 μg/mL EGFP-mRNA-NPs and incubated for 48 h. Live cell imaging was performed by fluorescent microscopy using the ZOE Fluorescent Cell Imager (Bio-Rad, CA, USA), and analysis was carried out using ImageJ (Java Version). For quantitative EGFP analysis, cells were trypsinized and centrifuged. The cell pellet was resuspended in FACS buffer. GFP fluorescence was assessed by using the BD LSRFortessa flow cytometer, and data were analyzed with FlowJo software (v10.10 version).

3.4.5 Patient-Derived Xenografts (PDX)

Protocols followed regarding animal studies were performed in strict pathogen-free conditions, in accordance with guidelines provided by the Animal Care Committee at the University of Ottawa (protocol # BMIe-4035). TNBC PDX HCI-001 and HCI-002 tumor chunks (2 mm × 4 mm) were surgically implanted into the mammary fat pad of NSG mice, and tumor growth was monitored every 3 days using calipers. PDX HCI-001 and HCI-002 tumors were originally generated from two different patients with TNBC and have been well characterized; tumor histology/immunohistology, clinical markers, drug treatment and response, whole exome sequencing, RNA sequencing, RPPA analysis, and growth curve, all have been described and

published in the spreadsheet of PDXNet[180]. For *ex vivo* experiments, tumors were collected and fragmented into a 48-well plate and exposed to either control-NP or EGFP-mRNA-NP for 48 h. For in *vivo* experiments, mice were randomized into two groups, one group receiving control-NP and one receiving EGFP-mRNA-NP. Once tumors reached a mean diameter of 1 cm, NPs were administered via intravenous (i.v.) or intratumoral (i.t.) routes (single dose at 7.3 mg/kg). At 48 h post-treatment, mice were humanely euthanized, and tumors were harvested and minced using a scalpel and incubated in DMEM media containing collagenase/hyaluronidase (STEMCELL Technologies, #07912) at 37 °C for 60 min. Afterward, the solution was passed through a 40-µm nylon mesh to generate a single-cell solution for flow cytometric analysis. For the gating, we first used forward and side scatter to gate single cells, excluding debris as well as doublets and triplets. Next, we gated on live cells by excluding dead cells based on 7-AAD staining, as dead cells can generate autofluorescence. Finally, we identified GFP-positive and GFP-negative cells by setting the cutoff gate using the control sample (NP alone without mRNA-GFP encapsulation).

3.5 Results

3.5.1 Development and Characterization of EGFP-mRNA-NPs

Among different NP platforms, PLGA-PEG polymeric NP systems were well explored and used in our study to deliver EGFP-mRNA. PLGA-PEG NPs consist of biodegradable, biocompatible polymers with a hydrophobic PLGA core and a hydrophilic PEG shell[226]. To encapsulate hydrophilic mRNA within the hydrophobic core of NPs and protect it from degradation, we employed the cationic lipid PEI-C_{14} (Figures S3.1-S3.3) to form ionic interactions with the phosphate backbone of mRNA.

EGFP-mRNA-NPs were synthesized via nanoprecipitation by blending EGFP-mRNA with PEI-C_{14} and $PLGA_{10K}$-PEG_{5K}, and then adding the mixture dropwise to nuclease-free water (Figure 3.1). After purification, dynamic light scattering (DLS, Malvern, UK) measurements were performed to determine NPs size and surface charge. EGFP-mRNA-NPs have a mean particle diameter of 71 nm with a low polydispersity index (0.10), as shown in Figure 3.2A. DLS analysis revealed that the mean surface charge of EGFP-mRNA-NPs is approximately −12 mV (Figure 3.2B)[161,226]. The smaller sizes of EGFP-mRNA-NPs compared to Empty-NPs can be attributed to the tight packaging of mRNA:PEI-C_{14} complexes within the PLGA core and strong hydrophobic interactions between the hydrophobic C-14 tails and the PLGA polymer. This suggests successful mRNA encapsulation within the NPs. Transmission electron microscopy (TEM, JEOL JEM-1400Flash, Japan) confirmed that EGFP-mRNA-NPs were spherical, with an actual size of around 40 nm (Figure 3.2C). Additionally, NPs were tested for serum stability by incubating them in 5% and 10% FBS at 37 °C for 6 h. Following the 6-h incubation, the particle sizes were measured, and no significant change in NPs size was observed compared to their initial sizes (Figure 3.2D)[227]. The encapsulation efficiency of mRNA is measured using the RiboGreen assay[228], revealing that our NPs encapsulated 96% of EGFP-mRNA feed.

3.5.2 EGFP-mRNA-NPs Effectively Protect and Deliver Functional mRNA to TNBC Cell Lines

To evaluate NPs' capacity to enter TNBC cells, escape endosomes, and deliver functional mRNA, we tested NPs using two different TNBC cell lines: mesenchymal MDA-MB-231 and epithelial SUM149[161]. Both cell lines were treated with either control-NPs (Empty-NP) or EGFP-mRNA-NP for 48 h, and the transfection efficacy was examined by fluorescence microscopy and flow cytometry (Figure 3.3). EGFP-mRNA-NPs successfully delivered mRNA to both cell lines, as

observed by GFP expression through fluorescence microscopy. Imaging analysis showed a significant number of cells expressing GFP after the treatment with EGFP-mRNA-NPs compared to Empty-NPs (Figure 3.3C)[205]. These results were corroborated by flow cytometry data, as EGFP-mRNA-NPs induced GFP protein expression around 65% of cells compared to Empty-NPs in MDA-MB-231 cells (Figure 3.3B,D). We did observe a difference in the transfection efficiency between different TNBC cell lines, with rates of approximately 65% and 30% for MDA-MB-231 and SUM149 cells, respectively (Figures 3.3D,E and S3.4 and S3.5). Overall, these results showed that our NPs can effectively deliver functional mRNA to the TNBC cell lines.

3.5.3 mRNA-NPs Can Express Genes of Interest within TNBC PDX Organotypic Cultures *Ex Vivo*

Next, we explored the delivery of functional mRNA agents to tumors using clinically relevant PDX tumors *ex vivo* before transitioning to *in vivo* testing. PDX models are considered more clinically accurate tumor models, as they retain many characteristics of human primary tumors, making them superior to cell line models. Due to the complex nature of PDX animal models, we first examined the transfection efficiency of mRNA-NPs *ex vivo* using PDX organotypic slice cultures. These PDX organotypic slice cultures are 3D structures containing human tumor cells, extracellular matrices, and other tumor components, providing a more accurate alternative to the uniform 2D *in vitro* cell-line-based therapeutic analysis[161]. PDX organotypic cultures have been shown to correlate with in *vivo* results, offering a clinically relevant yet cost-effective and time-efficient testing method[161]. To this end, organotypic slices were made from PDX tumors and cultured *ex vivo*, as illustrated in Figure 3.4A. TNBC PDX tumor HCI-001[180] was surgically engrafted into NSG mice, and when tumors reached 1–2 cm in diameter, they were collected and

dissected to prepare PDX organotypic slice cultures[161]. EGFP-mRNA-NPs and Empty-NPs were added to the PDX organotypic cultures and incubated for 48 h, with mRNA transfection examined by using fluorescent microscopy and flow cytometry. As shown in Figure 3.4B, a significantly higher GFP signal was observed in the treated PDX organotypic tissue when compared to control tissue analyzed through imaging analysis. Additionally, PDX organotypic slices were dissociated into a single-cell suspension for flow cytometry studies. Our flow cytometry analysis, presented in Figure 3.4D, E, confirms the microscopy results. PDX organotypic slices treated with EGFP-mRNA-NPs exhibited a significantly higher number of GFP+ cells compared to those treated with empty NPs. Overall, the combination of our microscopy and flow data suggests efficient transfection and functioning of mRNA-NPs in a PDX slice culture.

3.5.4 mRNA-NPs Effectively Accumulate and Express Target Protein within TNBC PDX Tumors *In Vivo*

Translating *in vitro* effects to *in vivo* is vital for developing clinically relevant mRNA nanotherapies. Therefore, we investigated our in *vivo* profile of EGFP-mRNA-NPs using the TNBC PDX models. Unlike cell-line-based tumors, which are typically homogeneous and lack the complexity of human tumors, PDX tumors retain patient tumor heterogeneity and three-dimensional architecture, correlating with patient clinical outcomes[161,180,224]. To this end, HCI001 and HCI002 tumor chunks (2 mm × 4 mm) were surgically implanted into the mammary fat pad of NSG mice, and tumor growth was monitored every 3 days using calipers. After the tumors reached a mean diameter of 1 cm, we injected either Empty-NPs or EGFP-mRNA-NPs. HCI-001, derived from a patient with disease progression, is paclitaxel-resistant, while HCI-002, from a patient without prior exposure to chemotherapy, is paclitaxel-sensitive and responds better to

paclitaxel treatment compared to HCI-001[180,224]. Our previous studies have shown that these PDX tumors exhibit extensive vasculature, allowing NPs to accumulate in the tumors[161,224,225]. In this study, we investigated if EGFP-mRNA-NPs accumulate in PDX tumors via EPR-related mechanisms, escape endosomes, and deliver functional mRNA. To ensure consistency with our *in vitro* and *ex vivo* studies (illustrated in Figure 3.5A), we administered a single dose of mRNA-NPs either intravenously (i.v.) or intratumorally (i.t.) and analyzed their delivery effects on the PDX tumors 48 h post administration. The dose was determined based on our previous in *vivo* studies using nanoparticles loaded with small-molecule inhibitors and paclitaxel in the HCI-001 and HCI-002 TNBC models[161,224,225].

While i.v. administration of NPs has been widely used in nanomedicine, its administration has been substantially employed in solid tumors to increase in situ bioavailability and efficacy. Consistent with our *in vitro* and *ex vivo* results, we found that the in *vivo* intratumoral administration of EGFP-mRNA-NPs resulted in a significantly higher EGFP expression in all PDX tumor cells, as quantified by flow cytometry shown in Figure 3.5B,D. This is further supported by Figure 3.5E,F, which shows higher GFP expression in HCI-002 tumors 48 h post-i.v. injection compared to Empty-NPs. Additionally, these data confirm that, when administrated via i.v. tail vein injection, EGFP-mRNA-NPs effectively protected mRNA in the bloodstream, accumulated in PDX tumors, and delivered functional mRNA into the tumor cells, resulting in significantly increased GFP expression within the tumor cells.

In contrast, GFP expression was undetectable in vital organs (Figure S3.7). Notably, both PDX HCI-001 and PDX HCI-002 expressed GFP after i.t. administration of EGFP-mRNA-NPs.

However, HCI-002 showed a higher relative expression compared to HCI001 (Figure 3.5C, D). This variability may be attributed to differences in individual patient's tumor responses, underscoring the importance of using patient-derived tumors in screening and optimizing mRNA-based therapies. These findings highlight the potential of i.t. and i.v. administrations of mRNA-NPs in personalized cancer treatment, suggesting a promising avenue for enhancing the efficacy of nanomedicine-based interventions.

3.6 Discussion

mRNA technology holds vast potential for treating a variety of diseases, with the current success of COVID-19 vaccines accelerating the development of mRNA-based drugs[201,202]. In cancer therapy, mRNA-based therapies are mainly explored for gene restoration, gene editing, and inducing cells to produce cytokines/antigens that activate/improve immune responses[151]. For example, NPs carrying PTEN mRNA have been shown to restore PTEN, a tumor suppressor, thereby inhibiting tumor growth in PTEN null or mutated prostate cancer mouse models[205]. Similarly, NPs containing p53 mRNA have reprogrammed the immune tumor microenvironment of hepatocellular carcinoma (HCC) tumors, improving antitumor effects by restoring p53 expression[206]. Deletions or mutations in PTEN and/or p53 are observed in 50–80% of the TNBC subtypes and their metastatic cases, indicating significant potential for PTEN and p53 NPs in TNBC therapies[229–231]. However, current cancer therapies are often evaluated using cell-line-based tumor models, which pose significant challenges for clinical translation due to their lack of predictive value. They fail to retain histologic characteristics, genomic signatures, and tumor heterogeneity of patient tumors, leading to discrepancies between preclinical results and clinical outcomes[222,223]. Additionally, TNBC, in particular, is difficult to treat due to its

heterogeneity and lack of specific targets, making chemotherapy the primary treatment option, which is associated with drug resistance, CSC enrichment, and tumorigenesis[224].

In this context, PDX models represent human tumors' complexity and heterogeneity, exhibiting high clinical concordance. PDX models are created by surgically implanting patient tumors into immunodeficient mice, preserving tumor microenvironment, heterogeneity, and three-dimensional architecture[114,224]. In this study, we demonstrated the effective delivery of mRNA to both mesenchymal MDA-MB-231 and epithelial SUM149 TNBC cell lines, which are typically difficult to transfect. This indicates that our NPs can successfully enter the cells via endocytic pathways, efficiently escape endosomes, and deliver their cargo. We chose two different PDX tumors from two patients with varying chemotherapy exposure, resulting in different sensitivity to chemotherapy, as we previously validated[224]. Our results demonstrated that NPs could effectively transfect PDX tumors without significant differences in transfection efficiency between the two different PDX tumor models, suggesting that our mRNA-NPs may overcome PDX heterogeneity regardless of chemoresistance or chemosensitivity. Additionally, intravenous administration of mRNA-NPs resulted in effective accumulation in PDX tumors via EPR-related mechanisms, protecting the mRNA from degradation and delivering functional mRNA into tumor cells. These results align with previous studies that demonstrated the efficacy of polymeric NPs for mRNA delivery in cell-line-based prostate and HCC tumor models[151,202,205]. However, our study highlights the potential of these NPs in clinically relevant TNBC PDX models. This suggests that our mRNA-NPs platform can be used to deliver therapeutic mRNAs, such as PTEN-mRNA, to PTEN-deficient PDX tumors or p53-mRNA to p53-mutated tumors. Such studies involving the

evaluation of mRNA-NPs in clinically relevant PDX models can bridge the gap in translating mRNA-NPs to clinical applications for cancer therapy[114].

PDX tumors represent a heterogeneous tumor microenvironment of human tumors, encompassing various cell populations, including tumor cells, extracellular matrices, and vasculature[180,224]. While we did achieve efficient delivery of mRNA to PDX tumors overall, further in *vivo* studies need to be performed to determine if mRNA is delivered differentially between tumor cells, tumor-associated macrophages, and other cell populations[232]. It is also important to investigate any differences in the mRNA transfection efficiency among the diverse cell populations in two PDX tumor models. The complexity and heterogeneity of TNBC in different patients cannot be fully represented by only two PDX models. Therefore, further testing of mRNA delivery efficacy using a broader range of PDX tumors is needed to address this limitation. Nonetheless, the consistent results from two different PDX tumor models in our studies suggest a degree of commonality, with significant implications. Additionally, since EGFP-mRNA lacks therapeutic potential, further studies are needed to validate our NPs using therapeutic mRNAs, such as tumor suppressors PTEN and p53, in TNBC PDX models. Furthermore, since our current PDX models use immunocompromised mice, developing TNBC PDX tumors in humanized mouse models for evaluating PTEN/p53 mRNA-NPs will greatly improve the predictive values and advance personalized mRNA nanotherapies toward clinical application.

Although LNP platforms are well-studied for mRNA delivery[201], their potential for cancer applications and tumor accumulation remains underexplored. In contrast, polymeric NP platforms[233] offer versatility with advantages such as controlled and sustained release and stimuli

responsiveness, yet their use in mRNA delivery is insufficiently examined. Previously, we showed that polymeric NPs can efficiently accumulate in TNBC PDX tumors[224]. In this study, we used simple polymeric NP systems that encapsulated a high mRNA load and successfully transfected TNBC PDX tumors after either intratumoral or intravenous administration. These studies indicate that polymeric NPs are effective for mRNA delivery and suitable for cancer applications, opening the door for the exploration of a vast range of polymeric mRNA-NP platforms.

3.7 Conclusion

mRNA-based therapies hold significant potential in treating major diseases including cancer. However, current cell-line-based tumor models do not accurately represent the complexity and heterogeneity of human tumors, often leading to unsuccessful translation of *in vivo* results to clinical trials. PDX tumors offer a more accurate representation of actual human tumors and demonstrate clinical concordance. In this study, we investigated the effect of mRNA-NPs on clinically relevant PDX tumors using EGFP mRNA as a model mRNA and TNBC as the target cancer. Our NPs exhibited high transfection efficiency *in vitro* TNBC cells and *ex vivo* TNBC PDX organotypic cultures. Following intratumoral or intravenous administration, the NPs accumulated in TNBC PDX tumors and successfully delivered the functional mRNA, resulting in GFP expression within the PDX tumors. Since our model system uses human tumors, it will minimize the translational gap from bench to bedside. Additionally, the use of PDX models in our NPs study will pave the way for new and improved approaches in NPs optimization, enhancing the success rate in human clinical trials involving NPs and cancer.

3.8 Figures

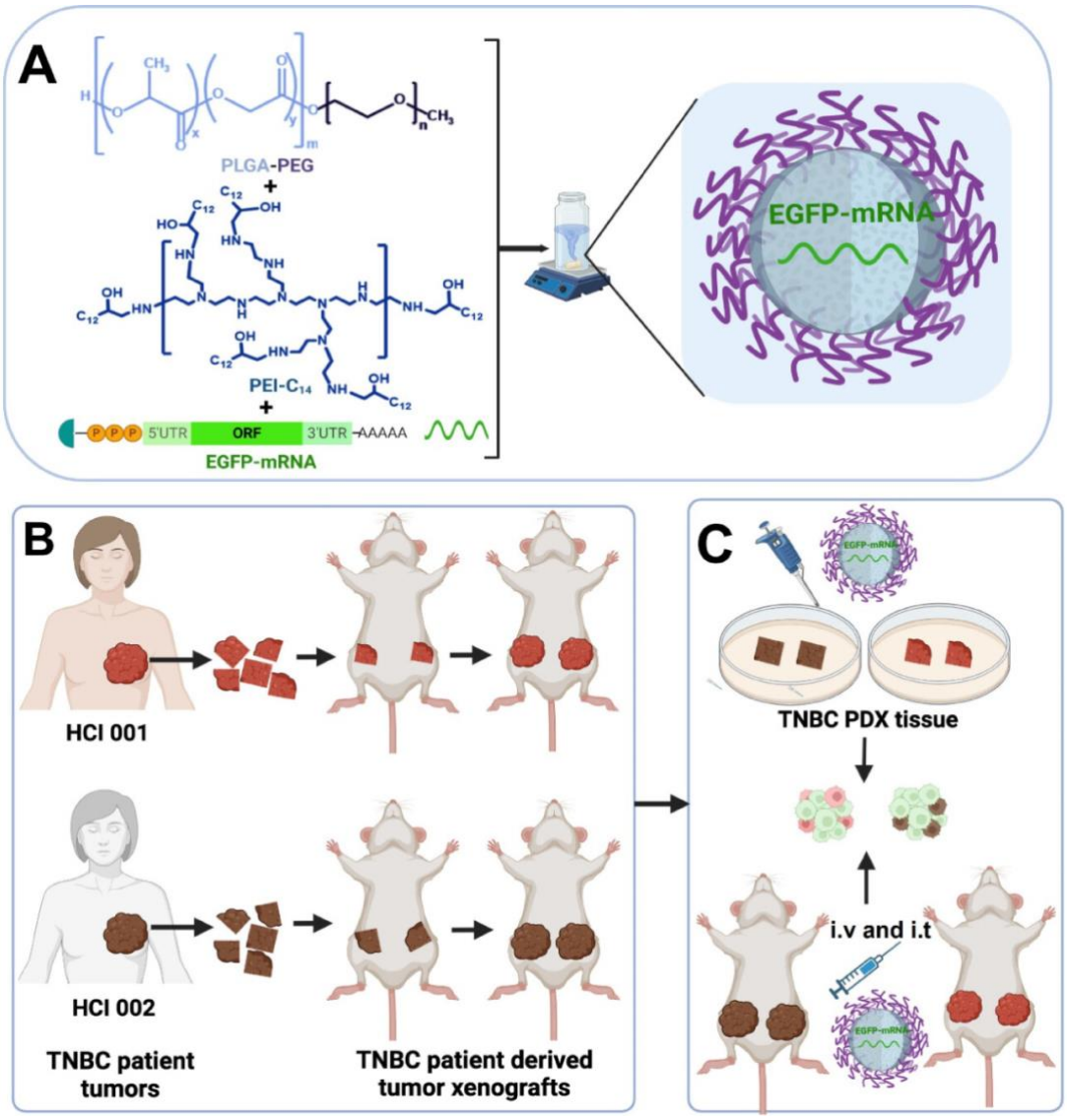

Figure 3.1. (A) The upper panel outlines the schematic diagram of the EGFP-mRNA-NPs synthesis by nanoprecipitation with PEI-C_{14} and PLGA-PEG. (B) The lower left panel outlines the TNBC PDX model development. PDX tumor chunks were surgically implanted into the mammary fat pad of NSG mice to expand and develop TNBC PDX tumors. (C) *Ex vivo* and in *vivo* experimental study plan. To evaluate the effects of EGFP-mRNA-NPs, they were added to TNBC PDX *ex vivo* organotypic slice cultures or in *vivo* administered via i.v. or i.t.

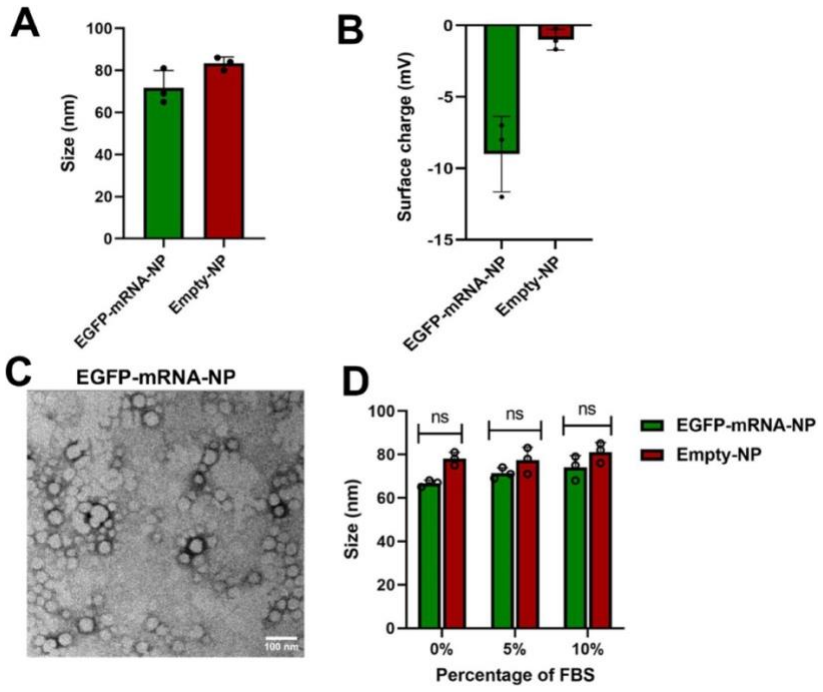

Figure 3.2. Physicochemical characterization of EGFP-mRNA-NPs. (A, B) Size and surface charge of EGFP-mRNA-NPs and Empty-NPs, measured using dynamic light scattering, by diluting 20 µL of NPs in 1 mL sterile water; $n = 3$ data represent means ± SD. (C) Size and morphology of EGFP-mRNA-NP by transmission electron microscopy (scale bar-100 nm). (D) Size of NPs in different percentages of FBS (5–10%), $n = 3$, statistical analysis between Empty-NPs and EGFP-mRNA-NPs, and between three biological replicates by two-way ANOVA (ns-no significant difference).

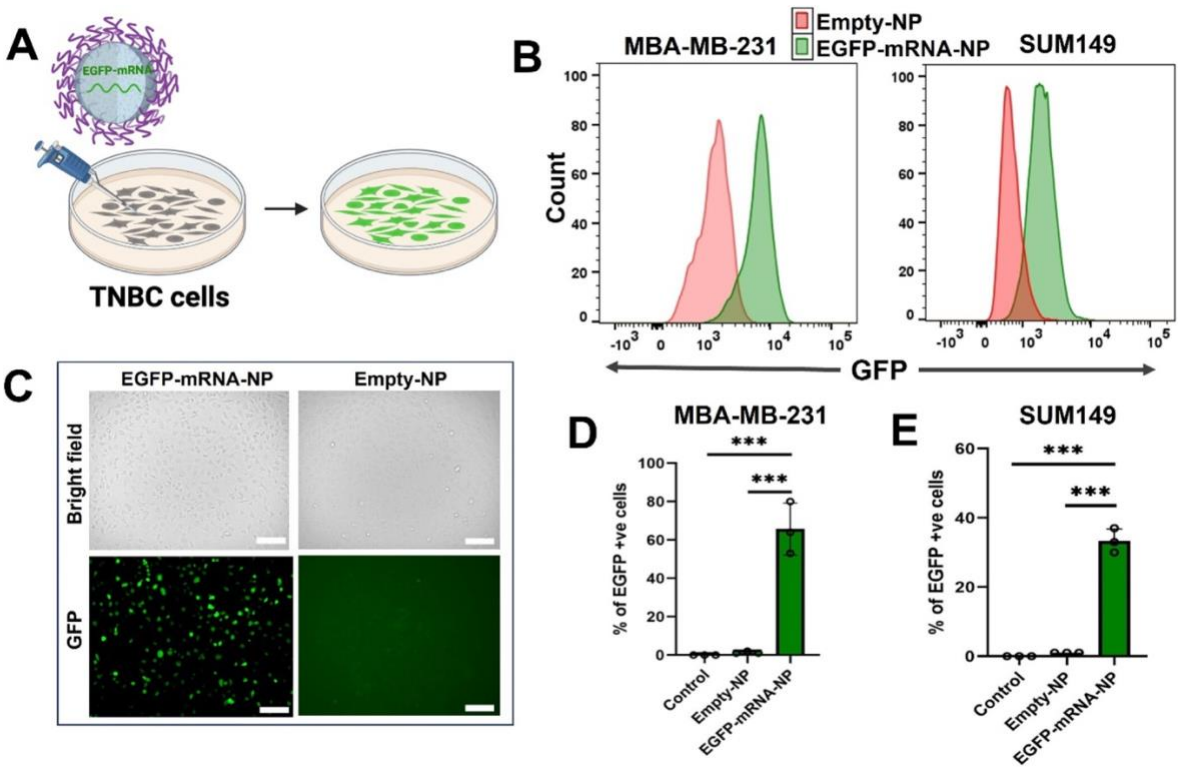

Figure 3.3. EGFP-mRNA-NPs efficiently deliver mRNA to the TNBC cell lines, MDA-MB-231 and SUM149. (A) Model representation of NP treatment to TNBC cells and production of EGFP. (B) Representative flow cytometry histography showing GFP expression in MDA-MB-231 and SUM149 cell lines 48 h post-treatment with EGFP-mRNA-NPs or control-NPs. (C) Fluorescence microscopy images of TNBC MDA-MB-231 cells 48 h after treatment with 10 µg/mL EGFP-mRNA-NPs or Empty-NPs (scale bar-100 µm). (D, E) Flow cytometry analysis of GFP expression in two different TNBC cell lines, MDA-MB-231 and SUM149 48 h post-treatment with EGFP-mRNA-NPs or control-NPs; $n = 3$. Data represent means ± SD, one-way ANOVA statistical difference with control- or Empty-NPs *** $p < 0.001$.

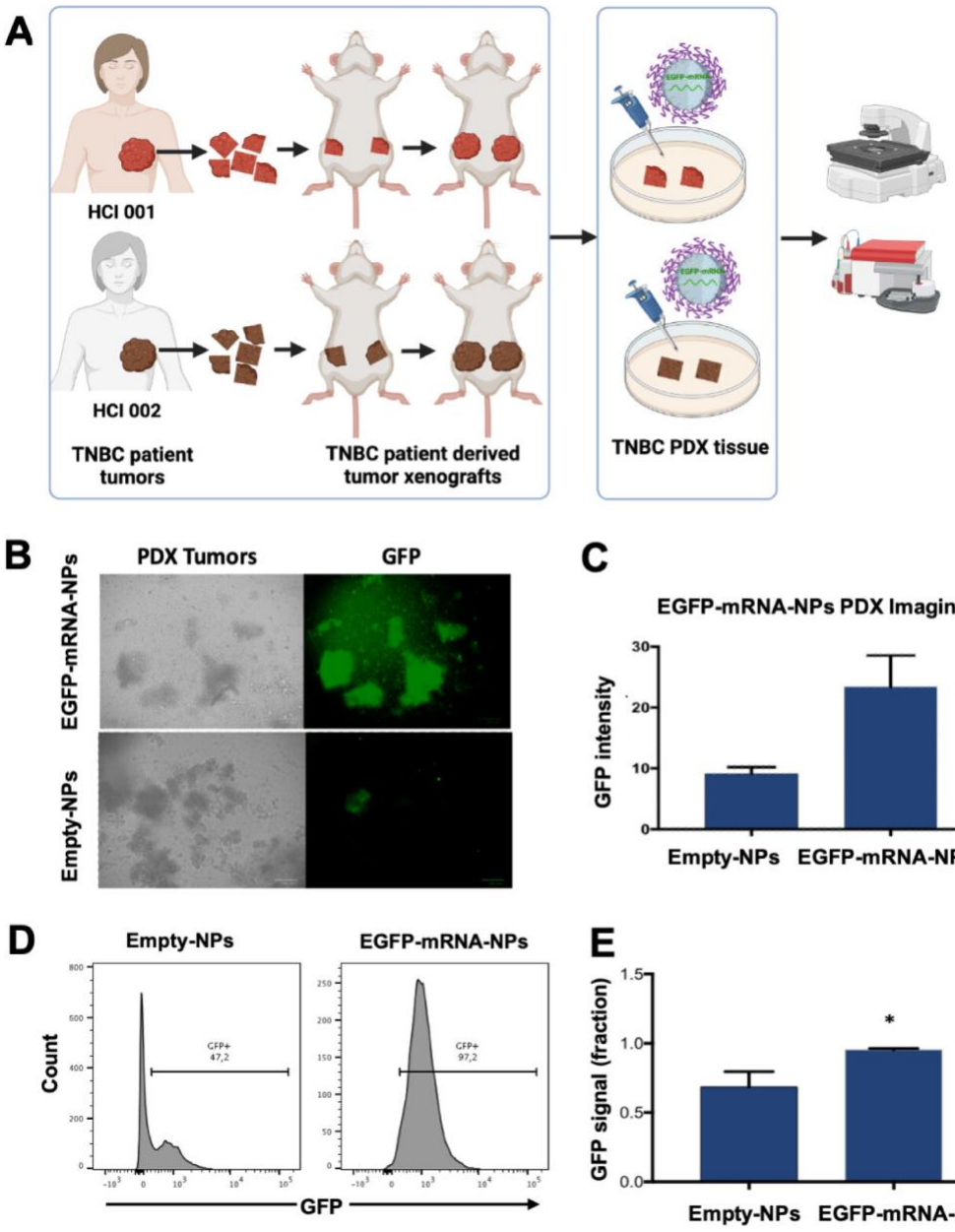

Figure 3.4. EGFP-mRNA-NPs induce GFP expression in TNBC PDX organotypic tissue *ex vivo*. (A) Schematic representation of the extraction and *ex vivo* preparation of TNBC PDX tumors and organotypic cultures. (B) Representative fluorescence microscopy images of TNBC PDX (HCI-001) organotypic tissues 48 h after treatment with 4 µg/mL EGFP-mRNA-NP or control-NPs. Left panel: phase contrast; right panel: fluorescence image. (C) Quantification of GFP intensity using ImageJ. (D) Representative flow cytometric histography of GFP expression in single cells dissociated from TNBC PDX (HCI-001) organotypic cultures after 48 h of treatment with EGFP-mRNA-NPs or Empty-NPs. The analysis includes both live and dead cells, noting some autofluorescence is observed from the dead cells in the Empty-NP treated group. (E) Summary of flow cytometry analysis of GFP expression from PDX organotypic culture of HCI-001. Data represent means ± SEM, $n = 3$, $*p < 0.05$.

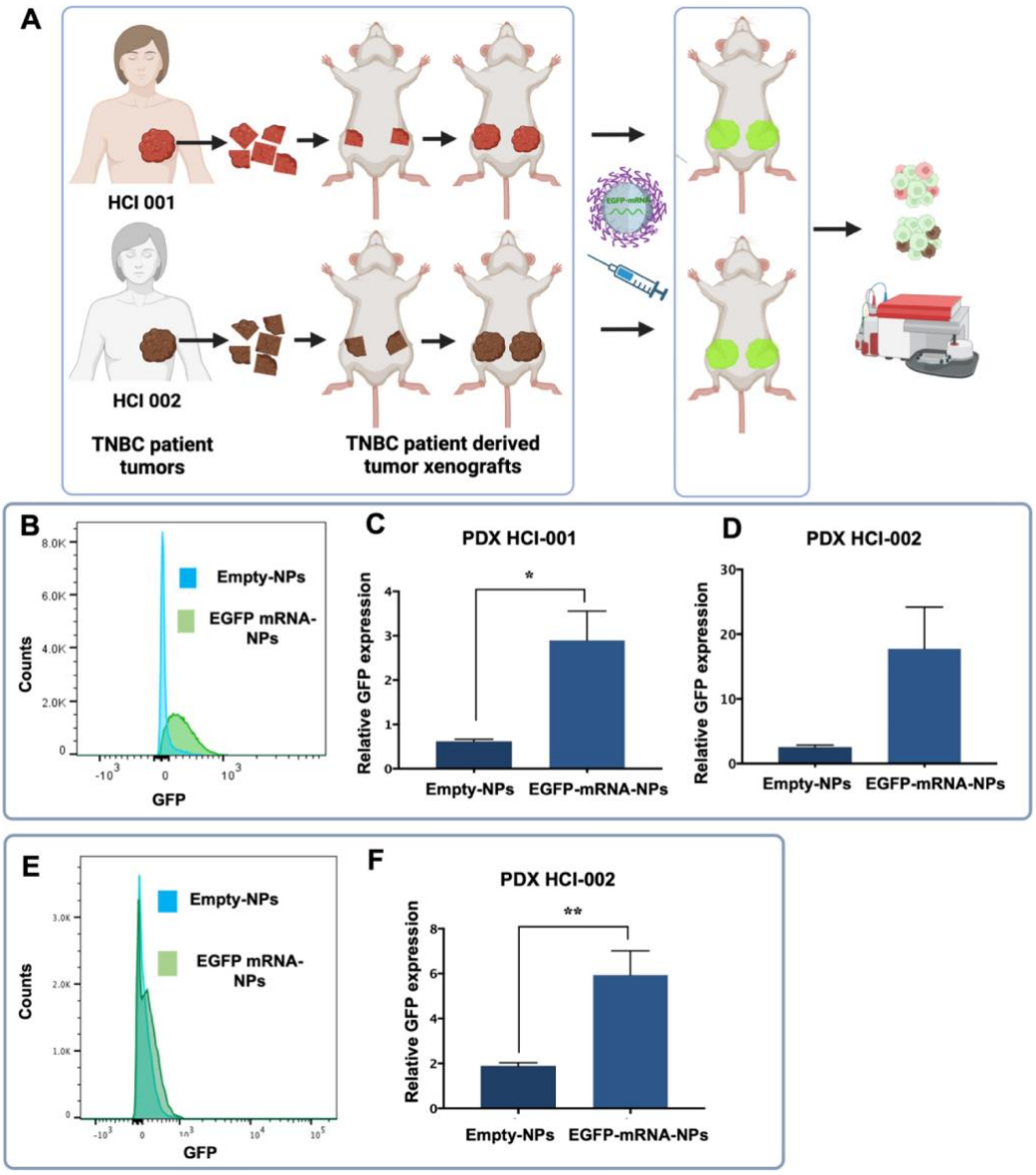

Figure 3.5. EGFP-mRNA-NPs accumulate and express GFP in TNBC PDX tumors in *vivo*. (A) Schematic representation of the PDX model and the administration of EGFP-mRNA-NP for in *vivo* analysis. (B) Representative flow cytometric histography of GFP expression in PDX tumors (HCI-002) 48 h post intratumoral injection (i.t.) of 7.3 mg/kg EGFP-mRNA-NPs (single dose). (C,D) Summary of flow cytometric analysis of two PDX tumors HCI-001 (C) and HCI-002 (D) after i.t. injection of EGFP-mRNA-NPs or Empty-NPs, respectively. (E) Representative flow cytometric histography of GFP expression in PDX tumors (HCI-002) 48 h post intravenous injection (i.v.) of 7.3 mg/kg EGFP-mRNA-NP (single dose). The analyses exclude dead cells, identified by 7-AAD staining. (F) Summary of flow cytometric analysis of PDX (HCI-002) after i.v. injection of EGFP-mRNA-NPs or Empty-NPs. Data represent means ± SEM (Empty-NPs: 1.44, 1.85, 2.10, and 2.12; EGFP-mRNA-NPs: 8.90, 6.12, 4.17, and 4.55). $N = 3$ mice/group for i.t. injections, $n = 4$ mice/group for i.v. injections $^{*}p < 0.05$, $^{**}p < 0.01$.

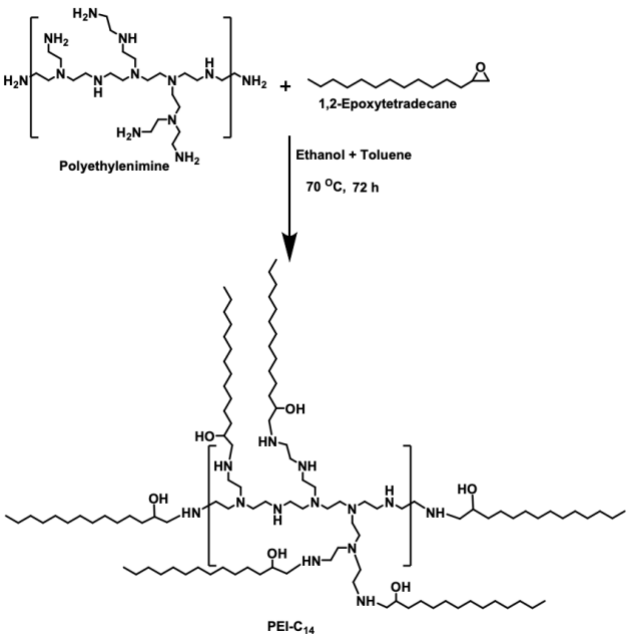

Figure S3.1. PEI-C14 lipid synthetic route: epoxide ring opening by polyethylenimine in presence of ethanol and toluene solvents at 70 °C

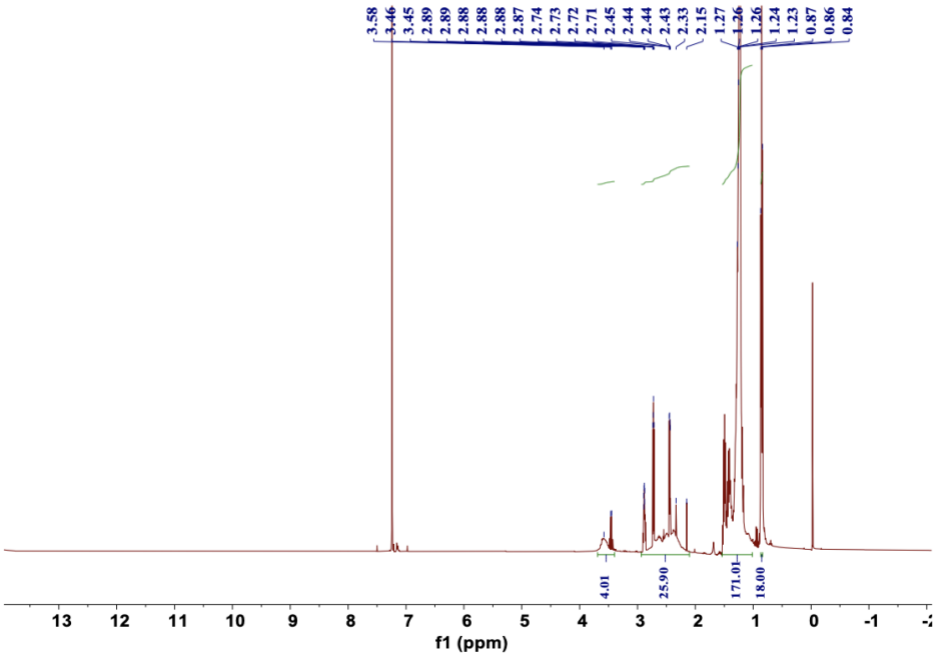

Figure S3.2. 1H (400 MHz Bruker AVANCE) NMR Spectrum of PEI-C14 lipid; 1H NMR (400 MHz, CDCl3) δ 3.71 – 3.30 (m, 4H), 2.91 – 2.10 (m, 26H), 1.51-1.24 (d, m 171H), 0.92 – 0.76 (m, 18H).

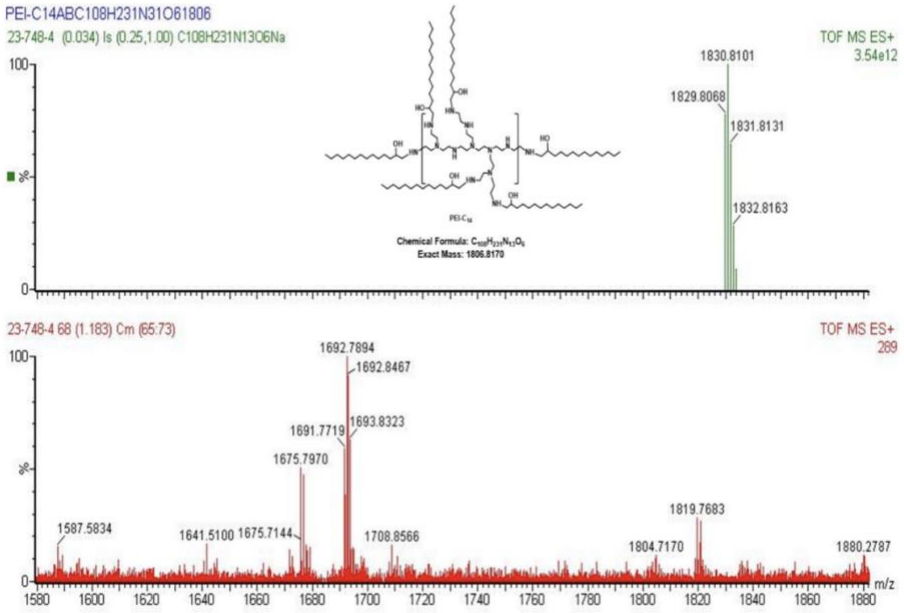

Figure S3.3. Mass spectrum of PEI-C14 lipid. Exact mass of lipid 1806.8170; founded as M+Na 1830.8101.

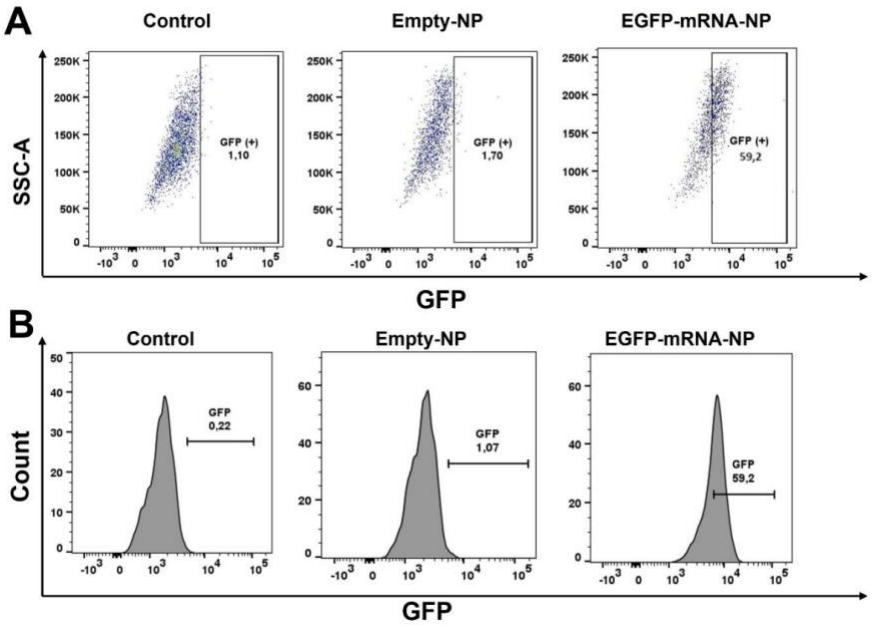

Figure S3.4. Flow cytometry SSC-A plots (A) and histograms (B) for GFP positive cells; EGFP-mRNA-NP and Empty-NP treatment to MDA-MB-231 cells after 48 h recorded GFP by flow cytometry; Control is non-treated cells (Plots are representing from one of the biological replicates).

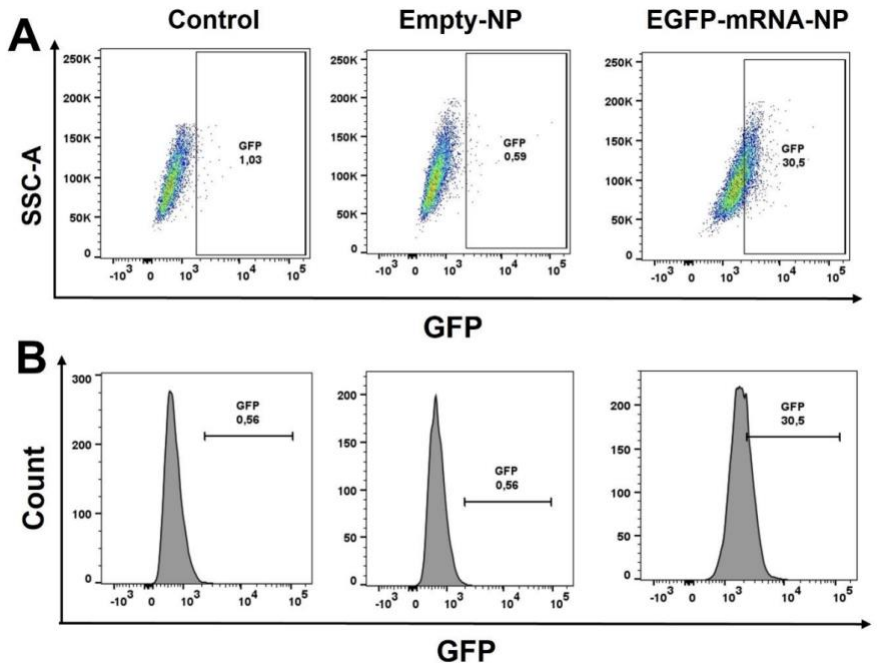

Figure S3.5. Flow cytometry SSC-A plots (A) and histograms (B) for GFP positive cells; EGFP-mRNA-NP and Empty-NP treatment to SUM-149 cells after 48 h recorded GFP by flow cytometry; Control is non-treated cells (Plots are representing from one of the biological replicates).

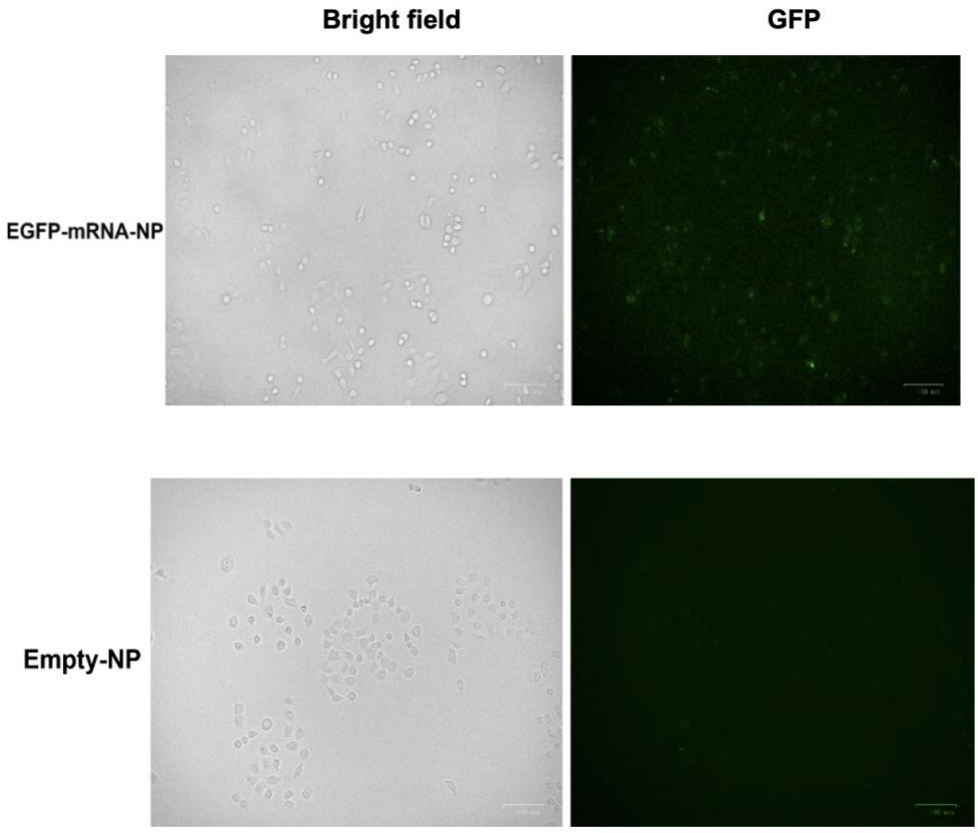

Figure S3.6. GFP fluorescence images of SUM-149 cells after 48 h treatment with EGFP-mRNA-NPs and Empty-NPs.

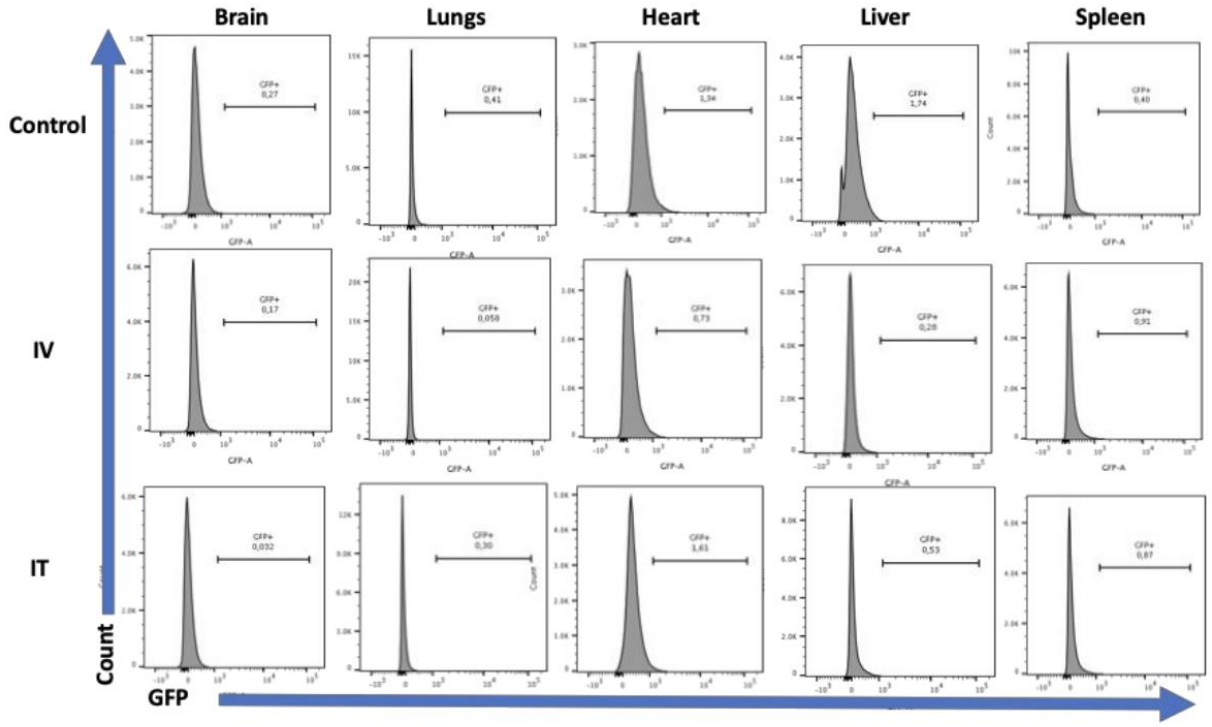

Figure S3.7. Representative flow cytometric histograms of GFP expression in different organs 48 hours post administration of EGFP-mRNA-NPs or control empty-NPs. The analyses exclude dead cells, identified by 7-AAD staining. Data represent means ± SEM, n=3 mice/group for i.t. injections, n=4 mice/group for i.v. injections.

EGFP mRNA (N1-Methylpseudouridine/m1Ψ) ORF sequence:

ATGGTGAGCAAGGGCGAGGAGCTGTTCACCGGGGTGGTGCCCATCCTGGTCG
AGCTGGACGGCGACGTAAACGGCCACAAGTTCAGCGTGTCCGGCGAGGGCGA
GGGCGATGCCACCTACGGCAAGCTGACCCTGAAGTTCATCTGCACCACCGGCA
AGCTGCCCGTGCCCTGGCCCACCCTCGTGACCACCCTGACCTACGGCGTGCA
GTGCTTCAGCCGCTACCCCGACCACATGAAGCAGCACGACTTCTTCAAGTCCG
CCATGCCCGAAGGCTACGTCCAGGAGCGCACCATCTTCTTCAAGGACGACGGC
AACTACAAGACCCGCGCCGAGGTGAAGTTCGAGGGCGACACCCTGGTGAACC
GCATCGAGCTGAAGGGCATCGACTTCAAGGAGGACGGCAACATCCTGGGGCA
CAAGCTGGAGTACAACTACAACAGCCACAACGTCTATATCATGGCCGACAAGCA
GAAGAACGGCATCAAGGTGAACTTCAAGATCCGCCACAACATCGAGGACGGCA
GCGTGCAGCTCGCCGACCACTACCAGCAGAACACCCCCATCGGCGACGGCCC
CGTGCTGCTGCCCGACAACCACTACCTGAGCACCCAGTCCGCCCTGAGCAAAG
ACCCCAACGAGAAGCGCGATCACATGGTCCTGCTGGAGTTCGTGACCGCCGC
CGGGATCACTCTCGGCATGGACGAGCTGTACAAGTAA

CHAPTER 4: NANOPARTICLES CODELIVERING MRNA AND SIRNA FOR SIMULTANEOUS RESTORATION AND SILENCING OF GENE/PROTEIN EXPRESSION IN VITRO AND IN VIVO

4.1 Preface

This chapter contains original research showing the co-delivery of nanoparticles encapsulating RNA agents for simultaneous gene expression and knockdown. This research was published in ACS Nanoscience Au[215].

Manturthi, S.,* El-Sahli, S.,* Bo, Y., Durocher, E., Kirkby, M., Popatia, A., Mediratta, K., Daniel, R., Lee, SH., Iqbal, U., Cote, M., Wang, L., & Gadde, S. (2024). Nanoparticles Codelivering mRNA and SiRNA for Simultaneous Restoration and Silencing of Gene/Protein Expression *In Vitro* and *In Vivo*. *ACS Nanoscience Au*, *4*(6), 416-425.

Author Contributions:

LW, SG, SE and SM conceived and planned the study. SE. and SM contributed equally to the manuscript. All authors were involved in data collection, analysis, and final editing.

4.2 Abstract

RNA-based agents (siRNA, miRNA, and mRNA) can selectively manipulate gene expression/proteins and are set to revolutionize a variety of disease treatments. Nanoparticle (NP) platforms have been developed to deliver functional mRNA or siRNA inside cells to overcome their inherent limitations. Recent studies have focused on siRNA to knock down proteins causing drug resistance or mRNA technology to introduce tumor suppressors. However, cancer needs multitargeted approaches to selectively manipulate multiple gene expressions/proteins. In this proof-of-concept study, we developed NPs containing Luc-mRNA and siRNA-GFP as model agents ((M+S)-NPs) and showed that NPs can simultaneously deliver functional mRNA and siRNA and impact the expression of two genes/proteins in *vitro*. Additionally, after *in vivo* administration, (M+S)-NPs successfully knocked down GFP while introducing luciferase into a TNBC mouse model, indicating that our NPs have the potential to develop RNA-based anticancer therapeutics. These studies pave the way to develop RNA-based, multitargeted approaches for complex diseases like cancer.

4.3 Introduction

RNA-based therapies have the capacity to selectively manipulate gene expressions and hold the potential to revolutionize current therapeutic strategies for various diseases, including cancer[202,234,235]. RNA-based agents such as siRNA, miRNA, and mRNA can downregulate, augment, or correct specific gene products that are otherwise undruggable with small molecules[204,236]. mRNA agents, typically over 2000 nucleotides long, include conventional mRNA, self-amplifying mRNA (saRNA), trans-amplifying mRNA (taRNA), and circular mRNA (circRNA)[151]. These mRNA agents can be designed to carry optimized genetic information and be translated for the production of encoded proteins without integrating into the host genome[151,201,202,237]. mRNA technology offers greater flexibility for targeting various diseases, including cancer, cardiovascular diseases, as well as vaccines[151,237,238]. In cancer treatment, mRNA applications are multifaceted. They can encode tumor suppressors to inhibit cancer cell proliferation, tumor antigens to trigger immune responses, and chimeric antigen receptors (CARs) or T cell receptors (TCRs) for T cell therapies[151,208]. While mRNA therapies can produce specific proteins in the target cells, RNA interference (RNAi), a natural defense mechanism against exogenous genes, can specifically knock down target gene expression[239,240]. RNAi agents, such as siRNA and miRNA, modulate target genes by mediating targeted mRNA degradation (siRNA and miRNA) or mRNA translation repression (miRNA). Both siRNA and miRNA-based RNAi therapies have shown significant potential in cancer therapies, specifically in knocking down/modulating the expression of genes/proteins involved in drug resistance and cancer stem cell (CSC) enrichment, inducing cell death, and sensitizing cancer cells to chemotherapeutic drugs[241,242].

Despite their potential, mRNA and RNAi therapies face several challenges in clinical applications[234]. RNA agents, such as mRNA, siRNA, and miRNA, possess undesirable physicochemical and pharmacological properties, are susceptible to degradation and unwanted immune reactions, and must be effectively delivered into the target cells[234,235,242]. Therefore, sophisticated delivery platforms are essential for developing safe and effective nucleic acid-based therapies[203]. Nanotherapeutic strategies offer several advantages over conventional therapies. Nanoparticle-based drug delivery platforms can encapsulate various therapeutic agents irrespective of their physicochemical properties, protect them from degradation, and deliver them into the cells[217]. However, delivering RNA agents is more challenging than traditional therapeutic agents due to the large size of mRNA (over 2000 nucleotides) and the phosphate backbone common to all RNA agents, which complicates their encapsulation in NPs[201,203,217,240]. Additionally, NPs must escape the endosome and release functional RNA agents into the cytosol to be effective. To overcome these challenges, advanced NP platforms will be required[235,240]. In this context, recent lipid NPs have shown success in delivering either mRNA or siRNA, with examples including ONPATTRO (patisiran), an siRNA-containing NP currently in the clinic for treating hereditary amyloidogenic transthyretin (TTR) amyloidosis, and the Moderna Spikevax and Pfizer-BioNTech COVID-19 vaccines, which are NPs containing mRNA encoding the SARS-CoV-2 spike glycoprotein[237,243]. Despite these successes, strategies targeting a single protein or cytokine are insufficient for complex diseases like cancer and cardiovascular diseases, the leading causes of mortality worldwide[216].

Triple-negative breast cancer (TNBC) is a highly heterogeneous disease that accounts for a disproportionate number of breast cancer-related deaths[162]. Effective treatment strategies must

address significant challenges related to drug resistance, cancer stem cell enrichment, and tumorigenesis, which represent critical unmet medical needs[161,163]. Multiple genes and proteins are implicated in tumor progression and metastasis, including mutations in tumor suppressor genes[244,245]. We recently showed that TNBC stem cells exist in two phenotypically distinct, yet interconvertible, epithelial-like and mesenchymal-like populations, regulated by Wnt and YAP signaling pathways[246]. We demonstrated that simultaneous inhibition of these pathways is essential for developing effective therapy[161,245,246]. Additionally, using clinically relevant TNBC patient-derived xenograft (PDX) models, we also showed that nanotherapies targeting multiple signaling pathways involved in CSC enhancement, in combination with chemotherapy, can arrest PDX tumor growth, suppress CSCs, and diminish tumor regeneration[161,224,225]. In complex diseases like TNBC, CSCs and tumor cells can modulate tumor microenvironments and phenotypical states or enter dormancy to develop resistance to single-agent therapies. Simultaneous targeting of multiple pathways can eliminate both bulk tumor cells and CSCs, ultimately leading to better patient outcomes. In this context, restoring tumor suppressor genes via mRNA to control tumor growth while silencing genes/proteins involved in drug resistance and tumorigenesis using RNAi presents a potent therapeutic strategy for TNBCs.

To date, a variety of NP systems have been developed to encapsulate and deliver two or more drugs with diverse physicochemical properties, including hydrophobic, hydrophilic, small molecules, proteins/peptides, and RNAi agents[161,218,242,247]. These systems are designed to provide different release kinetics, such as spontaneous, controlled, stimuli-responsive, or sequential release[248,249]. However, the codelivery NPs containing both mRNA and siRNA to simultaneously restore and knock down the expression of two different genes have not yet been reported in the

literature. Here, we developed a codelivery 2-in-1 NP system containing both mRNA and siRNA to simultaneously restore and knock down the expressions of two distinct genes. Compared to delivering two agents separately as single-agent NPs or in separate vehicles, combining them in a single 2-in-1 NP system ensures synchronized pharmacological action at both tissue and cellular levels[216,224,242]. Since the biophysicochemical properties of NPs critically influence their nanobio interactions, endosomal escape, and intracellular delivery, encapsulating both agents in a single NP (2-in-1) platform maximizes their codelivery within the tumor microenvironments. This approach ensures that both agents are effectively delivered into the cells and remain functional within the cellular context. As a proof-of-concept, we used Luc-mRNA and siRNA against GFP to develop our NPs, studying their effects *in vitro* and *in vivo* using GFP+ cells as a model. Our results demonstrated that NPs successfully encapsulated both mRNA and siRNA, protected them from degradation, delivered functional agents into the cells, and simultaneously and effectively knocked down and restored the target gene expression in both *in vitro* and *in vivo* settings.

4.4 Materials and methods

4.4.1 Materials and Reagents

mPEG–PLGA was procured from PolySciTech. Polyethylenimine (PEI) and 1,2- epoxytetradecane were purchased from Sigma-Aldrich. EGFP-mRNA and Luc-mRNA were purchased from GenScript Biotech. GFP-siRNA was purchased from Integrated DNA Technologies. Cy5-siRNA universal negative control was purchased from Sigma-Aldrich. Centrifuge filters were obtained from Pall Corporation. DMSO solvent was obtained from Fisher Scientific. Copper grids were obtained from Ted Pella Inc. UranyLess EM stain was procured from Electron Microscopy Sciences. RiboGreen assay reagent and luciferase reagent kit were purchased from Thermo Fisher

Scientific. Dulbecco's modified Eagle's medium was purchased from Wisent Bioproducts, and trypsin for cell splitting was obtained from Corning Inc.

4.4.2 Nanoparticle Synthesis and Characterization

All NPs were synthesized using the nanoprecipitation method by mixing PLGA–PEG, PEI-C_{14}, and mRNA/siRNAs in appropriate ratios. To mRNA (0.08 nmol) or siRNA (4 nmol) in 100 μL of sterile water, PEI-C_{14} lipid (0.1 mM (0.2 mM for dual drug NPs)) was added with 500 μL of DMSO and mixed gently. Subsequently, a solution of mPEG–PLGA (0.2 mM (0.4 mM for dual drug NPs)) in 500 μL DMF was added dropwise. After 10 min of spinning, 2 mL sterile water was added to the NP solution and spinning was continued for 2 h. For empty NP synthesis, a similar concentration of PEI-C_{14} and mPEG–PLGA was used without mRNA or siRNA. Then, NP solutions were concentrated for two rounds for 10 min. The resulting NPs were characterized for size and surface charge and stored at 4 °C. The particle size distribution and morphological appearance of NPs were examined under transmission electron microscopy. Briefly, 10 μL of the sample was spread onto a Cu grid (300 mesh) for 30 s and allowed to stain using 10 μL of UranyLess. The grid was dried before visualizing under a JEM-1400Plus transmission electron microscope operated at 120 kV. The images were acquired on FIJI ImageJ software. Also, NPs were tested for stability by incubating them for 6 h in 5% or 10% fetal bovine serum (FBS) at 37 °C and then measuring the size. The efficiency (EE%) of mRNA in the NPs was measured using the RiboGreen (Thermo Fisher Scientific) assay as previously described[250]. Briefly, single- or dual-drug NPs (15 μL) and 1× TE buffer (235 μL) were mixed as one solution. From this NP solution, three different volumes were taken in a replicate manner in a 96-well black well plate. Next, 1% Triton X-100 buffer was added to each sample. RNA standard solutions were prepared

in 1× TE buffer in the same plate. After 10–15 min, fluorescent RiboGreen reagent was added to NP solutions and RNA standard solutions. The resulting solution's fluorescence intensity was read at an excitation of 490 nm and an emission of 520 nm, using the plate reader BioTek Synergy Neo2 Hybrid Multimode. To measure the amount of mRNA and determine the encapsulation efficiency, we employed a standard curve.

For the siRNA encapsulation efficiency (EE%), the Cy5-labeled siRNA fluorescence intensity was measured. Briefly, in a black 96-well plate, Cy5-siRNA standard solutions (six concentrations) were placed with increasing concentrations. Each Cy5-siRNA concentration's volume was made up to 100 μL with DMSO. In the same plate, Cy5-siRNA-based single- or dual-drug NPs (50 μL) and DMSO (50 μL) were mixed in other wells in a replicate manner. Fluorescence intensity was read at an excitation of 650 nm and an emission of 670 nm, using the plate reader BioTek Synergy Neo2 Hybrid Multimode. A standard curve was made to determine the amount of siRNA and the efficiency of encapsulation.

4.4.3 *In Vitro* Studies

The MDA-MB-231 breast cancer cell line and HT1080 cell line were purchased from the American Type Culture Collection (ATCC, Manassas, VA, USA), and both cell lines were maintained in DMEM media supplemented with 10% FBS and 1% penicillin/streptomycin.

To generate the GFP+ MDA-MB-231, and GFP+ HT1080 monoclonal cell lines, retroviral vectors encoding GFP were produced by cotransfection of HEK293T cells (ATCC) with MLV LTR-GFP, Gag-Pol, and a plasmid encoding VSV-G (all kind gifts of Dr. James Cunningham, Brigham and Women's Hospital) using the JetPrime (Polyplus-transfection) reagent following the

manufacturer's protocol. Supernatants containing the retroviral pseudotypes were filtered (0.45 μm) and used to transduce MDA-MB-231 and HT1080 cells in the presence of Polybrene (3 μg/mL). 48 to 72 h later, transduced cells were seeded at very low density in 10 cm-dishes. Cells were incubated at 37 °C until the generation of colonies, which were selected based on GFP expression as visualized using the ZOE imager (Bio-Rad) and picked using cloning cylinders.

4.4.4 GFP Knockdown

GFP+ cells were seeded in a 12-well plate at 50 000 cells per well. At 60% confluency, cells were treated with (S)-NP (1 nmol) or (M+S)-NP (1 nmol + 0.016 nmol) and incubated for 48 h. Then, the cells were trypsinized and centrifuged. The cell pellet was resuspended with a 1× FACS buffer. GFP knockdown was assessed quantitatively using the BD LSRFortessa flow cytometer, and data were analyzed with FlowJo software.

4.4.5 (Cy5-siRNA+EGFP-mRNA)-NP Co-Delivery to HT1080 Cells

In a 12-well plate, HT1080 cells were seeded with a density of 50 000 cells per well. After 1 day, cells were treated with (Cy5-siRNA+EGFP-mRNA)-NP (1 nmol+0.016 nmol) and incubated for 48 h. GFP production in live cell imaging was performed by fluorescence microscopy using the ZOE Fluorescent Cell Imager (Bio-Rad, CA, USA). Subsequently, cells were trypsinized and centrifuged. The cell pellet was resuspended in a FACS buffer. The percentage of GFP production and Cy5 cellular entry were assessed quantitatively using the BD LSRFortessa flow cytometer, and data were analyzed with FlowJo software.

4.4.6 Luciferase Assay

In a white 96-well plate, at a density of 7×10^3 cells per well (GFP+ or GFP−), the cells were seeded in triplicate 1 day before treatment. Single (0.016 nmol) or dual-drug NPs (1 nmol + 0.016 nmol) were added to cells with fresh media and incubation was continued for 48 h. Then, the medium was removed and each well was added with 50 μL of 1× luciferase lysis buffer and the cells were lysed by a single freeze–thaw cycle. Subsequently, 50 μL of luciferin reagent was added to each well and luminescence reading was initiated using the BioTek Synergy Neo2 Hybrid Multimode Reader.

4.4.7 *In Vivo* Studies

The animal studies were approved by the Animal Care and Use Committee at the University of Ottawa (protocol # BMIe-4035). The MDA-MB-231-GFP+ breast cancer cells were mixed in a 1:1 ratio with Matrigel and injected under aseptic conditions into the mammary fat pads (2×10^6 cells per fat pad) of NSG mice. When the tumor reached a mean diameter of approximately 1 cm, tumor-bearing NSG mice were treated via intratumoral injection (IT) of 50 μL (M+S)-NPs ((2.5 nmol siRNA-GFP + 0.4 nmol Luc mRNA)/mouse) or empty NPs. After 20 h postinjection, relative bioluminescent intensity in tumors and different organs in mice was quantified using the PerkinElmer IVIS Spectrum In Vivo Imaging System (IVIS). Following IVIS, mice were humanely euthanized 24 h postinjection. The tumors were harvested and minced using a scalpel and incubated in DMEM media containing collagenase/hyaluronidase (STEMCELL Technologies, #07912) at 37 °C for 60 min. Afterward the solution was passed through a 40 μm nylon mesh for the creation of a single-cell solution. GFP knockdown was analyzed via flow cytometry, and

luciferase expression was assessed by bioluminescence. $n = 4$ for control empty-NPs and $n = 3$ for mRNA/siRNA NPs.

4.4.8 Flow Cytometry

Dissociated cancer cells were filtered through a 40 μm strainer and suspended in PBS supplemented with 2% FBS and 2 mM EDTA. 1 μL portion of mouse IgG (1 mg/mL) was added and incubated at 4 °C for 10 min. Afterward, the cells were resuspended in 1× binding buffer (eBioscience, San Diego, CA, USA) and incubated with Annexin-V (eBioscience) for 15 min at room temperature. The cells were then washed twice and 7-aminoactinomycin D (7-AAD, eBioscience, San Diego, CA) was added to exclude dead cells. Flow cytometry was performed on a Cyan-ADP 9 or the BD LSRFortessa. Data were analyzed with FlowJo software (Ashland, OR, USA).

4.4.9 Statistical analysis

Data are represented as means ± standard deviation (SD) or standard error (SE). Statistical significance was determined using ANOVA or student's *t*-test wherever appropriate and reported as (*) for $p < 0.05$, (**) for $p < 0.01$, (***) for $p < 0.001$, (****) for $p < 0.0001$, and n for no significant difference. Unless otherwise stated, experiments have a minimum of three biological repeats.

4.5 Results

4.5.1 Development and Characterization of Codelivery NPs

For this proof-of-concept study, we first developed single and dual RNA agents containing NPs via a self-assembling process using a $PLGA_{10K}$–PEG_{5K} polymer. PLGA–PEG polymeric NPs were chosen due to their biodegradability, biocompatibility, stability, scalability, and versatility in various drug delivery applications[233]. To address the hydrophilic nature of RNA's phosphate backbone and facilitate encapsulation within the NPs, we used PEI-C_{14} as a cationic lipid (Figures S4.1 and S4.2). Both single and dual-drug NPs were synthesized using the nanoprecipitation method by blending siRNA and/or mRNA with PEI-C_{14}, followed by the addition of $PLGA_{10K}$–PEG_{5K}, and dropwise addition to nuclease-free water[161]. The resulting NPs were Luc-mRNA containing (M)-NPs, siRNA-GFP containing (S)-NPs, and Luc-mRNA + siRNA-GFP containing (M+S)-NPs (Figure 4.1). NPs were instantly formed with PEI-C_{14}:siRNA and PEI-C_{14}:mRNA complexes embedded in the PLGA hydrophobic core stabilized by a PEG shell[251].

After synthesis, NPs were collected and purified using centrifugal filters and characterized for their physicochemical properties. Hydrodynamic size and surface charge were measured by dynamic light scattering (DLS). All three NPs have uniform sizes ranging between 50 and 60 nm, with low PDI of 0.15–0.28 (Figure S4.4) and surface charges between −0.2 and −20 mV (Figure 4.2A,B,E). TEM characterization of NPs showed all three NP formulations have a spherical shape, and the actual sizes are 40–50 nm, which are lower than DLS sizes as expected (Figure 4.2C). The % of encapsulation efficiency (EE%) of siRNA, measured using Cy5-labeled siRNA, was approximately 92% and 85% for single and dual drug NPs, respectively. EE of Luc-mRNA,

determined by RiboGreen assay, was 100% and 91% for single and dual drug NPs, respectively[228]. We then studied the serum stability of our NPs by incubating them for 6 h at different serum concentrations (up to 10%). Results indicated that NPs remained stable in the presence of serum proteins, as there were no significant changes in NP sizes before and after incubation (Figure 4.2D)[227].

4.5.2 Co-Delivery NPs Capable of Protecting and Delivering Both Functional mRNA and siRNA *In vitro*

To evaluate our NP's capacity to escape endosomes and deliver functional mRNA and/or siRNA, we performed a flow cytometry study. For this purpose, we developed NPs loaded with Cy5-labeled siRNA to mimic siRNA-GFP and EGFP mRNA as model mRNA (Cy5-siRNA+EGFP mRNA)-NPs). The codelivery NPs' size, surface charge, and stability are similar to those of (M+S)-NPs (Figure S4.3A-D). HT1080 cells were treated with (Cy5-siRNA+EGFP-mRNA)-NPs and control NPs for 48 h, and the NP delivery capacity was analyzed by flow cytometry. The Cy5 label could track siRNA in NPs, while GFP expression from the cells revealed functional mRNA delivery[205,252].

After 48 h of treatment, we observed a significant percentage of cells associated with Cy5 (100%) (Figures 4.3B, C and S4.5-4.7) and GFP (25%) (Figures 4.3D-F and S4.5-S4.7) signals, demonstrating that NPs can deliver agents intracellularly and are functional. Despite some Cy5 signal bleeding into the GFP channel, there was a 3-fold increase in the GFP signal in the cells. These results indicate that the NPs successfully entered the cells and delivered both mRNA and siRNA.

Next, we explored whether delivered mRNA and siRNA were functional and simultaneously processed by the cellular machinery to perform their intended functions. To achieve this, we developed monoclonal cell lines of MDA-MB-231 and HT1080 that stably express GFP, termed MDA-MB-231-GFP+ and HT1080-GFP+ throughout the manuscript. These cell lines were created by retroviral transduction and subsequent ring cloning. Before we explored the transfection capacities of dual agent (M+S)-NPs, we studied single agent (M)-NPs and (S)-NPs. To this end, HT1080 and MDA-MB-231 cells were treated with (M)-NPs, and their corresponding GFP+ cell lines were treated with (S)-NPs for 48 h, and luminescence (luciferase RLU) and flow cytometry assays were performed, respectively. Our results showed that, when compared to empty NPs, single agent (M)-NPs and (S)-NPs were successful in delivering functional agents in both cell lines, as shown in Figures 4.4A-E and S4.8-S4.11.

To evaluate the transfection efficiency of our codelivery NPs, we treated both GFP+ cells with (M+S)-NPs and control NPs for 48 h. We assessed the simultaneous delivery of Luc-mRNA and siRNA-GFP by (M+S)-NPs and their effects on the cells. Flow cytometry was used to analyze GFP knockdown induced by siRNA-GFP from (M+S)-NPs, while a luciferase assay was performed to measure the expression of the luciferase gene by Luc-mRNA delivered via the same (M+S)-NPs. The results indicated that our (M+S)-NPs successfully escaped endosomes and simultaneously knocked down GFP expression with siRNA-GFP while introducing the expression of the luciferase gene via Luc-mRNA (Figures 4.4F-I and S4.8-S4.11). Compared to empty NPs, (M+S)-NPs produced a strong bioluminescence signal in both cell lines, confirming the successful delivery of Luc-mRNA by codelivery NPs. Additionally, the mRNA transfection efficiency was higher in

HT1080-GFP+ than in MDA-MB-231-GFP+ cell lines. As expected, (M+S)-NPs delivered siRNA-GFP and also successfully knocked down GFP in both cell types, as evidenced by flow cytometry.

Overall, our *in vitro* studies with GFP+ cells showed that (M+S)-NPs can successfully escape the endosomes, simultaneously knocking down GFP expression and introducing luciferase gene expression into the cells.

4.5.3 Co-Delivery NPs Can Express Target Genes within TNBC Tumors While Simultaneously Silencing Another Gene In *Vivo*

To assess the translation of our (M+S)-NPs' *in vitro* effects into an in *vivo* setting, we studied their efficacy using a TNBC in *vivo* model. As a proof of concept, MDA-MB-231-GFP+ cells were implanted into the mammary gland of NSG mice to produce GFP+ TNBC tumors. Once tumors reached a mean diameter of 1 cm, mice were randomized into two cohorts and treated with (M+S)-NPs and empty NPs for 24 h. Luciferase induction was examined using an in *vivo* imaging system (IVIS) at 0 and 20 h post-treatment and with *ex vivo* bioluminescence at 24 h. GFP knockdown was measured using flow cytometry 24 h of treatment. At 0 h post-treatment, no luminescence was observed in either the control groups or (M+S)-NPs treated groups. However, at 20 h post-treatment, a strong luciferase bioluminescence was detected in the tumors of mice treated with (M+S)-NPs, while those treated with empty NPs showed no luminescence signal (Figure 4.5B). Subsequently, after 24 h treatment, tumors were extracted, single-cell suspensions were prepared, and luciferase bioluminescence and GFP were quantified using bioluminescence and flow cytometry, respectively. Compared to the control treatments, tumor cells treated with (M+S)-NPs

exhibited a significantly strong (>300-fold) luciferase signal (Figure 4.5C). In addition, (M+S)-NPs achieved approximately 20% knockdown of GFP expression in tumor cells (Figure 4.5D,E). These results unequivocally demonstrate that following administration, (M+S)-NPs can penetrate the tumor cells and deliver both mRNA and siRNA, enabling simultaneous knockdown of the target gene product while inducing the expression of another protein.

4.6 Discussion

RNAi and mRNA technologies hold immense potential to treat a variety of diseases by targeting genes that are undruggable for traditional therapies[204]. They offer versatile mechanisms for modulating gene and protein expression, including downregulation, augmentation, or correction. However, the full potential of RNA-based therapies remains unrealized due to inherent limitations, such as stability and unfavorable PK/PD properties. Effective delivery of RNA agents into cells is crucial to their treatment efficacy. In this context, advancements in NP-based drug delivery platforms have paved the way for novel NP systems capable of successfully delivering either siRNA or mRNA. Notably, current clinical successes, such as patisiran, a siRNA-based therapy for polyneuropathy in people with hereditary transthyretin-mediated amyloidosis, and mRNA-based COVID-19 vaccines, have accelerated RNA-based drug development for a variety of therapies[237,243].

In cancer, siRNA agents, alone or in combination with chemotherapeutic agents, are predominantly explored for their ability to silence proteins implicated in drug resistance[241,242]. Conversely, mRNA therapies are primarily studied for their potential to restore tumor suppressor gene/protein expressions, or to produce cytokines/antigens to improve antitumor immune

response[151]. However, cancer is a multifaceted disease, and genomic studies have highlighted that several factors are involved in cancer progression and survival[224,242]. Additionally, single-target therapies for cancer often encounter challenges such as drug resistance and tumorigenesis[225].

In TNBC, conventional chemotherapeutic treatments are frequently associated with drug resistance, the development of cancer stem cells, tumorigenesis, and adverse side effects. Our previous research has shown that multitargeted approaches can effectively control tumor growth and diminish CSC enrichment using clinically relevant tumor models[161,224]. In light of these findings, we reasoned that knocking down or restoring a single target gene may have limitations in effectively treating cancer, necessitating multitargeted approaches. To address this, we developed (M+S)-NPs using siRNA-GFP and Luc-mRNA as model agents to simultaneously restore one gene while silencing the other. This approach represents a promising strategy for overcoming the challenges associated with single-target therapies and advancing the treatment of complex diseases like cancer.

Our results showed that (M+S)-NPs effectively encapsulated both agents, protected them from degradation, and successfully delivered them inside the cells. Notably, despite the size difference between siRNA (20–21 nucleotides) and Luc-mRNA (>2000 nucleotides), the NPs efficiently encapsulated both within a single particle. The encapsulation efficiencies are comparable to those reported for single-agent formulations in the literature. Additionally, our NP's sizes are around 60 nm comparable to our previous NPs known to accumulate in tumors after intravenous administration[224]. *In vitro* and *in vivo* characterization of (M+S)-NPs confirmed their ability to effectively enter cells, escape endosomes, and release their cargo in the cytosol. Additionally,

(M+S)-NPs delivered siRNA-GFP and Luc-mRNA were functional and effective, as evidenced by a significant decrease in GFP expression and an increase in the Luciferase signal in both *in vitro* and *in vivo* studies (Figure 4.4 and 4.5). The significant GFP knockdown and luciferase expression achieved with (M+S)-NPs are comparable to those reported in current nanoparticle systems carrying single agents[205,253]. Within the cells, the two RNA agents are processed differently. While mRNA is recruited into ribosomes for translation, siRNA is incorporated into the multiprotein RNA-induced silencing complex (RISC), which recognizes and cleaves complementary mRNA[236,239]. Our NP results showed that these processes did not interfere with each other and operated independently. However, further studies are needed to understand the kinetics of this complex and any complementary interactions.

Diseases like cancer and cardiovascular diseases are complex and require multitargeted approaches. Our proof-of-concept study demonstrated the feasibility of precisely modulating the expression of multiple genes simultaneously. Drug resistance, CSC enhancement, and tumorigenesis are the primary challenges in current TNBC therapies. Our *in vivo* studies using the TNBC cell line model suggest that we could induce tumor suppressor gene expressions such as *PTEN*, *p53*, or tumor antigens for immunotherapy while simultaneously knocking down the genes/proteins involved in drug resistance/CSC developments[205,206]. Although GFP and luciferase are not directly interconnected, several signaling pathway crosstalks, such as MAPK/ERK and PI3K-Akt, Wnt and NF-kB, and JAK/STAT and RAS/MAPK, have been reported in tumors. Our approach can selectively enhance or interfere with these cross-talks to improve therapeutic outcomes. Additionally, our study suggests that we can synergistically promote antitumoral factors while minimizing protumoral factors via mRNA introduction, RNA interference, translational

inhibition, and/or translational repression. Overall, the studies presented here will pave the way for new therapeutic strategies for complex diseases such as cancer, with significant implications for drug development.

4.7 Conclusion

RNA-based strategies, such as RNAi and mRNA technologies, hold significant promise in treating major diseases, including cancer. Current studies primarily focus on introducing tumor suppressors using mRNA or knocking down proteins that cause drug resistance with siRNA. However, cancer's complexity necessitates multitargeted approaches. To address this, we developed codelivery NPs using Luc-mRNA and siRNA-GFP as model agents. Our NPs were efficiently transfected and successfully functioned in two different cancer cell lines *in vitro*. When administered to a TNBC mouse model created using the MDA-MB-231 GFP+ cell line, the codelivery NPs efficiently knocked down GFP while simultaneously introducing luciferase. This proof-of-concept has significant implications in developing RNA-based multitargeted therapies for complex diseases like cancer.

4.8 Figures

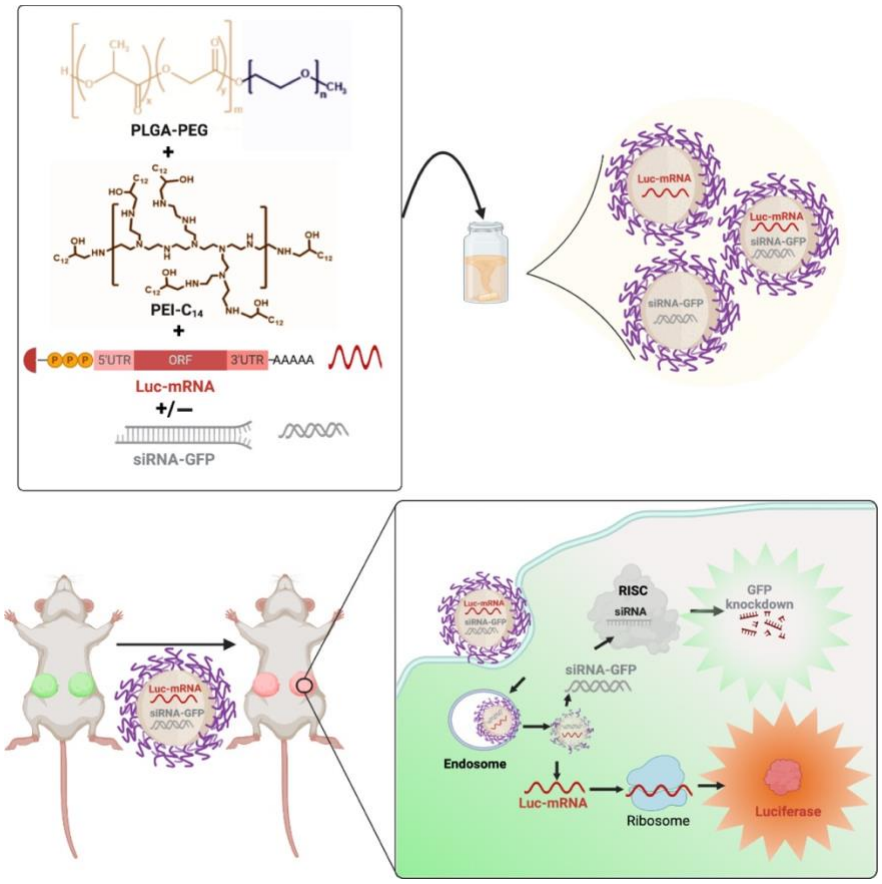

Figure 4.1. Schematic diagram of NP development (upper panel) and their *in vitro* and *in vivo* evaluation (lower panel).

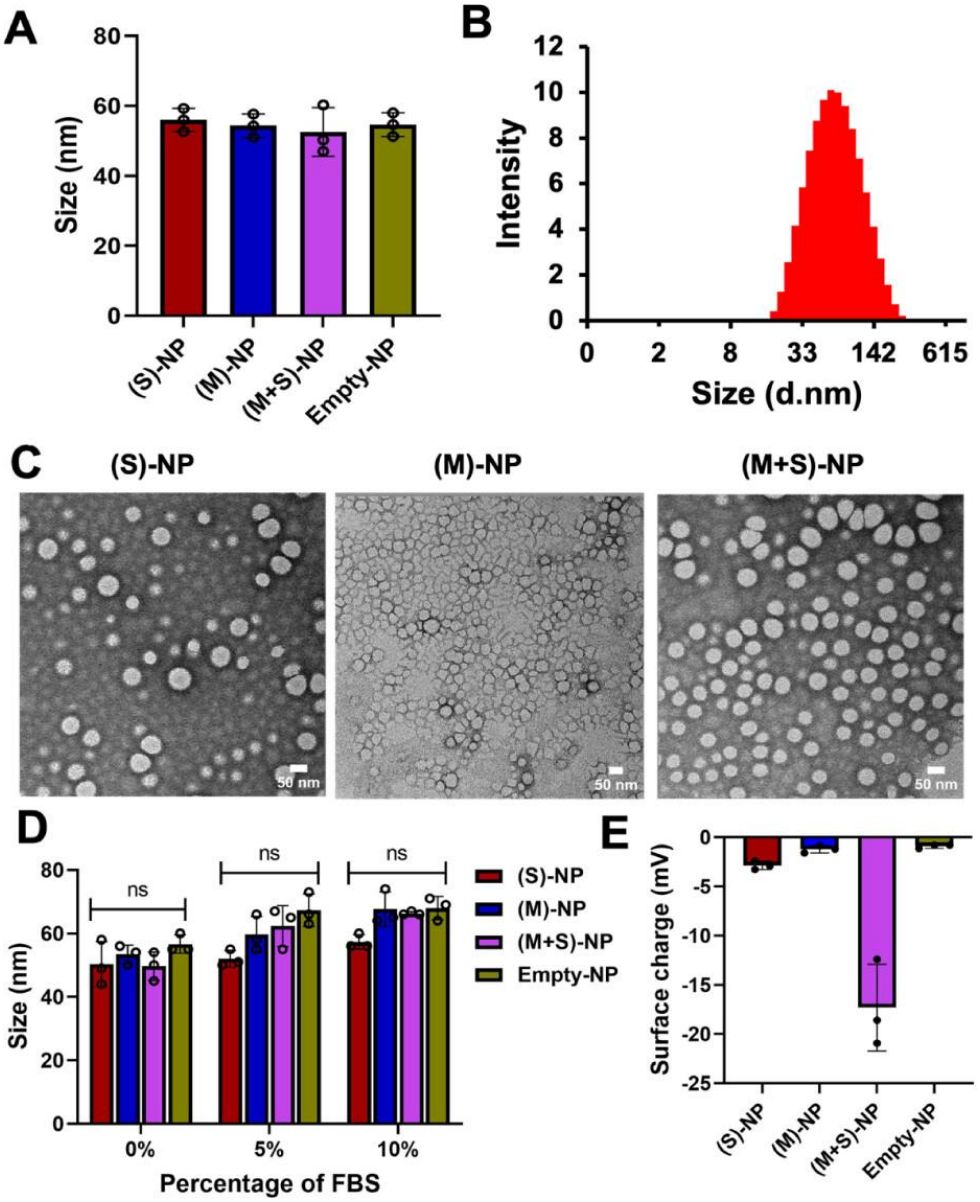

Figure 4.2. Physicochemical characterization of nanoparticles. (A) Size of single- and dual-drug NPs, along with control-NPs, measured by diluting 20 µL of NPs in 1 mL of sterile water using dynamic light scattering, $n = 3$. (B) Size distribution intensity of (M+S)-NPs, measured by DLS. (C) Size and morphology of single and dual-drug NPs by transmission electron microscopy (scale bar: 50 nm). (D) Stability of all the NPs in different percentages of FBS; NPs incubated for 6 h and size was measured; $n = 3$ (ns: no significant difference). (E) Surface of single and dual-drug NPs, along with control-NPs, measured by diluting 20 µL of NPs in 1 mL using dynamic light scattering $n = 3$.

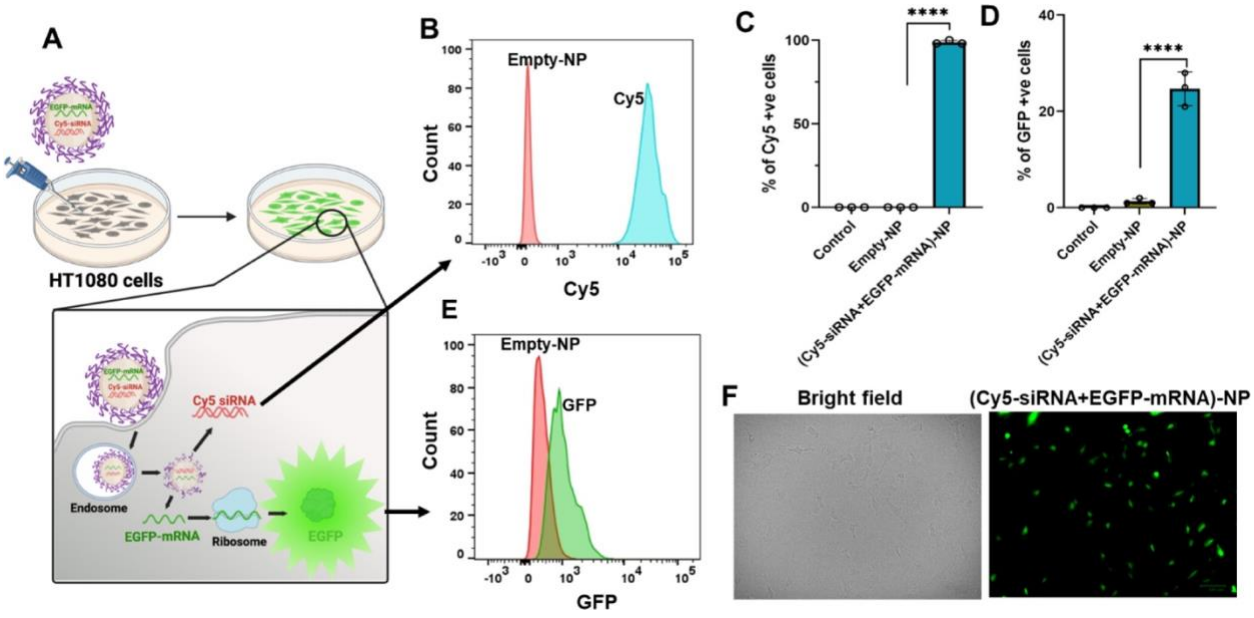

Figure 4.3. Cellular interactions of codelivery NPs. (A) Model representation of NP treatment to HT1080 cells; Cy5 cellular entry and expression of EGFP. (B,E) Representative flow cytometry histogram showing Cy5 and GFP expression in HT1080 cells 48 h post-treatment with Cy5-siRNA+EGFP-mRNA-NPs (1 nmol + 0.016 nmol) or control-NPs. (C,D) Percentage of Cy5 and GFP in HT1080 cells (control: nontreated) quantified by flow cytometry 48 h post-treatment with Cy5-siRNA+EGFP-mRNA-NPs (1 nmol + 0.016 nmol) or control-NPs (10 μM); $n = 3$ (data represent means ± SD, ****$p < 0.0001$). (F) Fluorescence microscopy images of HT1080 cells after 48 h of treatment with dual-drug NPs or empty NPs (scale bar: 100 μm).

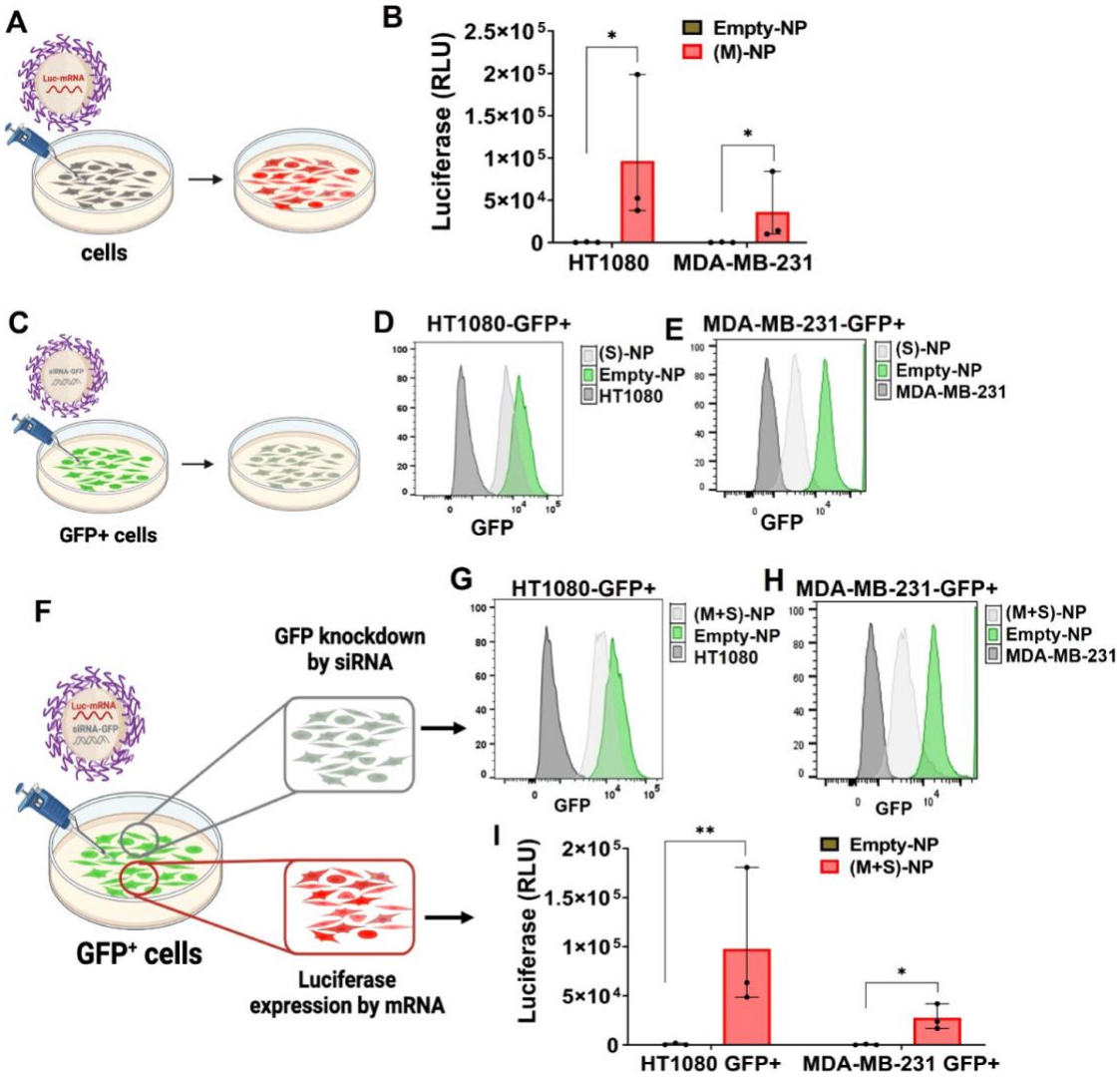

Figure 4.4. Single-drug NP's gene restoration and knockdown, and simultaneous gene restoration and knockdown mediated by codelivery dual-drug NPs using mRNA and siRNA in two cell lines. (A,B) Single drug (M)-NPs (0.016 nmol) and empty-NPs (10 μM) treated with HT1080 and MDA-MB-231 cells, and 48 h post-treatment with luciferase (RLU) measured by a plate reader, $n = 3$ (data represent means ± SD, $*p < 0.05$). (C) Single-drug (S)-NPs (1 nmol) and empty-NPs (10 μM) treated to GFP+ cells (HT1080 and MDA-MB-231). (D,E) Count of GFP knockdown was analyzed by flow cytometry histogram; no GFP cells were used as a positive control. (F) GFP+ cells (HT1080 and MDA-MB-231) were treated with (M+S)-NPs (~60 nm size) coloaded with siRNA-GFP (1 nmol) and Luc mRNA (0.016 nmol) for 48 h. (G,H) GFP knockdown count was analyzed via flow cytometry; no GFP cells were used as positive control. (I) Luciferase expression was measured in GFP+ cells by luminescence, $n = 3$ (data represent means ± SD, $*p < 0.05$, $**p < 0.01$).

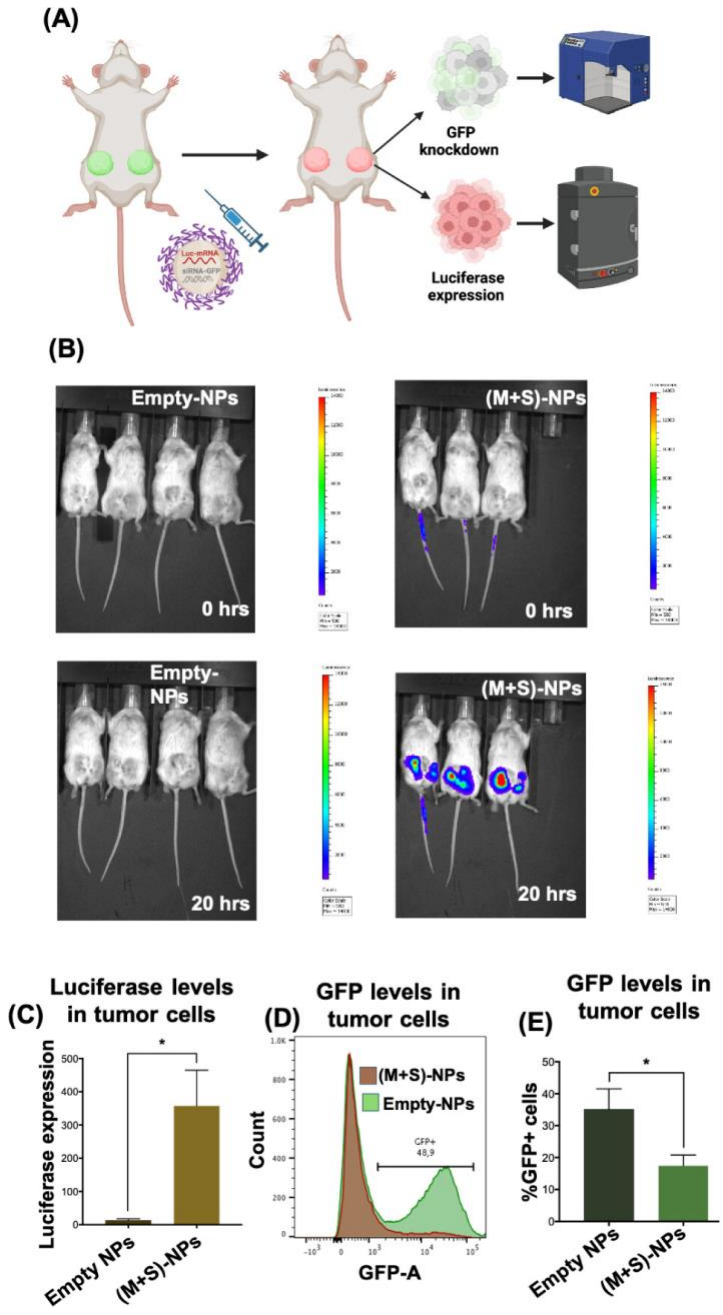

Figure 4.5. *In vivo*, codelivery NPs achieve simultaneous functional restoration and gene knockdown using mRNA and siRNA. GFP+ cells (MDA-MB-231) implanted into the mammary gland of NSG mice were treated via intratumoral injection (IT) with (M+S)-NPs coloaded with siRNA-GFP and Luc mRNA ((2.5 nmol siRNA-GFP + 0.4 nmol Luc mRNA)/mouse) for 24 h (A). Luciferase expression of Luc mRNA was measured using IVIS (B). GFP knockdown and luciferase expression were further analyzed via flow cytometry after dissociation of tumor into single cells (C,D), and the percentage of GFP+ cells was summarized (E). $n = 4$ for control-NPs and $n = 3$ for (M+S)-NPs; $*p < 0.05$.

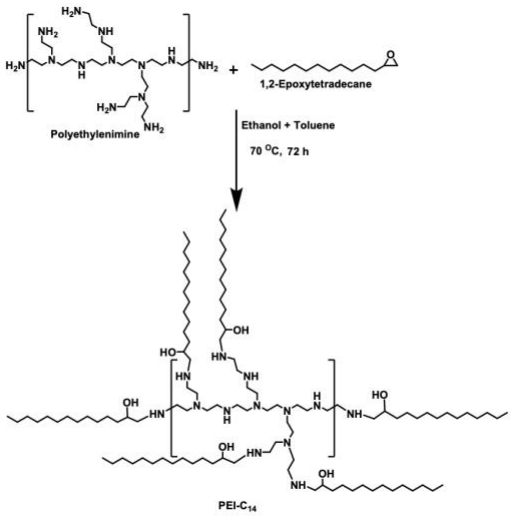

Figure S4.1. PEI-C14 lipid synthetic route: epoxide ring opening by polyethylenimine in presence of ethanol and toluene solvents at 70 °C.

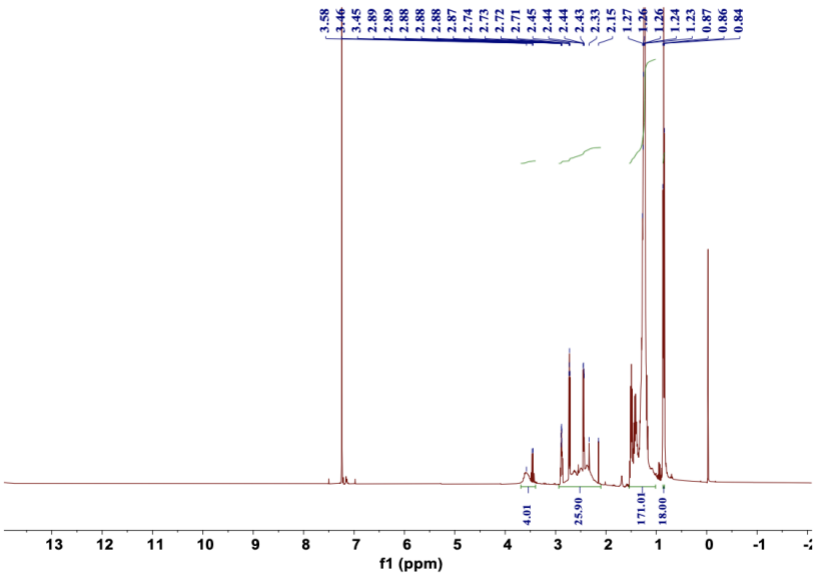

Figure S4.2. 1H (400 MHz Bruker AVANCE) NMR Spectrum of PEI-C14 lipid; 1H NMR (400 MHz, CDCl3) δ 3.71 – 3.30 (m, 4H), 2.91 – 2.10 (m, 26H), 1.51-1.24 (d, m 171H), 0.92 – 0.76 (m, 18H).

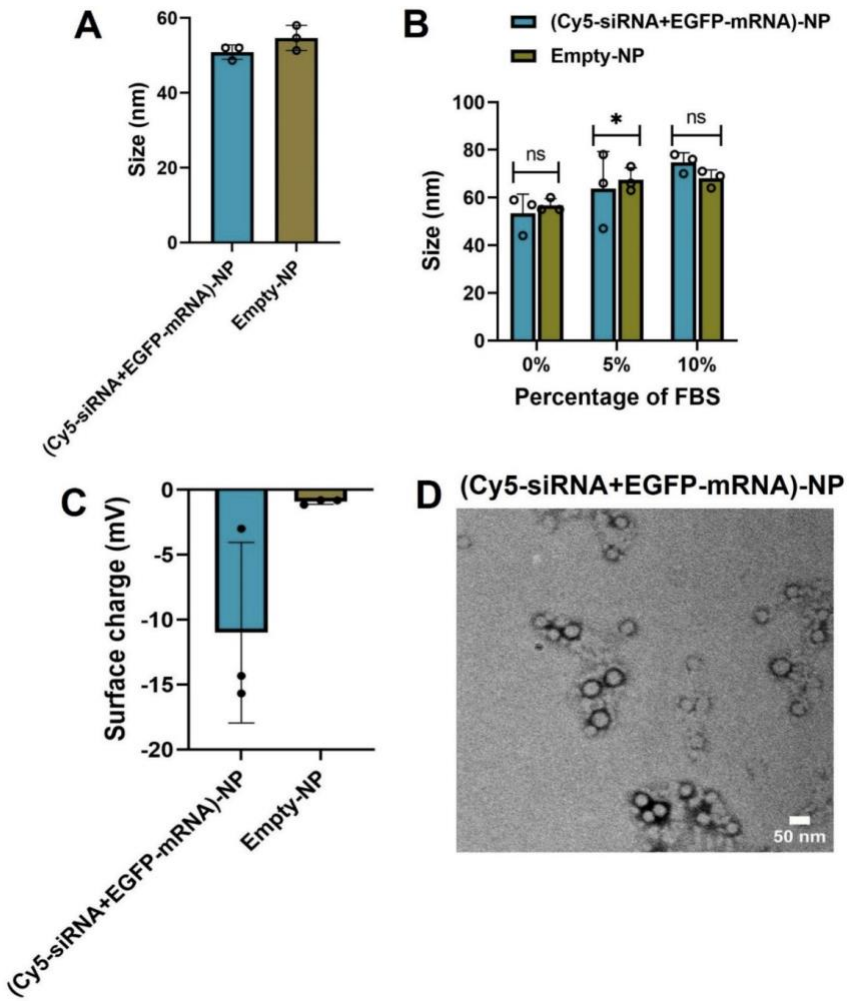

Figure S4.3. (A) Size of Cy5-siRNA+EGFP-mRNA-NPs along with control-NPs, measured by diluting 20 µL of NP in 980 µL sterile water using Dynamic light scattering n=3. (B) Stability of Cy5-siRNA+EGFP-mRNA-NPs in different percentages of FBS; NPs incubated for 6 hours and measured the size; n=3 (ns-no significant difference). (C) Surface of Cy5-siRNA+EGFP-mRNA-NPs along with control-NPs, measured by diluting 20 µL of NP in 980 µL sterile water using Dynamic light scattering n=3. (D) Size and morphology of Cy5-siRNA+EGFP-mRNA-NPs by transmission electron microscopy (scale bar-50 nm).

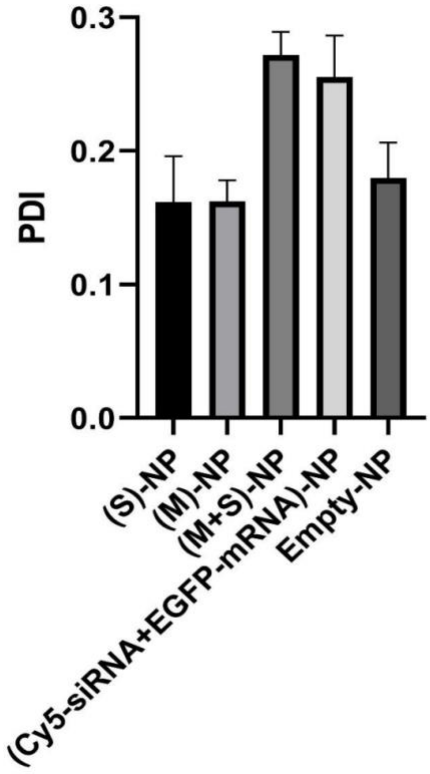

Figure S4.4. PDI (polydispersity index) of all single and dual NPs formulations analysed by DLS; n=3.

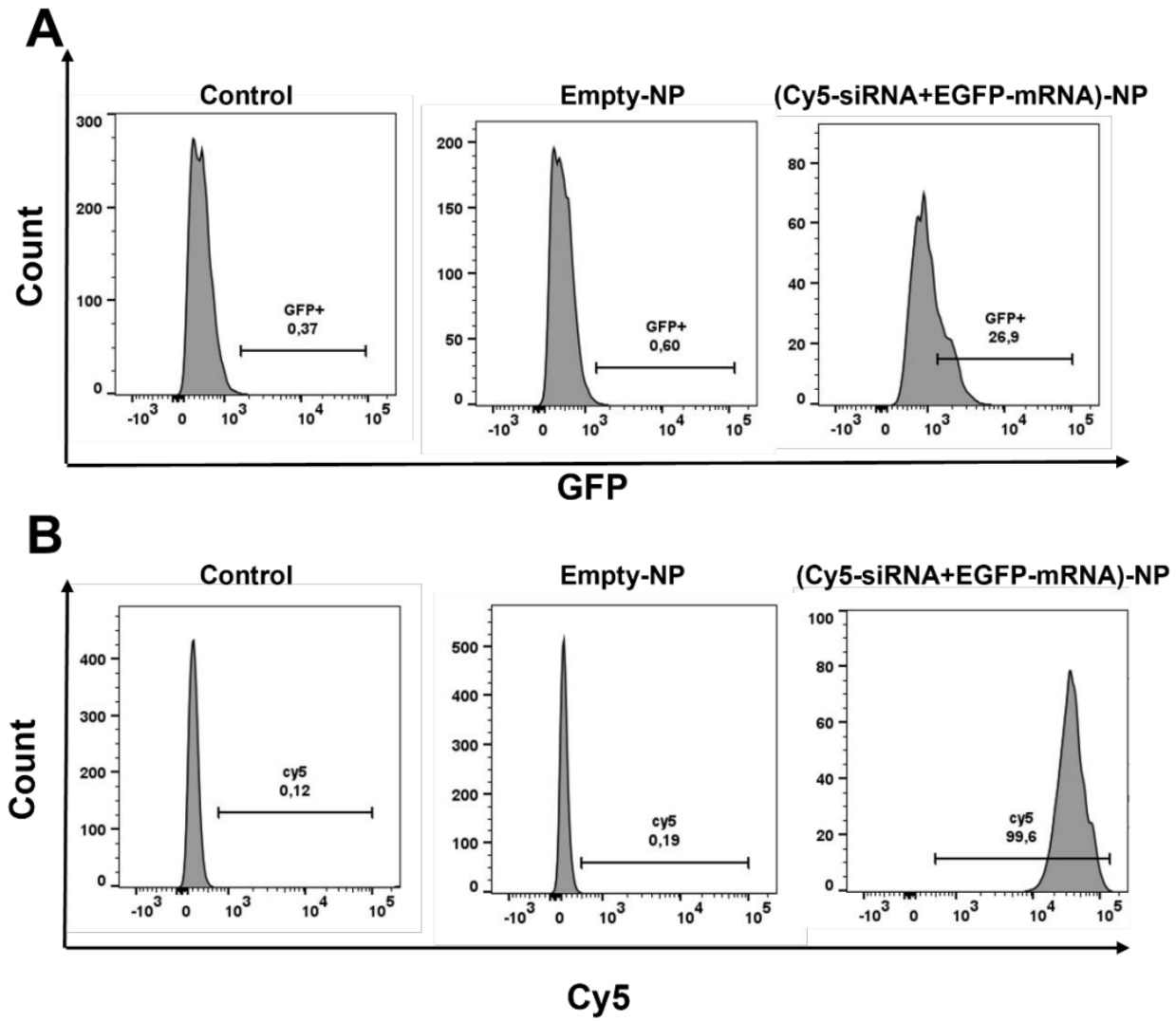

Figure S4.5. Representative flow cytometry histogram showing GFP (A) and Cy5 (B) expression in HT1080 cells after treated with (48 h post-treatment) Cy5-siRNA +EGFP-mRNANPs and Empty-NPs (control is non-treated).

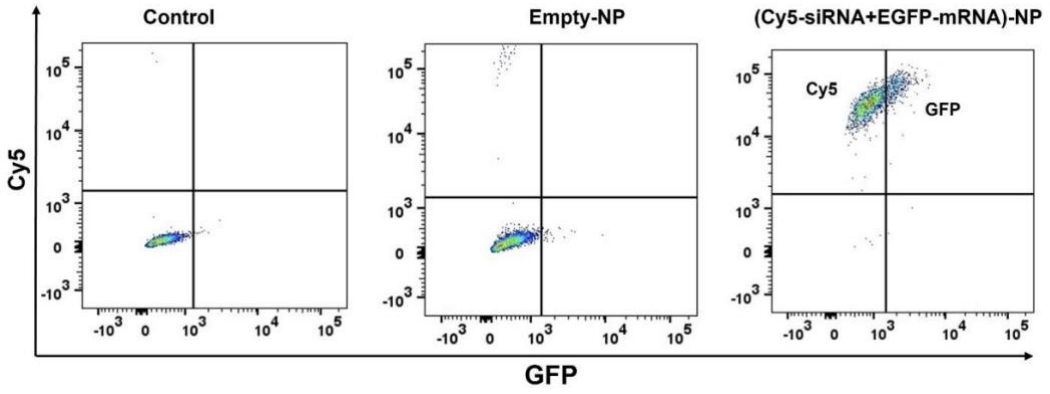

Figure S4.6. Cy5-siRNA+EGFP-mRNA-NPs or Empty-NPs treated to HT1080 cells. Representative flow cytometry histogram showing dual-drug in single plot, GFP population in x-axis and Cy5 population in y-axis; control is non-treated.

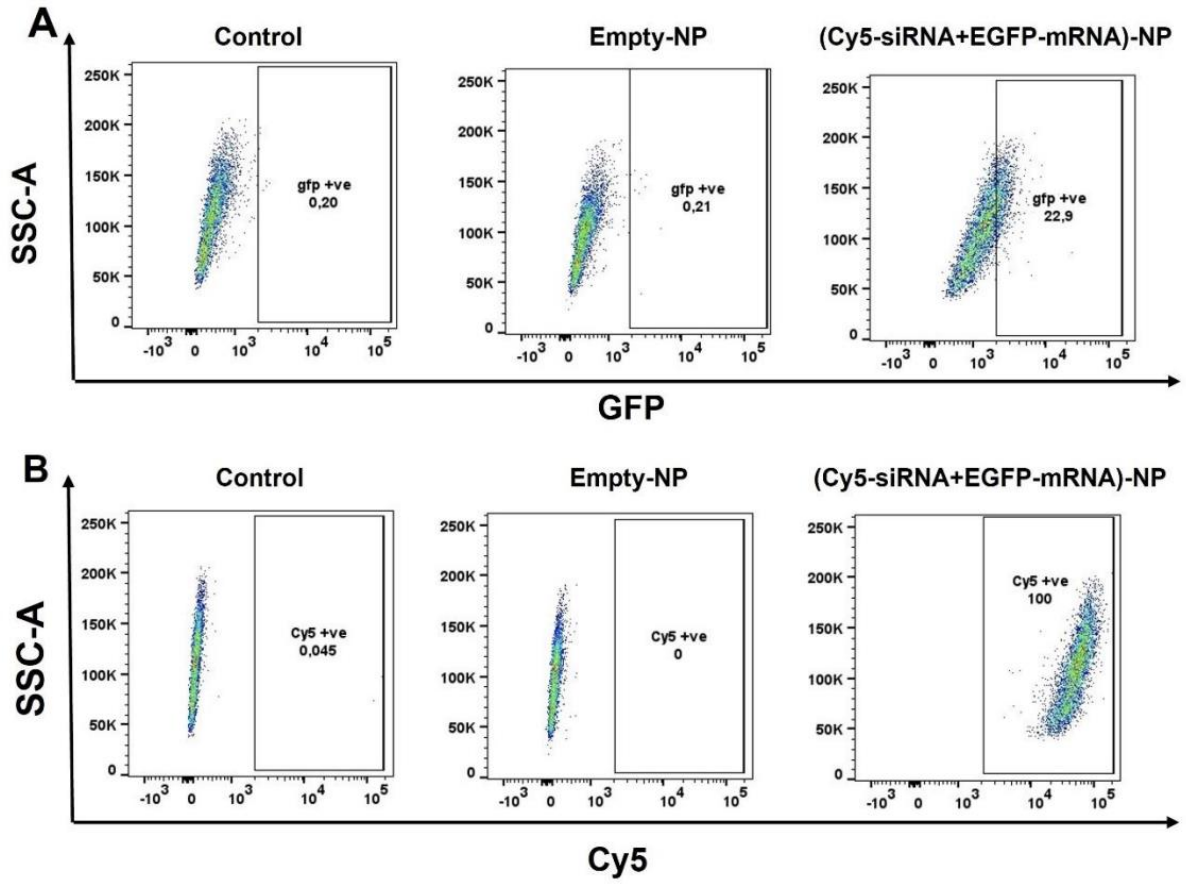

Figure S4.7. Representative flow cytometry SSC-A plots showing GFP (A), and Cy5 (B) expression in HT1080 cells 48 h post-treatment with Cy5-siRNA+EGFP-mRNA-NPs and Empty-NPs (control are non-treated).

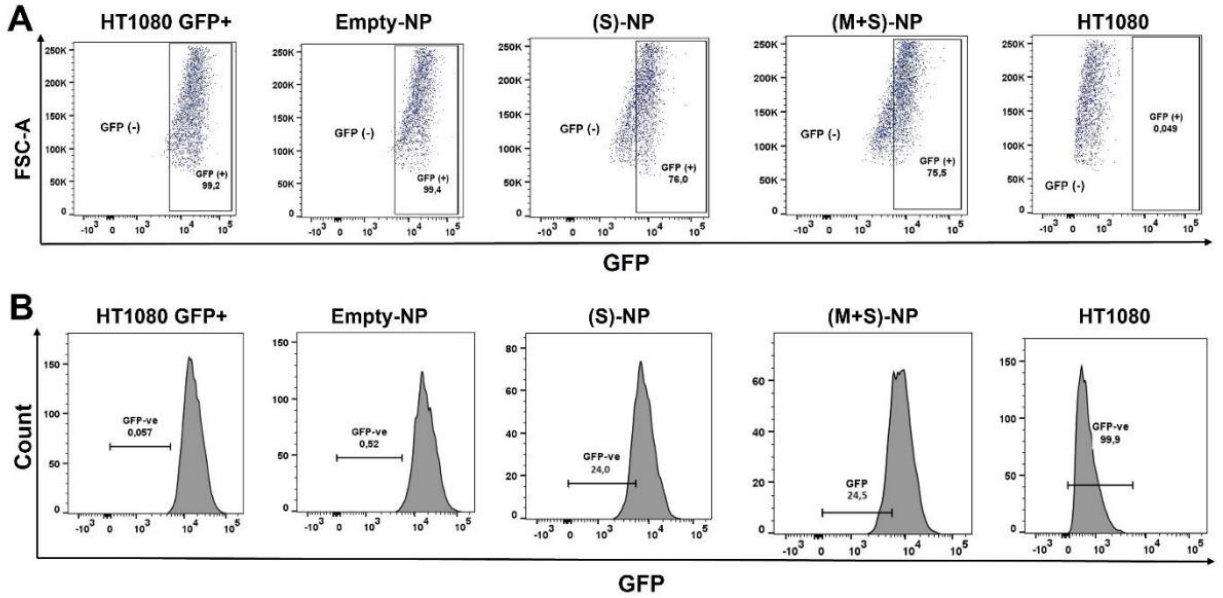

Figure S4.8. Single or dual-NPs along with Empty-NPs treated to HT1080 GFP (+) cells and 48 h post-treatment, the count of GFP knockdown was quantified by flow cytometry; (A) FSC A plots; (B) histograms representing count of GFP knockdown cells. HT1080 cells used as positive control.

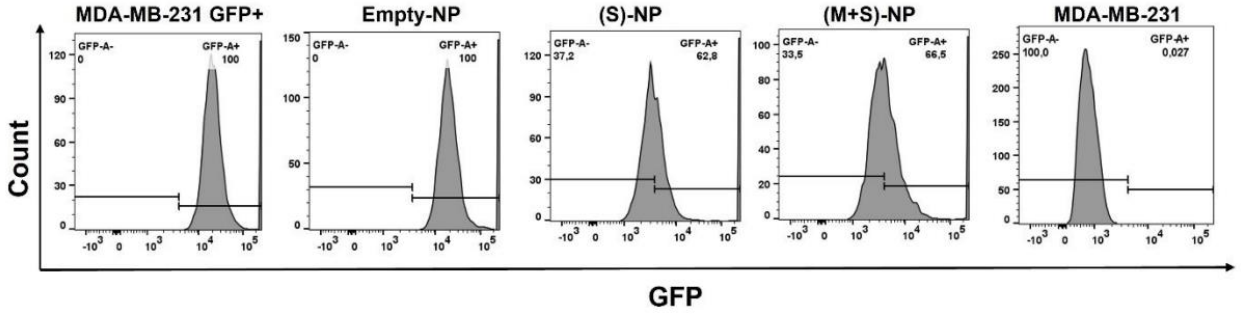

Figure S4.9. Single or dual-NPs along with Empty-NPs treated to MDA-MB-231 GFP (+) cells and 48 h post-treatment, the count of GFP knockdown was quantified by flow cytometry; histograms representing count of GFP knockdown cells. MDA-MB-231 cells used as positive control.

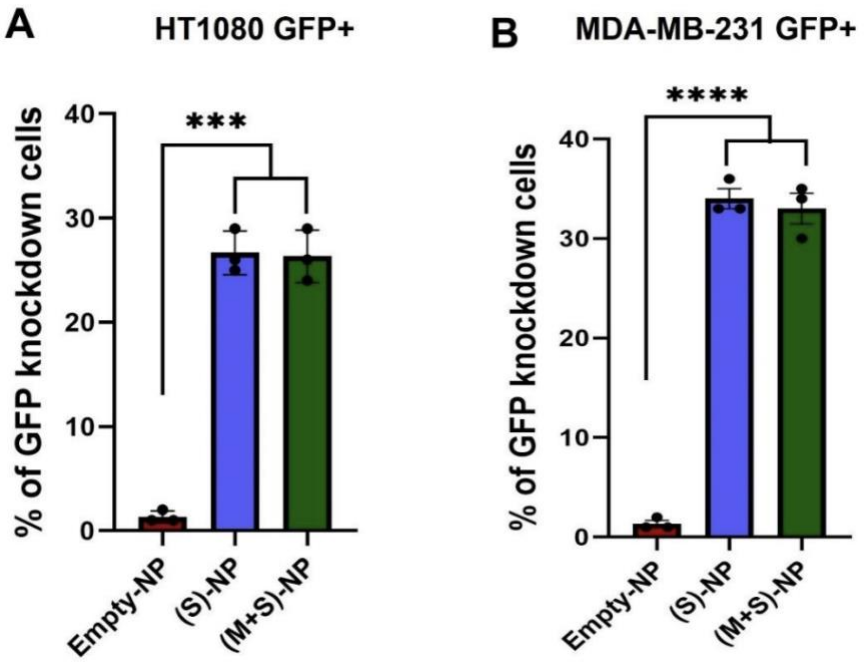

Figure S4.10. Percentage of GFP knockdown in (A) HT1080 GFP+ (B) MDA-MB-231 GFP+ was quantified with flow cytometry analysis; n=3 (Data represent means ± SD, ****p < 0.0001 ***p < 0.001)

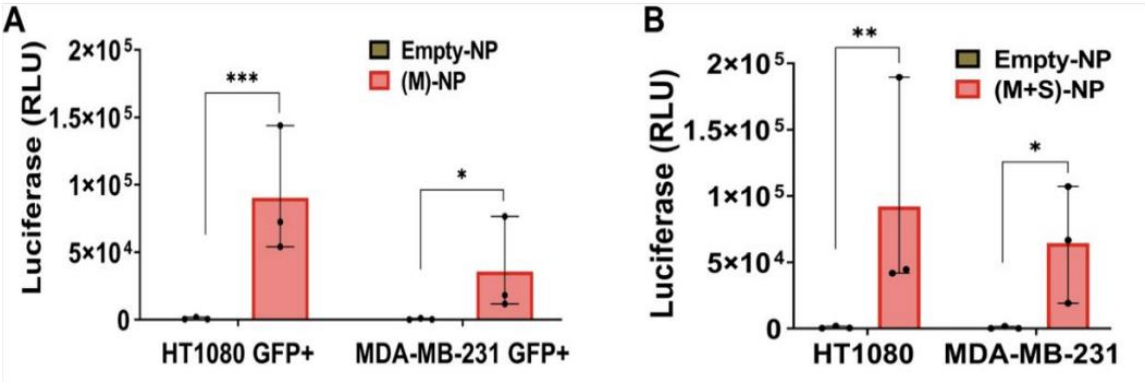

Figure S4.11. (A) Single drug (M)-NPs (0.016 nmol) and Empty-NPs (10 μM) treated to HT1080 GFP+ and MDA-MB-231 GFP+ cells, and 48 h post-treatment luciferase (RLU) measured by plate reader n=3 (Data represent means ± SD, *p < 0.05 ***p < 0.001). (B) HT1080 and MDA-MB-231 cells treated with (M+S)-NPs co-loaded with siRNA-GFP (1 nmol) and Luc mRNA (0.016 nmol) for 48 h, luciferase (RLU) measured by plate reader n=3 (Data represent means ± SD, *p < 0.05 **p < 0.01).

CHAPTER 5: CONCLUDING REMARKS & FUTURE DIRECTION

Breast cancer is the most prevalent cancer in women and, unfortunately, is one of the leading causes of cancer-related death[3]. TNBC, which lacks the ER, PR, and HER-2, is the most aggressive subtype and is commonly associated with the worst prognosis[33]. Chemotherapy remains the first line of treatment but comes with caveats, such as the adverse side effects that result from systemic delivery, as well as the enrichment of a tumor initiating subpopulation, known as CSCs[56]. In addition, TNBC tumors also tend to be more angiogenic, forming new blood vessels that aid in tumor growth and metastasis[101].

In an attempt to target multiple aspects of TNBC tumorigenesis at once, in chapter 2, I designed a triple drug therapy that inhibits bulk cells through the chemotherapy drug paclitaxel, CSCs through the inhibition of YAP signalling (a key CSC pathway) via FDA-approved verteporfin, and angiogenesis through CA4. While paclitaxel exerts its effects by stabilizing microtubules, thereby preventing depolymerization and inhibiting cell division in TNBC cells, CA4 functions through a complementary mechanism. Specifically, CA4 binds to tubulin and disrupts microtubule polymerization[254,255] , a mechanism thought to preferentially target immature endothelial cells within rapidly growing tumor vasculature, as these cells are particularly sensitive to disturbance in microtubule dynamics[255]. Verteporfin, in contrast, has been shown to interfere with YAP signalling, potentially by destabilizing the YAP-TEAD complex and promoting the upregulation of the YAP chaperon protein, 14-3-3 α, which prevents YAP's nuclear localization[95,167]. Together, these agents act on distinct but interconnected aspects of tumor biology, offering a multifaceted strategy to combat overall disease progression.

To develop a therapy that minimizes the side effects of drug treatment, we explored the use of nanoparticles as a vehicle for delivery. Nanomedicine has immensely helped overcome the limitations of free drug therapy as it allows for an increased drug accumulation within the tumor and diminished off-target effects. The results showed that the triple drug therapy (PVC-NP) was able to target TNBC tumorigenesis both *in vitro* and *in vivo* using a clinically translatable patient-derived xenograft (PDX) model. The triple drug treatment was also successful in targeting angiogenesis *in vivo* using a zebrafish model. These results pave the way for a safe, effective therapeutic strategy in clinical settings, maximizing the efficacy of treatment in TNBC patients while minimizing the drawbacks.

The results also reiterated the significance of HIF-1α in TNBC tumorigenesis, which has been previously elucidated by others[103,108], as verteporfin reduced paclitaxel-induced HIF-1α activity and indirectly inhibited VEGF, though the exact mechanism of action remains incompletely understood. Since HIF-1α mediates hypoxia-induced resistance to immunotherapy in TNBC[103], future work should also explore the effect of the triple drug therapy on the hypoxic tumor microenvironment and the subsequent immune evasion in TNBC tumors, as well as its potential to re-sensitize TNBC cells to treatment.

While the study discovers a novel clinically relevant combination, more work is required to explore the effect of PVC-NP on recurrence *in vivo* using a PDX model. This can be done through the serial transplantation assay, where secondary transplantations are performed using serial dilutions based on the CSC frequency *in vivo*[256]. This is considered the best strategy for determining CSCs due to its ability to measure self-renewal and multipotency[256]. Additionally, this study employed

immunodeficient mice to establish PDX models for preclinical analysis. While widely used, this approach precludes the evaluation of immune-tumor interactions, which are central drivers of disease progression in patients. To address this limitation, humanized PDX models have been developed, in which a functional immune system is reconstituted in the immunodeficient mice through the engraftment of human hematopoietic stem cells[257,258]. These models enable the study of the immune contribution to tumor growth providing us with greater insights into the clinical impact of therapeutic interventions. However, their application remains constrained by technical challenges, such as incomplete reconstitution of human immune function and difficulty in the maintenance of immune activity over time[257,259]. Despite these limitations, humanized PDX models represent a highly valuable tool, helping the advancement of translational cancer research.

RNA-based therapeutics offer a distinct advantage over conventional drug therapy by enabling precise targeting and modulation of the expression of genes of interest, which helps reduce the off-target effects often seen in cancer treatment[148]. With that in mind, in chapter 3, we explored the delivery of mRNA using polymeric NPs, maintaining clinical relevance by using two different TNBC PDX models. We demonstrated the successful delivery and tumor accumulation, laying the groundwork for further research and opening future avenues into targeted mRNA-based cancer therapy. Future work could explore the introduction of tumor suppressor genes via mRNA-loaded-NPs to TNBC tumors. Loss of PTEN, for example, is commonly observed in TNBC cases and is thought to contribute to the disease's aggressiveness and metastatic potential[260]. This was previously carried out in melanoma and prostate cancer, where polymeric NPs containing PTEN mRNA were able to promote immune cell infiltration and reduce the immunosuppressive tumor microenvironment. Furthermore, PTEN-mRNA-NP was found to sensitize tumors to

immunotherapy, and co-administration was shown to halt tumor growth[261]. The effect of PTEN-mRNA-NP on the CSC population *in vitro* and *in vivo* could also be investigated for its role in TNBC recurrence and treatment resistance.

Additionally, current mRNA delivery largely depends on lipid-NPs, while our study illustrates the efficiency of polymeric-NPs in mRNA delivery. Future work should conduct a comparative analysis between the two platforms to determine which offers a more effective delivery and leads to the best outcome in a clinical setting. Future studies may also use nanoparticles functionalized with ligands that selectively bind to receptors overexpressed in TNBC cells, enhancing the precision and efficiency of tumor targeting[262]. For example, Rahdari *et al.* (2021) explored the potency of c-peptide-conjugated lipid nanoparticles encapsulating paclitaxel[263]. C-peptide binds to integrin αvβ3 receptors, which are implicated in promoting angiogenesis and metastasis and are associated with poor prognosis[263,264]. Their findings showed a remarkable reduction in tumor growth *in vivo* with C-peptide-linked paclitaxel nanoparticles compared to either paclitaxel nanoparticles without C-peptide or free paclitaxel[263]. Other groups have examined the incorporation of different ligands targeting overexpressed molecules on TNBC cells, such as CD44[265]. However, this approach is limited by the pronounced heterogeneity of TNBC and the expression of these targets on non-tumor cells, raising the risk of off-target effects[266–268].

Even though mRNAs are a promising tool in halting tumorigenesis by restoring tumor suppressors or enhancing anti-cancer immunity, their therapeutic efficacy is often limited by factors such as the heterogeneity of tumors, resistance mechanisms acquired, and pathway redundancy where targeting a single pathway becomes ineffective as other pathways compensate[269–271]. The

combination with siRNAs to silence genes related to tumor growth could offer a multifaceted approach to target multiple aspects of tumorigenesis. Therefore, in chapter 4, we developed an NP platform co-encapsulating siRNA and mRNA. Both agents were delivered intracellularly, induced functional gene silencing and expression *in vitro* and *in vivo*. This paves the way for the simultaneous silencing of CSC-related players, such as YAP, while upregulating anti-cancer immunity in TNBC to target the multiple factors that contribute to its aggressive nature, improving future patient prognosis. Future studies should investigate the efficacy of the simultaneous delivery of these agents, with a focus on optimizing dosing schedules and establishing safety profiles. In addition, evaluating their use in combination with standard chemotherapeutics will be critical to overcoming drug resistance and reducing the risk of disease relapse.

Overall, these studies address critical challenges in preclinical research by using a clinically relevant model to evaluate novel drug combinations that disrupt multiple pathways of tumor growth and by developing platforms for more precise targeting of tumorigenic drivers. Together, this work introduces innovative strategies that lay the groundwork for further preclinical and clinical investigations, moving us closer to effective therapies for TNBC as well as better and improved patient outcomes.

REFERENCES

1. Filho, A. M. *et al.* The GLOBOCAN 2022 cancer estimates: Data sources, methods, and a snapshot of the cancer burden worldwide. *Int J Cancer* **156**, 1336–1346 (2025).
2. Arnold, M. *et al.* Current and future burden of breast cancer: Global statistics for 2020 and 2040. *Breast* **66**, 15–23 (2022).
3. Heer, E., Ruan, Y., Mealey, N., Quan, M. L. & Brenner, D. R. The incidence of breast cancer in Canada 1971-2015: trends in screening-eligible and young-onset age groups. *Can J Public Health* **111**, 787–793 (2020).
4. Lagacé, F. *et al.* Analysis of incidence, mortality trends, and geographic distribution of breast cancer patients in Canada. *Breast Cancer Res Treat* **178**, 683–691 (2019).
5. Kirkham, A. A. & Jerzak, K. J. Prevalence of Breast Cancer Survivors Among Canadian Women. *J Natl Compr Canc Netw* **20**, 1005–1011 (2022).
6. Sharma, R. Global, regional, national burden of breast cancer in 185 countries: evidence from GLOBOCAN 2018. *Breast Cancer Res Treat* **187**, 557–567 (2021).
7. Łukasiewicz, S. *et al.* Breast Cancer-Epidemiology, Risk Factors, Classification, Prognostic Markers, and Current Treatment Strategies-An Updated Review. *Cancers (Basel)* **13**, (2021).
8. Benz, C. C. Impact of aging on the biology of breast cancer. *Crit Rev Oncol Hematol* **66**, 65–74 (2008).
9. Wilkinson, A. N., Ng, C., Ellison, L. F. & Seely, J. M. Breast cancer incidence and mortality, by age, stage and molecular subtypes, by race/ethnicity in Canada. *Oncologist* (2024) doi:10.1093/oncolo/oyae283.
10. Chen, X., Wang, Q., Zhang, Y., Xie, Q. & Tan, X. Physical Activity and Risk of Breast Cancer: A Meta-Analysis of 38 Cohort Studies in 45 Study Reports. *Value Health* **22**, 104–128 (2019).
11. Fiolet, T. *et al.* Consumption of ultra-processed foods and cancer risk: results from NutriNet-Santé prospective cohort. *BMJ* **360**, k322 (2018).
12. Xiong, X. *et al.* Breast cancer: pathogenesis and treatments. *Signal Transduct Target Ther* **10**, 49 (2025).
13. Arpino, G. *et al.* Tumor characteristics and prognosis in familial breast cancer. *BMC Cancer* **16**, 924 (2016).
14. Hu, C. *et al.* A Population-Based Study of Genes Previously Implicated in Breast Cancer. *N Engl J Med* **384**, 440–451 (2021).
15. Fu, X., Tan, W., Song, Q., Pei, H. & Li, J. BRCA1 and Breast Cancer: Molecular Mechanisms and Therapeutic Strategies. *Front Cell Dev Biol* **10**, 813457 (2022).
16. Carbognin, L., Miglietta, F., Paris, I. & Dieci, M. V. Prognostic and Predictive Implications of PTEN in Breast Cancer: Unfulfilled Promises but Intriguing Perspectives. *Cancers (Basel)* **11**, (2019).
17. Beg, S. *et al.* Loss of PTEN expression is associated with aggressive behavior and poor prognosis in Middle Eastern triple-negative breast cancer. *Breast Cancer Res Treat* **151**, 541–53 (2015).
18. Kenemans, P., Verstraeten, R. A. & Verheijen, R. H. M. Oncogenic pathways in hereditary and sporadic breast cancer. *Maturitas* **61**, 141–50 (2008).

19. Pranavathiyani, G., Thanmalagan, R. R., Leimarembi Devi, N. & Venkatesan, A. Integrated transcriptome interactome study of oncogenes and tumor suppressor genes in breast cancer. *Genes Dis* **6**, 78–87 (2019).
20. Luo, J. *et al.* The oncogenic roles and clinical implications of YAP/TAZ in breast cancer. *Br J Cancer* **128**, 1611–1624 (2023).
21. Khramtsov, A. I. *et al.* Wnt/beta-catenin pathway activation is enriched in basal-like breast cancers and predicts poor outcome. *Am J Pathol* **176**, 2911–20 (2010).
22. Zhang, L. *et al.* TRAF4 promotes TGF-β receptor signaling and drives breast cancer metastasis. *Mol Cell* **51**, 559–72 (2013).
23. Arps, D. P., Healy, P., Zhao, L., Kleer, C. G. & Pang, J. C. Invasive ductal carcinoma with lobular features: a comparison study to invasive ductal and invasive lobular carcinomas of the breast. *Breast Cancer Res Treat* **138**, 719–26 (2013).
24. Kanbayashi, C. & Iwata, H. Current approach and future perspective for ductal carcinoma in situ of the breast. *Jpn J Clin Oncol* **47**, 671–677 (2017).
25. Shaath, H., Elango, R. & Alajez, N. M. Molecular Classification of Breast Cancer Utilizing Long Non-Coding RNA (lncRNA) Transcriptomes Identifies Novel Diagnostic lncRNA Panel for Triple-Negative Breast Cancer. *Cancers (Basel)* **13**, (2021).
26. Nolan, E., Lindeman, G. J. & Visvader, J. E. Deciphering breast cancer: from biology to the clinic. *Cell* **186**, 1708–1728 (2023).
27. Sopik, V., Sun, P. & Narod, S. A. The prognostic effect of estrogen receptor status differs for younger versus older breast cancer patients. *Breast Cancer Res Treat* **165**, 391–402 (2017).
28. Lashen, A. G., Toss, M. S., Mongan, N. P., Green, A. R. & Rakha, E. A. The clinical value of progesterone receptor expression in luminal breast cancer: A study of a large cohort with long-term follow-up. *Cancer* **129**, 1183–1194 (2023).
29. Gonzalez-Angulo, A. M. *et al.* High risk of recurrence for patients with breast cancer who have human epidermal growth factor receptor 2-positive, node-negative tumors 1 cm or smaller. *J Clin Oncol* **27**, 5700–6 (2009).
30. Cheang, M. C. U. *et al.* Ki67 index, HER2 status, and prognosis of patients with luminal B breast cancer. *J Natl Cancer Inst* **101**, 736–50 (2009).
31. Early Breast Cancer Trialists' Collaborative group (EBCTCG). Trastuzumab for early-stage, HER2-positive breast cancer: a meta-analysis of 13 864 women in seven randomised trials. *Lancet Oncol* **22**, 1139–1150 (2021).
32. Karim, A. M. *et al.* Triple-negative breast cancer: epidemiology, molecular mechanisms, and modern vaccine-based treatment strategies. *Biochem Pharmacol* **212**, 115545 (2023).
33. Zagami, P. & Carey, L. A. Triple negative breast cancer: Pitfalls and progress. *NPJ Breast Cancer* **8**, 95 (2022).
34. Chen, Z. *et al.* Classifications of triple-negative breast cancer: insights and current therapeutic approaches. *Cell Biosci* **15**, 13 (2025).
35. Hernandez, A. E. *et al.* Associations Between Neighborhood-Level Income and Triple-Negative Breast Cancer in a Majority-Minority Population. *Ann Surg Oncol* **31**, 988–996 (2024).

36. Prakash, O. *et al.* Racial Disparities in Triple Negative Breast Cancer: A Review of the Role of Biologic and Non-biologic Factors. *Front Public Health* **8**, 576964 (2020).
37. Bayard, S. *et al.* Screening mammography mitigates breast cancer disparities through early detection of triple negative breast cancer. *Clin Imaging* **80**, 430–437 (2021).
38. Lehmann, B. D. *et al.* Refinement of Triple-Negative Breast Cancer Molecular Subtypes: Implications for Neoadjuvant Chemotherapy Selection. *PLoS One* **11**, e0157368 (2016).
39. Hubalek, M., Czech, T. & Müller, H. Biological Subtypes of Triple-Negative Breast Cancer. *Breast Care (Basel)* **12**, 8–14 (2017).
40. Wang, D.-Y., Jiang, Z., Ben-David, Y., Woodgett, J. R. & Zacksenhaus, E. Molecular stratification within triple-negative breast cancer subtypes. *Sci Rep* **9**, 19107 (2019).
41. Lehmann, B. D. *et al.* Identification of human triple-negative breast cancer subtypes and preclinical models for selection of targeted therapies. *J Clin Invest* **121**, 2750–67 (2011).
42. Obidiro, O., Battogtokh, G. & Akala, E. O. Triple Negative Breast Cancer Treatment Options and Limitations: Future Outlook. *Pharmaceutics* **15**, (2023).
43. Bayles, C. E. *et al.* Upcycling the anthracyclines: New mechanisms of action, toxicology, and pharmacology. *Toxicol Appl Pharmacol* **459**, 116362 (2023).
44. Alalawy, A. I. Key genes and molecular mechanisms related to Paclitaxel Resistance. *Cancer Cell Int* **24**, 244 (2024).
45. Huang, Q., Mei, Z. & Han, X. Efficacy and safety of taxanes combined with chemotherapy drugs in advanced triple negative breast cancer: A meta-analysis of 26 randomized controlled trials. *Front Oncol* **12**, 972767 (2022).
46. Miller, K. *et al.* Paclitaxel plus Bevacizumab versus Paclitaxel Alone for Metastatic Breast Cancer. *New England Journal of Medicine* **357**, 2666–2676 (2007).
47. O'Shaughnessy, J. *et al.* Efficacy and Safety of Weekly Paclitaxel With or Without Oral Alisertib in Patients With Metastatic Breast Cancer: A Randomized Clinical Trial. *JAMA Netw Open* **4**, e214103 (2021).
48. Chaudhary, L. N. Early stage triple negative breast cancer: Management and future directions. *Semin Oncol* **47**, 201–208 (2020).
49. Timmins, H. C. *et al.* Weekly Paclitaxel-Induced Neurotoxicity in Breast Cancer: Outcomes and Dose Response. *Oncologist* **26**, 366–374 (2021).
50. Gokce Ceylan, G. & Gok Metin, Z. Symptom status, body perception, and risk of anxiety and depression in breast cancer patients receiving paclitaxel: a prospective longitudinal study. *Support Care Cancer* **30**, 2069–2079 (2022).
51. Zhao, T., Zhang, T., Zhang, Y., Zhou, B. & Lu, X. Paclitaxel Resistance Modulated by the Interaction between TRPS1 and AF178030.2 in Triple-Negative Breast Cancer. *Evid Based Complement Alternat Med* **2022**, 6019975 (2022).
52. Jia, D. *et al.* An autocrine inflammatory forward-feedback loop after chemotherapy withdrawal facilitates the repopulation of drug-resistant breast cancer cells. *Cell Death Dis* **8**, e2932 (2017).
53. He, J. *et al.* Inhibition of USP2 eliminates cancer stem cells and enhances TNBC responsiveness to chemotherapy. *Cell Death Dis* **10**, 285 (2019).

54. Yuan, H. *et al.* Albumin Nanoparticle of Paclitaxel (Abraxane) Decreases while Taxol Increases Breast Cancer Stem Cells in Treatment of Triple Negative Breast Cancer. *Mol Pharm* **17**, 2275–2286 (2020).
55. Park, S.-Y., Choi, J.-H. & Nam, J.-S. Targeting Cancer Stem Cells in Triple-Negative Breast Cancer. *Cancers (Basel)* **11**, (2019).
56. Fultang, N., Chakraborty, M. & Peethambaran, B. Regulation of cancer stem cells in triple negative breast cancer. *Cancer Drug Resist* **4**, 321–342 (2021).
57. Taurin, S. & Alkhalifa, H. Breast cancers, mammary stem cells, and cancer stem cells, characteristics, and hypotheses. *Neoplasia* **22**, 663–678 (2020).
58. O'Brien, C. A., Kreso, A. & Dick, J. E. Cancer stem cells in solid tumors: an overview. *Semin Radiat Oncol* **19**, 71–7 (2009).
59. Owens, T. W. & Naylor, M. J. Breast cancer stem cells. *Front Physiol* **4**, 225 (2013).
60. Lim, E. *et al.* Aberrant luminal progenitors as the candidate target population for basal tumor development in BRCA1 mutation carriers. *Nat Med* **15**, 907–13 (2009).
61. Pece, S. *et al.* Biological and molecular heterogeneity of breast cancers correlates with their cancer stem cell content. *Cell* **140**, 62–73 (2010).
62. Al-Hajj, M., Wicha, M. S., Benito-Hernandez, A., Morrison, S. J. & Clarke, M. F. Prospective identification of tumorigenic breast cancer cells. *Proc Natl Acad Sci U S A* **100**, 3983–8 (2003).
63. Zhang, X., Powell, K. & Li, L. Breast Cancer Stem Cells: Biomarkers, Identification and Isolation Methods, Regulating Mechanisms, Cellular Origin, and Beyond. *Cancers (Basel)* **12**, (2020).
64. Wei, Y. *et al.* ALDH1: A potential therapeutic target for cancer stem cells in solid tumors. *Front Oncol* **12**, 1026278 (2022).
65. Ginestier, C. *et al.* ALDH1 is a marker of normal and malignant human mammary stem cells and a predictor of poor clinical outcome. *Cell Stem Cell* **1**, 555–67 (2007).
66. Tsochantaridis, I. *et al.* Profiling of Aldehyde Dehydrogenase Isoforms in In Vitro Formed Tumorspheres. *Anticancer Res* **41**, 5481–5488 (2021).
67. Castaneda, M., den Hollander, P., Kuburich, N. A., Rosen, J. M. & Mani, S. A. Mechanisms of cancer metastasis. *Semin Cancer Biol* **87**, 17–31 (2022).
68. Velasco-Velázquez, M. A., Popov, V. M., Lisanti, M. P. & Pestell, R. G. The role of breast cancer stem cells in metastasis and therapeutic implications. *Am J Pathol* **179**, 2–11 (2011).
69. Lamouille, S., Xu, J. & Derynck, R. Molecular mechanisms of epithelial-mesenchymal transition. *Nat Rev Mol Cell Biol* **15**, 178–96 (2014).
70. Wendt, M. K., Taylor, M. A., Schiemann, B. J. & Schiemann, W. P. Down-regulation of epithelial cadherin is required to initiate metastatic outgrowth of breast cancer. *Mol Biol Cell* **22**, 2423–35 (2011).
71. Eslami Amirabadi, H. *et al.* Characterizing the invasion of different breast cancer cell lines with distinct E-cadherin status in 3D using a microfluidic system. *Biomed Microdevices* **21**, 101 (2019).
72. Fu, M. *et al.* The Hippo signalling pathway and its implications in human health and diseases. *Signal Transduct Target Ther* **7**, 376 (2022).
73. Liu, S. *et al.* Breast cancer stem cells transition between epithelial and mesenchymal states reflective of their normal counterparts. *Stem Cell Reports* **2**, 78–91 (2014).

74. Xu, H. *et al.* Enrichment of CD44 in basal-type breast cancer correlates with EMT, cancer stem cell gene profile, and prognosis. *Onco Targets Ther* **9**, 431–44 (2016).
75. Zheng, Q., Zhang, M., Zhou, F., Zhang, L. & Meng, X. The Breast Cancer Stem Cells Traits and Drug Resistance. *Front Pharmacol* **11**, 599965 (2020).
76. Ji, X. *et al.* Chemoresistance mechanisms of breast cancer and their countermeasures. *Biomed Pharmacother* **114**, 108800 (2019).
77. Khoury, T. *et al.* Aldehyde dehydrogenase 1A1 expression in breast cancer is associated with stage, triple negativity, and outcome to neoadjuvant chemotherapy. *Mod Pathol* **25**, 388–97 (2012).
78. Gillespie, M. S. *et al.* PRMT5-regulated splicing of DNA repair genes drives chemoresistance in breast cancer stem cells. *Oncogene* **44**, 862–876 (2025).
79. Wang, T. *et al.* JAK/STAT3-Regulated Fatty Acid β-Oxidation Is Critical for Breast Cancer Stem Cell Self-Renewal and Chemoresistance. *Cell Metab* **27**, 136-150.e5 (2018).
80. Harvey, K. F., Zhang, X. & Thomas, D. M. The Hippo pathway and human cancer. *Nat Rev Cancer* **13**, 246–57 (2013).
81. Bae, J. S., Kim, S. M. & Lee, H. The Hippo signaling pathway provides novel anti-cancer drug targets. *Oncotarget* **8**, 16084–16098 (2017).
82. Di Benedetto, A. *et al.* The Hippo transducers TAZ/YAP and their target CTGF in male breast cancer. *Oncotarget* **7**, 43188–43198 (2016).
83. Mizuno, T. *et al.* YAP induces malignant mesothelioma cell proliferation by upregulating transcription of cell cycle-promoting genes. *Oncogene* **31**, 5117–22 (2012).
84. Jung, O. *et al.* Nuclear phosphoinositide signaling promotes YAP/TAZ-TEAD transcriptional activity in breast cancer. *EMBO J* **43**, 1740–1769 (2024).
85. Quinn, H. M. *et al.* YAP and β-Catenin Cooperate to Drive Oncogenesis in Basal Breast Cancer. *Cancer Res* **81**, 2116–2127 (2021).
86. Wang, Z. *et al.* Regulation of Hippo signaling and triple negative breast cancer progression by an ubiquitin ligase RNF187. *Oncogenesis* **9**, 36 (2020).
87. Parambil, S. T. *et al.* YAP transduction drives triple-negative breast cancer aggressiveness through modulating the EGFR–AKT axis in patient-derived xenograft cells. *Med Oncol* **40**, 137 (2023).
88. Li, Y. *et al.* Role of inhibitor of yes-associated protein 1 in triple-negative breast cancer with taxol-based chemoresistance. *Cancer Sci* **110**, 561–567 (2019).
89. Cordenonsi, M. *et al.* The Hippo transducer TAZ confers cancer stem cell-related traits on breast cancer cells. *Cell* **147**, 759–72 (2011).
90. Bora-Singhal, N. *et al.* YAP1 Regulates OCT4 Activity and SOX2 Expression to Facilitate Self-Renewal and Vascular Mimicry of Stem-Like Cells. *Stem Cells* **33**, 1705–18 (2015).
91. Kumar, S. M. *et al.* Acquired cancer stem cell phenotypes through Oct4-mediated dedifferentiation. *Oncogene* **31**, 4898–4911 (2012).
92. Andrade, D. *et al.* YAP1 inhibition radiosensitizes triple negative breast cancer cells by targeting the DNA damage response and cell survival pathways. *Oncotarget* **8**, 98495–98508 (2017).
93. Li, Y.-W. *et al.* Apigenin suppresses the stem cell-like properties of triple-negative breast cancer cells by inhibiting YAP/TAZ activity. *Cell Death Discov* **4**, 105 (2018).

94. Nakano, N. *et al.* Hybrid molecule between platanic acid and LCL-161 as a yes-associated protein degrader. *J Biochem* **171**, 631–640 (2022).
95. Wei, H. *et al.* Verteporfin suppresses cell survival, angiogenesis and vasculogenic mimicry of pancreatic ductal adenocarcinoma via disrupting the YAP-TEAD complex. *Cancer Sci* **108**, 478–487 (2017).
96. Wang, Z. *et al.* Interplay of mevalonate and Hippo pathways regulates RHAMM transcription via YAP to modulate breast cancer cell motility. *Proceedings of the National Academy of Sciences* **111**, (2014).
97. Zhou, C. *et al.* Exploring Degradation of Intrinsically Disordered Protein Yes-Associated Protein Induced by Proteolysis TArgeting Chimeras. *J Med Chem* **67**, 15168–15198 (2024).
98. Liu, Z.-L., Chen, H.-H., Zheng, L.-L., Sun, L.-P. & Shi, L. Angiogenic signaling pathways and anti-angiogenic therapy for cancer. *Signal Transduct Target Ther* **8**, 198 (2023).
99. Nishida, N., Yano, H., Nishida, T., Kamura, T. & Kojiro, M. Angiogenesis in cancer. *Vasc Health Risk Manag* **2**, 213–219 (2006).
100. Linderholm, B. K. *et al.* Significantly higher levels of vascular endothelial growth factor (VEGF) and shorter survival times for patients with primary operable triple-negative breast cancer. *Ann Oncol* **20**, 1639–46 (2009).
101. Lee, H. & Kang, K.-T. Differential Angiogenic Responses of Human Endothelial Colony-Forming Cells to Different Molecular Subtypes of Breast Cancer Cells. *J Lipid Atheroscler* **10**, 111–122 (2021).
102. Taha, F. M. *et al.* Prognostic value of serum vascular endothelial growth factor in Egyptian females with metastatic triple negative breast cancer. *Clin Biochem* **42**, 1420–6 (2009).
103. Ma, S. *et al.* Hypoxia induces HIF1α-dependent epigenetic vulnerability in triple negative breast cancer to confer immune effector dysfunction and resistance to anti-PD-1 immunotherapy. *Nat Commun* **13**, 4118 (2022).
104. Liu, Q. *et al.* Targeting hypoxia-inducible factor-1alpha: A new strategy for triple-negative breast cancer therapy. *Biomed Pharmacother* **156**, 113861 (2022).
105. Han, D., Li, Z., Luo, L. & Jiang, H. Targeting Hypoxia and HIF1α in Triple-Negative Breast Cancer: New Insights from Gene Expression Profiling and Implications for Therapy. *Biology (Basel)* **13**, (2024).
106. Liu, X. *et al.* HIF-1-regulated expression of calreticulin promotes breast tumorigenesis and progression through Wnt/β-catenin pathway activation. *Proc Natl Acad Sci U S A* **118**, (2021).
107. Lu, H. *et al.* Chemotherapy triggers HIF-1-dependent glutathione synthesis and copper chelation that induces the breast cancer stem cell phenotype. *Proc Natl Acad Sci U S A* **112**, E4600-9 (2015).
108. Li, Y. *et al.* HIF-1α inhibitor YC-1 suppresses triple-negative breast cancer growth and angiogenesis by targeting PlGF/VEGFR1-induced macrophage polarization. *Biomed Pharmacother* **161**, 114423 (2023).
109. Mirabelli, P., Coppola, L. & Salvatore, M. Cancer Cell Lines Are Useful Model Systems for Medical Research. *Cancers (Basel)* **11**, (2019).
110. Ben-David, U. *et al.* Genetic and transcriptional evolution alters cancer cell line drug response. *Nature* **560**, 325–330 (2018).

111. Takahashi, H. *et al.* Biologically Aggressive Phenotype and Anti-cancer Immunity Counterbalance in Breast Cancer with High Mutation Rate. *Sci Rep* **10**, 1852 (2020).
112. Souto, E. P., Dobrolecki, L. E., Villanueva, H., Sikora, A. G. & Lewis, M. T. In Vivo Modeling of Human Breast Cancer Using Cell Line and Patient-Derived Xenografts. *J Mammary Gland Biol Neoplasia* **27**, 211–230 (2022).
113. Liu, K. *et al.* Evaluating cell lines as models for metastatic breast cancer through integrative analysis of genomic data. *Nat Commun* **10**, 2138 (2019).
114. Sulaiman, A. & Wang, L. Bridging the divide: preclinical research discrepancies between triple-negative breast cancer cell lines and patient tumors. *Oncotarget* **8**, 113269–113281 (2017).
115. Simmons, J. K. *et al.* Animal Models of Bone Metastasis. *Vet Pathol* **52**, 827–41 (2015).
116. Jin, J., Yoshimura, K., Sewastjanow-Silva, M., Song, S. & Ajani, J. A. Challenges and Prospects of Patient-Derived Xenografts for Cancer Research. *Cancers (Basel)* **15**, (2023).
117. Owonikoko, T. K. *et al.* Patient-derived xenografts faithfully replicated clinical outcome in a phase II co-clinical trial of arsenic trioxide in relapsed small cell lung cancer. *J Transl Med* **14**, 111 (2016).
118. Roife, D. *et al.* Ex Vivo Testing of Patient-Derived Xenografts Mirrors the Clinical Outcome of Patients with Pancreatic Ductal Adenocarcinoma. *Clin Cancer Res* **22**, 6021–6030 (2016).
119. Hoffman, R. M. Patient-derived orthotopic xenografts: better mimic of metastasis than subcutaneous xenografts. *Nat Rev Cancer* **15**, 451–2 (2015).
120. Giuliano, M. *et al.* Circulating and disseminated tumor cells from breast cancer patient-derived xenograft-bearing mice as a novel model to study metastasis. *Breast Cancer Res* **17**, 3 (2015).
121. Santoro, M. M. Antiangiogenic cancer drug using the zebrafish model. *Arterioscler Thromb Vasc Biol* **34**, 1846–53 (2014).
122. Seano, G. *et al.* Modeling human tumor angiogenesis in a three-dimensional culture system. *Blood* **121**, e129-37 (2013).
123. Veldman, M. B. & Lin, S. Zebrafish as a developmental model organism for pediatric research. *Pediatr Res* **64**, 470–6 (2008).
124. Shehwana, H. & Konu, O. Comparative Transcriptomics Between Zebrafish and Mammals: A Roadmap for Discovery of Conserved and Unique Signaling Pathways in Physiology and Disease. *Front Cell Dev Biol* **7**, 5 (2019).
125. Zhuo, Y., Zhao, Y.-G. & Zhang, Y. Enhancing Drug Solubility, Bioavailability, and Targeted Therapeutic Applications through Magnetic Nanoparticles. *Molecules* **29**, (2024).
126. Amidon, G. L., Lennernäs, H., Shah, V. P. & Crison, J. R. A theoretical basis for a biopharmaceutic drug classification: the correlation of in vitro drug product dissolution and in vivo bioavailability. *Pharm Res* **12**, 413–20 (1995).
127. Lin, A. *et al.* Off-target toxicity is a common mechanism of action of cancer drugs undergoing clinical trials. *Sci Transl Med* **11**, (2019).
128. Li, X. *et al.* Proteolysis-targeting chimeras (PROTACs) in cancer therapy. *Mol Cancer* **21**, 99 (2022).

129. Santos, R. *et al.* A comprehensive map of molecular drug targets. *Nat Rev Drug Discov* **16**, 19–34 (2017).
130. Pradhan, R. *et al.* Recent Advances in Targeted Nanocarriers for the Management of Triple Negative Breast Cancer. *Pharmaceutics* **15**, (2023).
131. Bazzazan, M. A., Fattollazadeh, P., Keshavarz Shahbaz, S. & Rezaei, N. Polymeric nanoparticles as a promising platform for treating triple-negative breast cancer: Current status and future perspectives. *Int J Pharm* **664**, 124639 (2024).
132. Di Costanzo, F., Gasperoni, S., Rotella, V. & Di Costanzo, F. Targeted delivery of albumin bound paclitaxel in the treatment of advanced breast cancer. *Onco Targets Ther* **2**, 179–88 (2009).
133. Wu, J. The Enhanced Permeability and Retention (EPR) Effect: The Significance of the Concept and Methods to Enhance Its Application. *J Pers Med* **11**, (2021).
134. Liu, J. *et al.* A Sequentially Responsive Nanosystem Breaches Cascaded Bio-barriers and Suppresses P-Glycoprotein Function for Reversing Cancer Drug Resistance. *ACS Appl Mater Interfaces* **12**, 54343–54355 (2020).
135. Fraguas-Sánchez, A. I., Lozza, I. & Torres-Suárez, A. I. Actively Targeted Nanomedicines in Breast Cancer: From Pre-Clinal Investigation to Clinic. *Cancers (Basel)* **14**, (2022).
136. Li, Y., Lu, X., Lin, Q. & Li, W. Is nab-paclitaxel better than conventional taxanes as neoadjuvant therapy for breast cancer? A meta-analysis. *J Int Med Res* **48**, 300060520943473 (2020).
137. Untch, M. *et al.* NAB-Paclitaxel Improves Disease-Free Survival in Early Breast Cancer: GBG 69-GeparSepto. *J Clin Oncol* **37**, 2226–2234 (2019).
138. Park, I. H. *et al.* An Open-Label, Randomized, Parallel, Phase III Trial Evaluating the Efficacy and Safety of Polymeric Micelle-Formulated Paclitaxel Compared to Conventional Cremophor EL-Based Paclitaxel for Recurrent or Metastatic HER2-Negative Breast Cancer. *Cancer Res Treat* **49**, 569–577 (2017).
139. Bardia, A. *et al.* Sacituzumab Govitecan in Metastatic Triple-Negative Breast Cancer. *N Engl J Med* **384**, 1529–1541 (2021).
140. Lv, Y. *et al.* Mechanism of action and future perspectives of ADCs in combination with immune checkpoint inhibitors for solid tumors. *Clin Exp Med* **25**, 139 (2025).
141. Xu, X., Yu, T. & Wang, Z. Combining antibody-drug conjugates with immune checkpoint inhibitors: A new paradigm for breast cancer therapy. *Cancer Treat Rev* **140**, 103012 (2025).
142. Tolaney, S. M. *et al.* Sacituzumab govitecan (SG) + pembrolizumab (pembro) vs chemotherapy (chemo) + pembro in previously untreated PD-L1–positive advanced triple-negative breast cancer (TNBC): Primary results from the randomized phase 3 ASCENT-04/KEYNOTE-D19 study. *Journal of Clinical Oncology* **43**, (2025).
143. Villacampa, G. *et al.* Safety and efficacy of antibody-drug conjugates plus immunotherapy in solid tumours: A systematic review and meta-analysis. *Cancer Treat Rev* **131**, 102847 (2024).
144. Kumari, M. *et al.* PGMD/curcumin nanoparticles for the treatment of breast cancer. *Sci Rep* **11**, 3824 (2021).
145. Mukhopadhyay, R. *et al.* Gemcitabine Co-Encapsulated with Curcumin in Folate Decorated PLGA Nanoparticles; a Novel Approach to Treat Breast Adenocarcinoma. *Pharm Res* **37**, 56 (2020).

146. Setten, R. L., Rossi, J. J. & Han, S.-P. The current state and future directions of RNAi-based therapeutics. *Nat Rev Drug Discov* **18**, 421–446 (2019).
147. Xie, X. *et al.* Recent advances in targeting the 'undruggable' proteins: from drug discovery to clinical trials. *Signal Transduct Target Ther* **8**, 335 (2023).
148. Zhu, Y., Zhu, L., Wang, X. & Jin, H. RNA-based therapeutics: an overview and prospectus. *Cell Death Dis* **13**, 644 (2022).
149. Lam, J. K. W., Chow, M. Y. T., Zhang, Y. & Leung, S. W. S. siRNA Versus miRNA as Therapeutics for Gene Silencing. *Mol Ther Nucleic Acids* **4**, e252 (2015).
150. Dönmez, Y. & Gündüz, U. Reversal of multidrug resistance by small interfering RNA (siRNA) in doxorubicin-resistant MCF-7 breast cancer cells. *Biomed Pharmacother* **65**, 85–9 (2011).
151. Liu, C. *et al.* mRNA-based cancer therapeutics. *Nat Rev Cancer* **23**, 526–543 (2023).
152. Shi, Y., Shi, M., Wang, Y. & You, J. Progress and prospects of mRNA-based drugs in pre-clinical and clinical applications. *Signal Transduct Target Ther* **9**, 322 (2024).
153. Kanasty, R., Dorkin, J. R., Vegas, A. & Anderson, D. Delivery materials for siRNA therapeutics. *Nat Mater* **12**, 967–77 (2013).
154. Dana, H. *et al.* Molecular Mechanisms and Biological Functions of siRNA. *Int J Biomed Sci* **13**, 48–57 (2017).
155. Chernikov, I. V, Vlassov, V. V & Chernolovskaya, E. L. Current Development of siRNA Bioconjugates: From Research to the Clinic. *Front Pharmacol* **10**, 444 (2019).
156. Wan, X. *et al.* In Vivo Delivery of siRNAs Targeting EGFR and BRD4 Expression by Peptide-Modified Redox Responsive PEG-PEI Nanoparticles for the Treatment of Triple-Negative Breast Cancer. *Mol Pharm* **18**, 3990–3998 (2021).
157. Yin, L. *et al.* A prodrug nanodevice co-delivering docetaxel and ROR1 siRNA for enhanced triple negative breast cancer therapy. *Acta Biomater* **193**, 498–513 (2025).
158. Schilb, A. L. *et al.* Efficacy of Targeted ECO/miR-200c Nanoparticles for Modulating Tumor Microenvironment and Treating Triple Negative Breast Cancer as Non-invasively Monitored by MR Molecular Imaging. *Pharm Res* **38**, 1405–1418 (2021).
159. Okamoto, A. *et al.* Systemic Administration of siRNA with Anti-HB-EGF Antibody-Modified Lipid Nanoparticles for the Treatment of Triple-Negative Breast Cancer. *Mol Pharm* **15**, 1495–1504 (2018).
160. Zhang, C. *et al.* Chemotherapy drugs derived nanoparticles encapsulating mRNA encoding tumor suppressor proteins to treat triple-negative breast cancer. *Nano Res* **12**, 855–861 (2019).
161. El-Sahli, S. *et al.* A triple-drug nanotherapy to target breast cancer cells, cancer stem cells, and tumor vasculature. *Cell Death Dis* **12**, 8 (2021).
162. DeSantis, C., Ma, J., Bryan, L. & Jemal, A. Breast cancer statistics, 2013. *CA Cancer J Clin* **64**, 52–62 (2014).
163. Dent, R. *et al.* Triple-negative breast cancer: clinical features and patterns of recurrence. *Clin Cancer Res* **13**, 4429–34 (2007).
164. Malhotra, V. & Perry, M. C. Classical chemotherapy: mechanisms, toxicities and the therapeutic window. *Cancer Biol Ther* **2**, S2-4 (2003).
165. Jia, D. *et al.* Cardamonin reduces chemotherapy-enriched breast cancer stem-like cells in vitro and in vivo. *Oncotarget* **7**, 771–85 (2016).

166. Ma, F. *et al.* Aldehyde dehydrogenase 1 (ALDH1) expression is an independent prognostic factor in triple negative breast cancer (TNBC). *Medicine* **96**, e6561 (2017).
167. Wang, C. *et al.* Verteporfin inhibits YAP function through up-regulating 14-3-3σ sequestering YAP in the cytoplasm. *Am J Cancer Res* **6**, 27–37 (2016).
168. Bielenberg, D. R. & Zetter, B. R. The Contribution of Angiogenesis to the Process of Metastasis. *Cancer J* **21**, 267–73 (2015).
169. Su, M. *et al.* The anti-angiogenic effect and novel mechanisms of action of Combretastatin A-4. *Sci Rep* **6**, 28139 (2016).
170. Shen, C.-H. *et al.* Combretastatin A-4 inhibits cell growth and metastasis in bladder cancer cells and retards tumour growth in a murine orthotopic bladder tumour model. *Br J Pharmacol* **160**, 2008–27 (2010).
171. Saputra, E. C., Huang, L., Chen, Y. & Tucker-Kellogg, L. Combination Therapy and the Evolution of Resistance: The Theoretical Merits of Synergism and Antagonism in Cancer. *Cancer Res* **78**, 2419–2431 (2018).
172. Mukherjee, A. *et al.* Lipid-polymer hybrid nanoparticles as a next-generation drug delivery platform: state of the art, emerging technologies, and perspectives. *Int J Nanomedicine* **14**, 1937–1952 (2019).
173. Tran, S., DeGiovanni, P.-J., Piel, B. & Rai, P. Cancer nanomedicine: a review of recent success in drug delivery. *Clin Transl Med* **6**, 44 (2017).
174. Nel, A., Ruoslahti, E. & Meng, H. New Insights into 'Permeability' as in the Enhanced Permeability and Retention Effect of Cancer Nanotherapeutics. *ACS Nano* **11**, 9567–9569 (2017).
175. Izumchenko, E. *et al.* Patient-derived xenografts effectively capture responses to oncology therapy in a heterogeneous cohort of patients with solid tumors. *Ann Oncol* **28**, 2595–2605 (2017).
176. Zhang, L. *et al.* Self-assembled lipid--polymer hybrid nanoparticles: a robust drug delivery platform. *ACS Nano* **2**, 1696–702 (2008).
177. Emerling, B. M., Weinberg, F., Liu, J.-L., Mak, T. W. & Chandel, N. S. PTEN regulates p300-dependent hypoxia-inducible factor 1 transcriptional activity through Forkhead transcription factor 3a (FOXO3a). *Proc Natl Acad Sci U S A* **105**, 2622–7 (2008).
178. Chen, X. & Prywes, R. Serum-induced expression of the cdc25A gene by relief of E2F-mediated repression. *Mol Cell Biol* **19**, 4695–702 (1999).
179. Xi, Y. *et al.* Transgenic zebrafish expressing green fluorescent protein in dopaminergic neurons of the ventral diencephalon. *Dev Dyn* **240**, 2539–47 (2011).
180. DeRose, Y. S. *et al.* Tumor grafts derived from women with breast cancer authentically reflect tumor pathology, growth, metastasis and disease outcomes. *Nat Med* **17**, 1514–20 (2011).
181. Lee, C.-H., Yu, C.-C., Wang, B.-Y. & Chang, W.-W. Tumorsphere as an effective in vitro platform for screening anti-cancer stem cell drugs. *Oncotarget* **7**, 1215–26 (2016).
182. Thomas, D. *et al.* Increased cancer stem cell invasion is mediated by myosin IIB and nuclear translocation. *Oncotarget* **7**, 47586–47592 (2016).
183. Li, S. & Li, Q. Cancer stem cells and tumor metastasis (Review). *Int J Oncol* **44**, 1806–12 (2014).

184. Yu, F.-X., Zhao, B. & Guan, K.-L. Hippo Pathway in Organ Size Control, Tissue Homeostasis, and Cancer. *Cell* **163**, 811–28 (2015).
185. Guo, L., Chen, Y., Luo, J., Zheng, J. & Shao, G. YAP1 overexpression is associated with poor prognosis of breast cancer patients and induces breast cancer cell growth by inhibiting PTEN. *FEBS Open Bio* **9**, 437–445 (2019).
186. Feitsma, H. & Cuppen, E. Zebrafish as a cancer model. *Mol Cancer Res* **6**, 685–94 (2008).
187. Delov, V., Muth-Köhne, E., Schäfers, C. & Fenske, M. Transgenic fluorescent zebrafish Tg(fli1:EGFP)y[1] for the identification of vasotoxicity within the zFET. *Aquat Toxicol* **150**, 189–200 (2014).
188. Wong, C. C.-L. *et al.* Hypoxia-inducible factor 1 is a master regulator of breast cancer metastatic niche formation. *Proc Natl Acad Sci U S A* **108**, 16369–74 (2011).
189. Mimeault, M. & Batra, S. K. Hypoxia-inducing factors as master regulators of stemness properties and altered metabolism of cancer- and metastasis-initiating cells. *J Cell Mol Med* **17**, 30–54 (2013).
190. Wong, A. D., Ye, M., Ulmschneider, M. B. & Searson, P. C. Quantitative Analysis of the Enhanced Permeation and Retention (EPR) Effect. *PLoS One* **10**, e0123461 (2015).
191. Peer, D. *et al.* Nanocarriers as an emerging platform for cancer therapy. *Nat Nanotechnol* **2**, 751–60 (2007).
192. Logue, S. E. *et al.* Inhibition of IRE1 RNase activity modulates the tumor cell secretome and enhances response to chemotherapy. *Nat Commun* **9**, 3267 (2018).
193. Bhola, N. E. *et al.* TGF-β inhibition enhances chemotherapy action against triple-negative breast cancer. *J Clin Invest* **123**, 1348–58 (2013).
194. Kumbhar, B. V., Bhandare, V. V., Panda, D. & Kunwar, A. Delineating the interaction of combretastatin A-4 with αβ tubulin isotypes present in drug resistant human lung carcinoma using a molecular modeling approach. *J Biomol Struct Dyn* **38**, 426–438 (2020).
195. Abbassi, R. H. *et al.* Lower Tubulin Expression in Glioblastoma Stem Cells Attenuates Efficacy of Microtubule-Targeting Agents. *ACS Pharmacol Transl Sci* **2**, 402–413 (2019).
196. Zhao, Y. *et al.* YAP-induced resistance of cancer cells to antitubulin drugs is modulated by a Hippo-independent pathway. *Cancer Res* **74**, 4493–503 (2014).
197. Olsen, J. J. *et al.* The Role of Wnt Signalling in Angiogenesis. *Clin Biochem Rev* **38**, 131–142 (2017).
198. Samanta, D., Gilkes, D. M., Chaturvedi, P., Xiang, L. & Semenza, G. L. Hypoxia-inducible factors are required for chemotherapy resistance of breast cancer stem cells. *Proc Natl Acad Sci U S A* **111**, E5429-38 (2014).
199. Chen, R. *et al.* High mobility group protein B1 controls liver cancer initiation through yes-associated protein -dependent aerobic glycolysis. *Hepatology* **67**, 1823–1841 (2018).
200. El-Sahli, S. *et al.* Nanoparticle-Mediated mRNA Delivery to Triple-Negative Breast Cancer (TNBC) Patient-Derived Xenograft (PDX) Tumors. *ACS Pharmacol Transl Sci* **8**, 460–469 (2025).
201. Hou, X., Zaks, T., Langer, R. & Dong, Y. Lipid nanoparticles for mRNA delivery. *Nat Rev Mater* **6**, 1078–1094 (2021).

202. Huang, X. *et al.* The landscape of mRNA nanomedicine. *Nat Med* **28**, 2273–2287 (2022).
203. Paunovska, K., Loughrey, D. & Dahlman, J. E. Drug delivery systems for RNA therapeutics. *Nat Rev Genet* **23**, 265–280 (2022).
204. Hopkins, A. L. & Groom, C. R. The druggable genome. *Nat Rev Drug Discov* **1**, 727–30 (2002).
205. Islam, M. A. *et al.* Restoration of tumour-growth suppression in vivo via systemic nanoparticle-mediated delivery of PTEN mRNA. *Nat Biomed Eng* **2**, 850–864 (2018).
206. Kong, N. *et al.* Synthetic mRNA nanoparticle-mediated restoration of p53 tumor suppressor sensitizes p53-deficient cancers to mTOR inhibition. *Sci Transl Med* **11**, (2019).
207. Hotz, C. *et al.* Local delivery of mRNA-encoded cytokines promotes antitumor immunity and tumor eradication across multiple preclinical tumor models. *Sci Transl Med* **13**, eabc7804 (2021).
208. Parayath, N. N., Stephan, S. B., Koehne, A. L., Nelson, P. S. & Stephan, M. T. In vitro-transcribed antigen receptor mRNA nanocarriers for transient expression in circulating T cells in vivo. *Nat Commun* **11**, 6080 (2020).
209. Wang, H.-X. *et al.* CRISPR/Cas9-Based Genome Editing for Disease Modeling and Therapy: Challenges and Opportunities for Nonviral Delivery. *Chem Rev* **117**, 9874–9906 (2017).
210. Katti, A., Diaz, B. J., Caragine, C. M., Sanjana, N. E. & Dow, L. E. CRISPR in cancer biology and therapy. *Nat Rev Cancer* **22**, 259–279 (2022).
211. Mendez-Gomez, H. R. *et al.* RNA aggregates harness the danger response for potent cancer immunotherapy. *Cell* **187**, 2521-2535.e21 (2024).
212. Wang, B. *et al.* Delivery of mRNA Encoding Interleukin-12 and a Stimulator of Interferon Genes Agonist Potentiates Antitumor Efficacy through Reversing T Cell Exhaustion. *ACS Nano* **18**, 15499–15516 (2024).
213. Bitounis, D., Jacquinet, E., Rogers, M. A. & Amiji, M. M. Strategies to reduce the risks of mRNA drug and vaccine toxicity. *Nat Rev Drug Discov* **23**, 281–300 (2024).
214. Chaudhary, N., Weissman, D. & Whitehead, K. A. mRNA vaccines for infectious diseases: principles, delivery and clinical translation. *Nat Rev Drug Discov* **20**, 817–838 (2021).
215. Manturthi, S. *et al.* Nanoparticles Codelivering mRNA and SiRNA for Simultaneous Restoration and Silencing of Gene/Protein Expression In Vitro and In Vivo. *ACS nanoscience Au* **4**, 416–425 (2024).
216. Shi, J., Kantoff, P. W., Wooster, R. & Farokhzad, O. C. Cancer nanomedicine: progress, challenges and opportunities. *Nat Rev Cancer* **17**, 20–37 (2017).
217. Poon, W., Kingston, B. R., Ouyang, B., Ngo, W. & Chan, W. C. W. A framework for designing delivery systems. *Nat Nanotechnol* **15**, 819–829 (2020).
218. Patel, Y. *et al.* Development of Pro-resolving and Pro-efferocytic Nanoparticles for Atherosclerosis Therapy. *ACS Pharmacol Transl Sci* **7**, 3086–3095 (2024).
219. Nguyen, L. N. M. *et al.* The mechanisms of nanoparticle delivery to solid tumours. *Nature Reviews Bioengineering* **2**, 201–213 (2024).

220. Dasgupta, A., Sofias, A. M., Kiessling, F. & Lammers, T. Nanoparticle Delivery to Tumours: From EPR and ATR Mechanisms to Clinical Impact. *Nature reviews bioengineering* **2**, 714–716 (2024).
221. Bertrand, N., Wu, J., Xu, X., Kamaly, N. & Farokhzad, O. C. Cancer nanotechnology: the impact of passive and active targeting in the era of modern cancer biology. *Adv Drug Deliv Rev* **66**, 2–25 (2014).
222. Hidalgo, M. *et al.* Patient-derived xenograft models: an emerging platform for translational cancer research. *Cancer Discov* **4**, 998–1013 (2014).
223. Liu, Y. *et al.* Patient-derived xenograft models in cancer therapy: technologies and applications. *Signal Transduct Target Ther* **8**, 160 (2023).
224. Sulaiman, A. *et al.* Nanoparticles Loaded with Wnt and YAP/Mevalonate Inhibitors in Combination with Paclitaxel Stop the Growth of TNBC Patient-Derived Xenografts and Diminish Tumorigenesis. *Adv Ther (Weinh)* **3**, (2020).
225. Sulaiman, A. *et al.* Co-targeting Bulk Tumor and CSCs in Clinically Translatable TNBC Patient-Derived Xenografts via Combination Nanotherapy. *Mol Cancer Ther* **18**, 1755–1764 (2019).
226. Gadde, S. *et al.* Development of therapeutic polymeric nanoparticles for the resolution of inflammation. *Adv Healthc Mater* **3**, 1448–1456 (2014).
227. Smith, T. K. T. *et al.* Characterization of Redox-Responsive LXR-Activating Nanoparticle Formulations in Primary Mouse Macrophages. *Molecules* **24**, (2019).
228. Riley, R. S. *et al.* Ionizable lipid nanoparticles for in utero mRNA delivery. *Sci Adv* **7**, (2021).
229. Craig, D. W. *et al.* Genome and transcriptome sequencing in prospective metastatic triple-negative breast cancer uncovers therapeutic vulnerabilities. *Mol Cancer Ther* **12**, 104–16 (2013).
230. Khan, F. *et al.* Loss of PTEN in high grade advanced stage triple negative breast ductal cancers in African American women. *Pathol Res Pract* **214**, 673–678 (2018).
231. Comprehensive molecular portraits of human breast tumours. *Nature* **490**, 61–70 (2012).
232. Miller, M. A. *et al.* Predicting therapeutic nanomedicine efficacy using a companion magnetic resonance imaging nanoparticle. *Sci Transl Med* **7**, 314ra183 (2015).
233. Kamaly, N., Yameen, B., Wu, J. & Farokhzad, O. C. Degradable Controlled-Release Polymers and Polymeric Nanoparticles: Mechanisms of Controlling Drug Release. *Chem Rev* **116**, 2602–63 (2016).
234. Kulkarni, J. A. *et al.* Author Correction: The current landscape of nucleic acid therapeutics. *Nat Nanotechnol* **16**, 841 (2021).
235. Mendes, B. B. *et al.* Nanodelivery of nucleic acids. *Nature reviews. Methods primers* **2**, (2022).
236. Qin, S. *et al.* mRNA-based therapeutics: powerful and versatile tools to combat diseases. *Signal Transduct Target Ther* **7**, 166 (2022).
237. Buschmann, M. D. *et al.* Nanomaterial Delivery Systems for mRNA Vaccines. *Vaccines (Basel)* **9**, (2021).
238. Gao, M. *et al.* Modulating Plaque Inflammation via Targeted mRNA Nanoparticles for the Treatment of Atherosclerosis. *ACS Nano* **17**, 17721–17739 (2023).
239. Hu, B. *et al.* Therapeutic siRNA: state of the art. *Signal Transduct Target Ther* **5**, 101 (2020).

240. Kulkarni, J. A., Witzigmann, D., Chen, S., Cullis, P. R. & van der Meel, R. Lipid Nanoparticle Technology for Clinical Translation of siRNA Therapeutics. *Acc Chem Res* **52**, 2435–2444 (2019).
241. Scully, M. A., Wilhelm, R., Wilkins, D. E. & Day, E. S. Membrane-Cloaked Nanoparticles for RNA Interference of β-Catenin in Triple-Negative Breast Cancer. *ACS Biomater Sci Eng* **10**, 1355–1363 (2024).
242. Gadde, S. Multi-drug delivery nanocarriers for combination therapy. *Medchemcomm* **6**, 1916–1929 (2015).
243. Akinc, A. *et al.* The Onpattro story and the clinical translation of nanomedicines containing nucleic acid-based drugs. *Nat Nanotechnol* **14**, 1084–1087 (2019).
244. Chai, C., Wu, H. H., Abuetabh, Y., Sergi, C. & Leng, R. Regulation of the tumor suppressor PTEN in triple-negative breast cancer. *Cancer Lett* **527**, 41–48 (2022).
245. Sulaiman, A. *et al.* Co-inhibition of mTORC1, HDAC and ESR1α retards the growth of triple-negative breast cancer and suppresses cancer stem cells. *Cell Death Dis* **9**, 815 (2018).
246. Sulaiman, A. *et al.* Dual inhibition of Wnt and Yes-associated protein signaling retards the growth of triple-negative breast cancer in both mesenchymal and epithelial states. *Mol Oncol* **12**, 423–440 (2018).
247. Detappe, A. *et al.* Molecular bottlebrush prodrugs as mono- and triplex combination therapies for multiple myeloma. *Nat Nanotechnol* **18**, 184–192 (2023).
248. Huang, J. *et al.* Core-Shell Distinct Nanodrug Showing On-Demand Sequential Drug Release To Act on Multiple Cell Types for Synergistic Anticancer Therapy. *ACS Nano* **13**, 7036–7049 (2019).
249. Ling, X. *et al.* Glutathione-Scavenging Poly(disulfide amide) Nanoparticles for the Effective Delivery of Pt(IV) Prodrugs and Reversal of Cisplatin Resistance. *Nano Lett* **18**, 4618–4625 (2018).
250. Billingsley, M. M. *et al.* Ionizable Lipid Nanoparticle-Mediated mRNA Delivery for Human CAR T Cell Engineering. *Nano Lett* **20**, 1578–1589 (2020).
251. Xu, X. *et al.* Enhancing tumor cell response to chemotherapy through nanoparticle-mediated codelivery of siRNA and cisplatin prodrug. *Proc Natl Acad Sci U S A* **110**, 18638–43 (2013).
252. Zhu, X. *et al.* Long-circulating siRNA nanoparticles for validating Prohibitin1-targeted non-small cell lung cancer treatment. *Proc Natl Acad Sci U S A* **112**, 7779–84 (2015).
253. Xu, X. *et al.* Ultra-pH-Responsive and Tumor-Penetrating Nanoplatform for Targeted siRNA Delivery with Robust Anti-Cancer Efficacy. *Angew Chem Int Ed Engl* **55**, 7091–7094 (2016).
254. Chavez, J. D., Keller, A., Zhou, B., Tian, R. & Bruce, J. E. Cellular Interactome Dynamics during Paclitaxel Treatment. *Cell Rep* **29**, 2371-2383.e5 (2019).
255. Jaroch, K. *et al.* Combretastatins: In vitro structure-activity relationship, mode of action and current clinical status. *Pharmacol Rep* **68**, 1266–1275 (2016).
256. Rycaj, K. & Tang, D. G. Cell-of-Origin of Cancer versus Cancer Stem Cells: Assays and Interpretations. *Cancer Res* **75**, 4003–11 (2015).
257. Jin, K.-T. *et al.* Development of humanized mouse with patient-derived xenografts for cancer immunotherapy studies: A comprehensive review. *Cancer Sci* **112**, 2592–2606 (2021).

258. Meraz, I. M. *et al.* An Improved Patient-Derived Xenograft Humanized Mouse Model for Evaluation of Lung Cancer Immune Responses. *Cancer Immunol Res* **7**, 1267–1279 (2019).
259. Zhao, Y. *et al.* Development of a new patient-derived xenograft humanised mouse model to study human-specific tumour microenvironment and immunotherapy. *Gut* **67**, 1845–1854 (2018).
260. Wang, D.-Y., Gendoo, D. M. A., Ben-David, Y., Woodgett, J. R. & Zacksenhaus, E. A subgroup of microRNAs defines PTEN-deficient, triple-negative breast cancer patients with poorest prognosis and alterations in RB1, MYC, and Wnt signaling. *Breast Cancer Res* **21**, 18 (2019).
261. Lin, Y.-X. *et al.* Reactivation of the tumor suppressor PTEN by mRNA nanoparticles enhances antitumor immunity in preclinical models. *Sci Transl Med* **13**, (2021).
262. Samad, M. A. *et al.* Nanotechnology-based drug delivery for breast cancer treatment: Current applications and future directions. *European Journal of Medicinal Chemistry Reports* **14**, 100268 (2025).
263. Rahdari, T. *et al.* Advancing triple-negative breast cancer treatment through peptide decorated solid lipid nanoparticles for paclitaxel delivery. *Sci Rep* **15**, 6043 (2025).
264. Beer, A. J. *et al.* Patterns of alphavbeta3 expression in primary and metastatic human breast cancer as shown by 18F-Galacto-RGD PET. *J Nucl Med* **49**, 255–9 (2008).
265. Gómez-Pastor, S. *et al.* CD-44 targeted nanoparticles for combination therapy in an in vitro model of triple-negative breast cancer: Targeting the tumour inside out. *Colloids Surf B Biointerfaces* **249**, 114504 (2025).
266. Raj, A., Chandran C, S., Dua, K., Kamath, V. & Alex, A. T. Targeting overexpressed surface proteins: A new strategy to manage the recalcitrant triple-negative breast cancer. *Eur J Pharmacol* **981**, 176914 (2024).
267. Choi, A. S. *et al.* Can targeted nanoparticles distinguish cancer metastasis from inflammation? *J Control Release* **362**, 812–819 (2023).
268. Woythe, L. *et al.* Valency and affinity control of aptamer-conjugated nanoparticles for selective cancer cell targeting. *J Control Release* **355**, 228–237 (2023).
269. Marusyk, A., Janiszewska, M. & Polyak, K. Intratumor Heterogeneity: The Rosetta Stone of Therapy Resistance. *Cancer Cell* **37**, 471–484 (2020).
270. Han, Y. *et al.* Synthetic RNA Therapeutics in Cancer. *J Pharmacol Exp Ther* **386**, 212–223 (2023).
271. Logue, J. S. & Morrison, D. K. Complexity in the signaling network: insights from the use of targeted inhibitors in cancer therapy. *Genes Dev* **26**, 641–50 (2012).

APPENDIX

Rights and Permissions

Figure 1.1 and 1.3 in Chapter 1 were adapted and recreated through BioRender.com. Permission granted through Creative Commons Attribution 4.0 International License. (Creative Commons — Attribution- 4.0 International — CC BY 4.0) https://creativecommons.org/licenses/by/4.0/ and the older version: Creative Commons Attribution 2.5 Generic License. (Creative Commons — Attribution- 2.5 Generic— CC BY 2.5) https://creativecommons.org/licenses/by/2.5/, respectively.

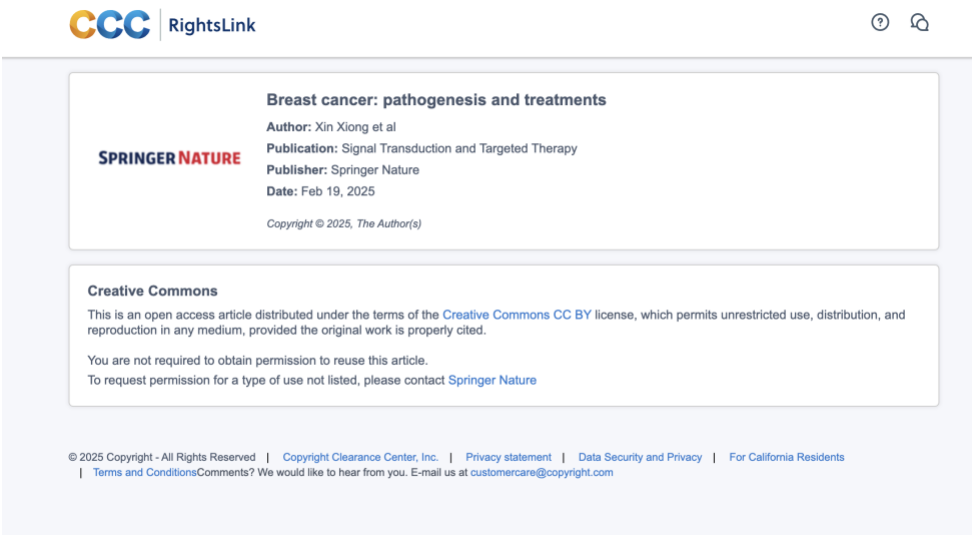

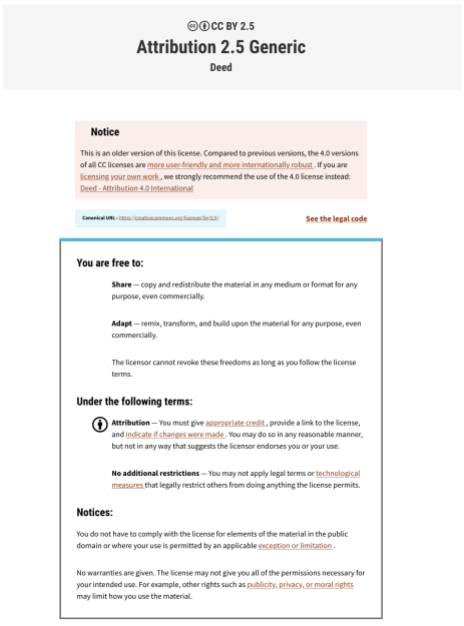

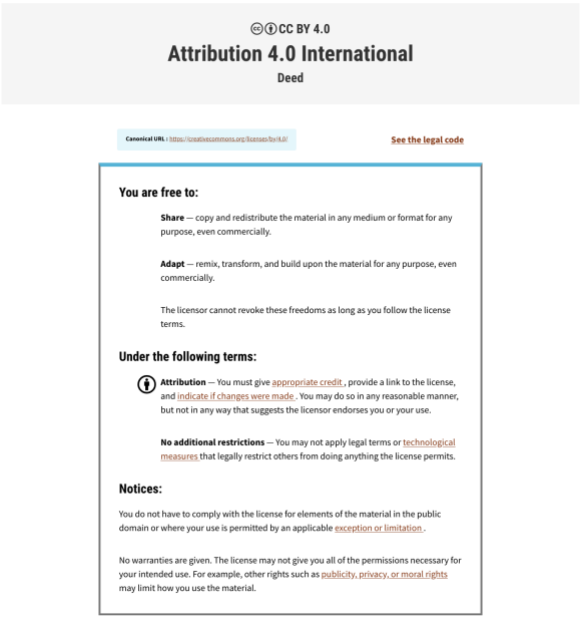

Chapter 2 is reproduced (content unedited and unmodified) from El-Sahli, S., *et al.* (2021). "A triple-drug nanotherapy to target breast cancer cells, cancer stem cells, and tumor vasculature." *Cell death & disease*, permission under the terms of Creative Commons Attribution 4.0 international license (CC BY 4.0). Minor formatting changes were made to comply with thesis style requirements. No other modifications were made.

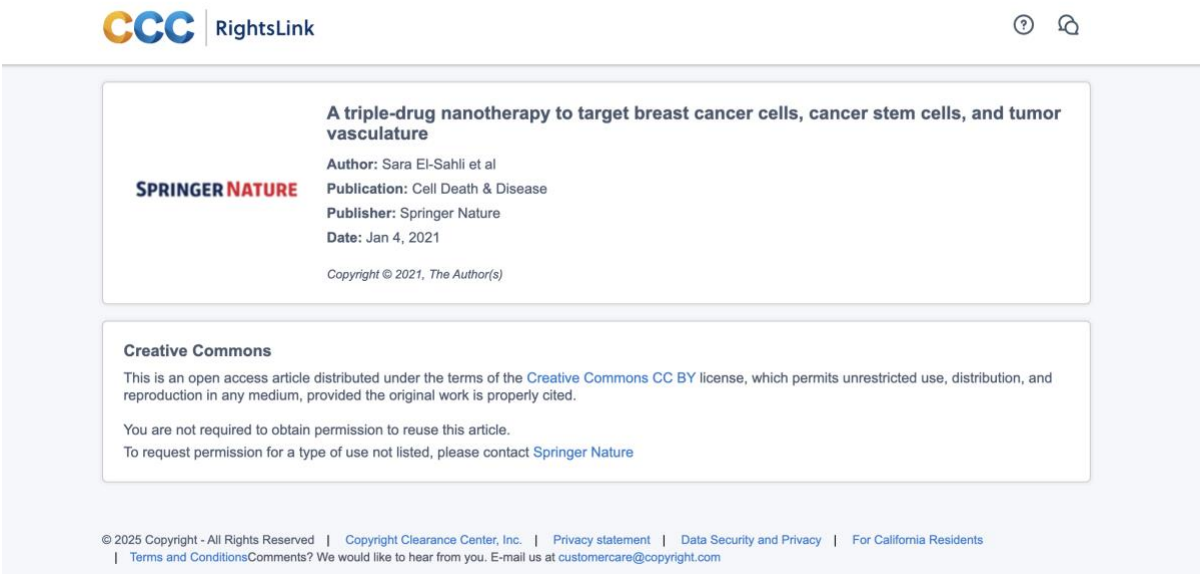

Chapter 3 is reproduced (content unedited and unmodified) from El-Sahli, S., et al. (2025). "Nanoparticle-Mediated mRNA Delivery to Triple-Negative Breast Cancer (TNBC) Patient-Derived Xenograft (PDX) Tumors." *ACS Pharmacology & Translational Science*, permission under the terms of Creative Commons Attribution–NonCommercial–NoDerivatives 4.0 International License (CC BY-NC-ND 4.0). Minor formatting changes were made to comply with thesis style requirements. No other modifications were made.
https://doi.org/10.1021/acsptsci.4c00597

Chapter 4 is reproduced (content unedited and unmodified) from Manturthi, S.*, & El-Sahli, S.*, et al. (2024). "Nanoparticles Codelivering mRNA and SiRNA for Simultaneous Restoration and Silencing of Gene/Protein Expression In Vitro and In Vivo." *ACS Nanoscience Au*, permission under the terms of Creative Commons Attribution–NonCommercial–NoDerivatives 4.0 International License (CC BY-NC-ND 4.0). Minor formatting changes were made to comply with thesis style requirements. No other modifications were made.
https://doi.org/10.1021/acsnanoscienceau.4c00040

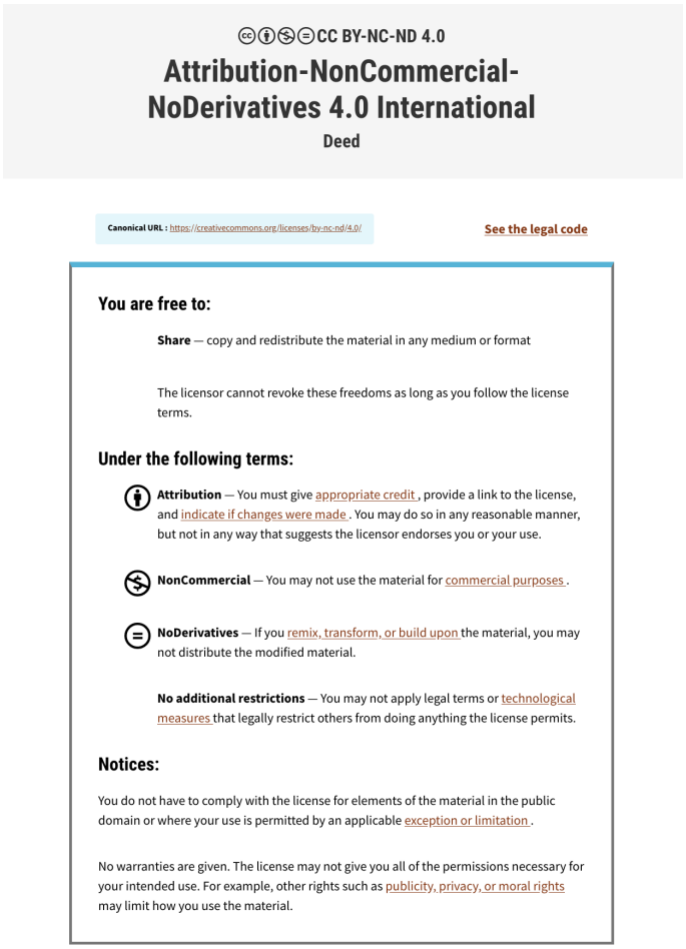

CC BY-NC-ND 4.0

Attribution-NonCommercial-NoDerivatives 4.0 International

Deed

Canonical URL : https://creativecommons.org/licenses/by-nc-nd/4.0/

See the legal code

You are free to:

Share — copy and redistribute the material in any medium or format

The licensor cannot revoke these freedoms as long as you follow the license terms.

Under the following terms:

Attribution — You must give appropriate credit , provide a link to the license, and indicate if changes were made . You may do so in any reasonable manner, but not in any way that suggests the licensor endorses you or your use.

NonCommercial — You may not use the material for commercial purposes .

NoDerivatives — If you remix, transform, or build upon the material, you may not distribute the modified material.

No additional restrictions — You may not apply legal terms or technological measures that legally restrict others from doing anything the license permits.

Notices:

You do not have to comply with the license for elements of the material in the public domain or where your use is permitted by an applicable exception or limitation .

No warranties are given. The license may not give you all of the permissions necessary for your intended use. For example, other rights such as publicity, privacy, or moral rights may limit how you use the material.

The following ACS guidelines were followed:

Section I: Scholarly posting & sharing policies

1. **Reuse/Republication of the Entire Work in Theses or Collections:** Authors may reuse all or part of the Submitted, Accepted or Published Work **(see definitions below)** in a thesis or dissertation that the Author writes and is required to submit to satisfy the criteria of degree-granting institutions. Appropriate citation of the Published Work must be made. If the thesis or dissertation to be published is in electronic format, a direct link to the Published Work must also be included using the ACS Articles on Request author-directed link.

https://pubs.acs.org/page/copyright/journals/posting_policies.html

CURRICULUM VITAE

SARA EL-SAHLI

EDUCATION

2018-present **Doctorate in Biochemistry**, University of Ottawa, Ottawa, ON
Thesis title: *The development of different strategies using clinically translatable models for the treatment of triple negative breast cancer (TNBC)*

2014-2018 **Bachelor of Science**, Honours, Biochemistry, University of Ottawa, Ottawa, ON
Summa Cum Laude

PUBLICATIONS

El-Sahli, S.,* Manturthi, S.,* Durocher, E., Bo, Y., Akman, A., Sannan, C., ... & Wang, L.*, Gadde, S.* (2025). *Nanoparticle-Mediated mRNA Delivery to Triple-Negative Breast Cancer (TNBC) Patient-Derived Xenograft (PDX) Tumors.* [ACS Pharmacology & Translational Science]

Manturthi, S.*, El-Sahli, S.*, Bo, Y., Durocher, E., Kirkby, M., Popatia, A., ... & Wang, L.*, Gadde, S.* (2024). *Nanoparticles Codelivering mRNA and SiRNA for Simultaneous Restoration and Silencing of Gene/Protein Expression In Vitro and In Vivo*. [ACS Nanoscience Au]

Mediratta, K., El-Sahli, S., Marotel, M., Awan, M. Z., Kirkby, M., Salkini, A., ... & Wang, L. (2024). *Targeting CD73 with flavonoids inhibits cancer stem cells and increases lymphocyte infiltration in a triple-negative breast cancer mouse model*. [Frontiers in Immunology]

Laframboise, S., Bailey, T., Dang, A., Rose, M., Zhou, Z., Berg, M., Holland, S., Aftab Abdul, S., O'Connor, K., El-Sahli, S., Boucher, D., Fairman, G., Deng, Shaw, Noblett, N., D'Addario, A., Empey, Sinclair, K. (2023). *Analysis of financial challenges faced by graduate students in Canada*. [Biochemistry and Cell Biology]

Ke, D., El-Sahli, S.,* & Wang, L.,*. (2022). *The Potential of Natural Products in the Treatment of Triple-Negative Breast Cancer.* [Current Cancer Drug Targets]

St-Denis-Bissonnette, F., Khoury, R., Mediratta, K., El-Sahli, S., Wang, L.,* & Lavoie, J.,*. (2022). *Applications of Extracellular Vesicles in Triple-Negative Breast Cancer.* [Cancers]

El-Sahli, S., Hua, K.,*, Sulaiman, A.,*, Chambers, J., Li, L., Farah, E., McGarry, S., Liu, D., Zheng, P., Lee, SH., Cui, J., Ekker, M., Cote, M., Alain, T., Li, X., D'Costa, V., Wang, L.,* Gadde, S.,*. (2021). *A triple-drug nanotherapy to target breast cancer cells, cancer stem cells and tumor vasculature.* [Cell Death & Disease]

El-Sahli, S., & Wang, L.,* (2020). *Cancer Stem Cell-Associated Pathways in the Metabolic Reprogramming of Breast Cancer.* [International Journal of Molecular Sciences]

Mediratta, K., El-Sahli, S., D'Costa, V.,* & Wang, L.,*. (2020). *Current Progresses and Challenges of Immunotherapy in Triple-Negative Breast Cancer.* [Cancers]

Sulaiman A, McGarry S, El-Sahli S, Li L, Chambers J, Phan A, Al-Kadi E, Kahiel Z, Farah E, Ji G, Lee SH, Inampudi KK, Alain T, Gadde S,* and Wang L*. (2020). *Nanoparticles loaded with Wnt and YAP/ mevalonate*

inhibitors in combination with paclitaxel stop the growth of TNBC patient-derived xenografts and diminish cancer stem cells and tumorigenesis. [Advanced therapeutics]

El-Sahli S, Xie Y, Wang L and Liu S. (2019). *Wnt Signaling in Cancer Metabolism and Immunity*. [Cancers]

Sulaiman A, El-Sahli S*, McGarry S*, Li L, Chambers J, Phan A, Côté M, Cron G, Alain T, Le Y, Lee SH, Liu S, Figeys D, Gadde S*and Wang W*. (2019). *Co-Targeting Bulk Tumor and CSCs in Clinically Translatable TNBC Patient-Derived Xenografts via Combination Nanotherapy*. [Molecular Cancer Therapeutics]

Sulaiman, A., McGarry, S., Lam, KM., El-Sahli, S., Chambers, J., Kaczmarek, S., Li, L., Addison, C., Dimitroulakos, J., Arnaout, A., Nessim, C., Yao, Z., Ji, G., Song, H., Liu, S., Xie, Y., Gadde, S., Li, X. & Wang L.,* (2018). *Co-inhibition of mTORC1, HDAC and ESR1α retards the growth of triple-negative breast cancer and suppresses cancer stem cells.* [Cell Death & Disease]

PRESENTATIONS

2023 An introduction to the Ottawa Science Policy Network (OSPN). *Department of Geography's Orientation Day,* Ottawa, ON, Canada

2023 The development of novel methods to treat triple negative breast cancer (TNBC). *Canadian Society for Molecular Biosciences (CSMB)*, Ottawa, ON, Canada

2023 Navigating graduate school-tips and tricks to succeed in grad school. *Canadian Society for Molecular Biosciences (CSMB)*, Ottawa, ON, Canada

2023 The development of novel methods to treat triple negative breast cancer (TNBC). *Faculty Research Day*, Ottawa, ON, Canada

2022 Targeting Triple Negative Breast Cancer (TNBC) using natural products. *Faculty Research Day*, Cornwall, ON, Canada

2022 Targeting Triple Negative Breast Cancer (TNBC) using natural products. *OISB Scientific Meeting*, Cornwall, ON, Canada

2021 The development of effective TNBC treatment through the co-inhibition of SCD1 and NF-kB pathways. *Faculty Research Day*, Ottawa, ON, Canada ***3rd place oral presentation award**

2021 A triple-drug nano-therapy targeting breast cancer cells, cancer stem cells, and tumor vasculature. *13ème édition de la Journée Phare*, Orford, QC, Canada

2019 Combination nanomedicine for the treatment of triple negative breast cancer. *Nanoparticle delivery systems for ruthenium-based therapeutics*, Halifax, NS, Canada

2019 The development of a triple drug nanotherapy to target TNBC cells, CSCs &tumor vasculature. *Department Poster Day*, Ottawa, ON, Canada ***1st place poster presentation award**

2018 Using a nanoparticle-containing triple drug treatment to target TNBC cells, CSC populations & tumor vasculature. *Journée phare*, Bromont, QC, Canada ***3rd place poster presentation award**

LEADERSHIP POSITIONS

2023-2024	**President: Ottawa Science Policy Network (OSPN),** Ottawa, ON
2021-2023	**VP Marketing: Ottawa Science Policy Network (OSPN)**, Ottawa, ON
2018, 2021	**Department representative: Graduate Student Association (GSAED),** Ottawa, ON
2019-2020	**President: Biochemistry, Microbiology & Immunology Graduate Student Association (BMIGSA)**, Ottawa, ON
2018-2019	**VP External: BMIGSA**, Ottawa, ON
2017	**Vice-President: Secure Her Education,** Ottawa, ON

TECHNICAL SKILLS

- Cell culture
- Flow cytometry
- Quantitative PCR
- Animal work: basic mouse skills, intravenous (IV) & intraperitoneal (IP) injections, Patient Derived Xenograft (PDX) transplantation surgery
- In Vivo Imaging Systems (IVIS)
- Western Blotting

WORK EXPERIENCE

Fall 2022	**Teaching assistant,** University of Ottawa**,** Ottawa, ON

HONOURS & AWARDS

2023-24	**Ontario Graduate Scholarship (OGS)**
2020-23	**CIHR-The Frederick Banting & Charles Best Canada Graduate Scholarship – Doctoral Award**
2020-21	**Leadership Award in graduate studies,** University of Ottawa, Faculty of Medicine
2020-21	**Excellence Award in graduate studies, PhD level**, University of Ottawa, Faculty of Medicine
2020-21	**Judith R. Raymond Scholarship**
2019-20	**Excellence Award in graduate studies, MSc level**, University of Ottawa, Faculty of Medicine
2018-19	**CIHR- Canada Graduate Scholarship - Master's Award**
2018-19	**Ontario Graduate Scholarship (OGS)**
2018	**Faculty Plaque in Biochemistry (highest standing in Biochemistry)**, University of Ottawa
2015-18	**Faculty of Science Dean's Honour List**, University of Ottawa
2015-18	**Excellence Scholarship**
2015-16	**Undergraduate Research Scholarship,** University of Ottawa